FAST MARCHING METHODS - PARALLEL IMPLEMENTATION AND ANALYSIS

A Dissertation

Submitted to the Graduate Faculty of the
Louisiana State University and
Agricultural and Mechanical College
in partial fulfillment of the
requirements for the degree of
Doctor of Philosophy

in

The Department of Mathematics

by
Maria Cristina Tugurlan
B.Sc., Technical University of Iasi, 1998
M.Sc., Louisiana State University, 2004
December 2008

Acknowledgments

I would like to express my sincere gratitude to my research advisor Professor Blaise Bourdin for the suggestion of the topic. This dissertation would have not been possible without his continuous support, help, guidance, and endless patience.

It is a pleasure to give thanks to all my professors at Louisiana State University, and especially to my committee members: Dr. Jimmie Lawson, Dr. Robert Lipton, Dr. Robert Perlis, Dr. Ambar Sengupta, Dr. Padmanabhan Sundar and Dr. Jing Wang, for all the help and support provided during my graduate studies.

I am grateful to the Department of Mathematics at Louisiana State University, for the great moral, professional and financial support.

I would also like to thank Dr. Robert Perlis for the financial support through the Louisiana Education Quality Support Fund LEQSF(2005), which allowed me to enjoy valuable research visits to France and Denmark. Special thanks go to Dr. Gregoire Allaire (L'*É*cole Polytechnique, France), Dr. Antonine Chambolle (L'*É*cole Polytechnique, France), Dr. Martin P. Bendsøe (Technical University of Denmark, Lyngby), and Dr. Mathias Stolpe (Technical University of Denmark, Lyngby) for their hospitality, valuable support, and interesting discussions.

Finally, I would like to express my deepest gratitude to my family for their support, encouragement and understanding over all these years. Also I want to thank Laurentiu for his patience, love and support.

Table of Contents

List of Figures

List of Algorithms

Abstract

Fast Marching represents a very efficient technique for solving front propagation problems, which can be formulated as partial differential equations with Dirichlet boundary conditions, called Eikonal equation:

$$\begin{cases} F(x)|\nabla T(x)| &= 1, \quad x \in \Omega \\ T(x) &= 0, \quad x \in \Gamma, \end{cases}$$

where Ω is a domain in $\mathbb{R}^n$, Γ is the initial position of a curve evolving with normal velocity $F > 0$. Fast Marching Methods are a necessary step in Level Set Methods, which are widely used today in scientific computing. The classical Fast Marching Methods, based on finite differences, are typically sequential. Parallelizing Fast Marching Methods is a step forward for employing the Level Set Methods on supercomputers.

The efficiency of the parallel Fast Marching implementation depends on the required amount of communication between sub-domains and on algorithm ability to preserve the upwind structure of the numerical scheme during execution. To address these problems, I develop several parallel strategies which allow fast convergence. The strengths of these approaches are illustrated on a series of benchmarks which include the study of the convergence, the error estimates, and the proof of the monotonicity and stability of the algorithms.

Introduction

Scientific computing allows scientists and engineers to gain understanding of real life problems in diverse areas, such as cosmology, climate control, computational fluid dynamics, health-care, design and manufacturing. The scientists and engineers develop computer programs that model the behavior of the studied system or phenomenon. Running these programs with multiple and various sets of input parameters helps them better comprehend past behavioral patterns and possibly predict future actions. Typically, these models require massive amounts of calculations and, therefore, executed on supercomputers or distributed computing platforms.

Nowadays, parallel computing is considered a standard tool for scientific computing. It is formally viewed as the simultaneous use of multiple processors to execute a program. Parallel programming is more intricate than its sequential counterpart and demands extra care. For instance, concurrency between tasks introduces several new classes of potential software bugs and requires revisiting many classical algorithms. Communication and synchronization between processors is typically one of the greatest barriers to getting good performances. All of these are aspects that I have encountered while preparing my thesis.

In order to set this work into perspective, let me describe first the front propagation problem that I want to solve employing parallel computing. It is known that interfaces propagation occur in a lot of settings, including ocean waves, material boundaries, optimal path planning, construction of geodesic path on surfaces, iso-intensity contours in images, computer vision and many more. I consider the case of a curve propagating in a domain with a normal velocity $F > 0$, the tangent direction of the movement being ignored. I want to track the motion of this in-

terface as it evolves. To describe interface motion, I formulate the boundary value problem and the partial differential equation with initial value known as Eikonal equation:

$$\begin{cases} F(x)|\nabla T(x)| &= 1, \quad x \in \Omega \\ T(x) &= 0, \quad x \in \Gamma, \end{cases}$$

where Ω is a domain in $\mathbb{R}^n$, Γ is the initial position of a curve evolving with normal velocity F, ∇ denotes the gradient, and $|\cdot|$ is the Euclidean norm. The solution T of the Eikonal equation can be view as: the *time of first arrival* of the curve Γ, or as the *distance* function to curve Γ, if $F = 1$. All the mathematical details on how to find the solution to Eikonal equation are presented in Chapter 1.

The primary goal of my thesis is to solve the Eikonal equation employing parallelized computational methods and algorithms. To solve this equation, I use the Fast Marching Method, a computational technique for tracking moving interfaces and modeling the evolution of boundaries. Fast Marching Methods are typically sequential, and hence not straight forward to parallelize [18, 23]. The Fast Marching algorithm is a necessary step in Level Set Methods, which, in today's scientific computing world, are widely used for simulating front motion related processes. Therefore, since they have a great impact on many applications, it is imperative to parallelize Fast Marching Methods to try to improve even more execution time and solution accuracy.

The idea of the parallel Fast Marching algorithm is to perform Fast Marching on sub-domains, update the boundary values at the interfaces and restart the algorithm until convergence is achieved. To update the boundary values at the interfaces we need to preserve the upwind structure of the numerical scheme and to synchronize the ghost-zones at each iteration. Therefore, the efficiency of the parallel Fast Marching implementation depends on the required amount of com-

munication between sub-domains and on algorithm ability to preserve the upwind structure of the numerical scheme during execution. To address these problems, I develop several strategies, among which the following are the most viable:

1. Ordered Overlap strategy: group the overlapping nodes of each sub-domain in a sorted list and use this list to recompute the boundary values;

2. Fast Sweeping strategy: perform a Fast Sweeping [28] at the interfaces and update the overlapping regions of the sub-domains.

The advantage of these strategies is to not keep a distributed list for the *narrow band*, which would require much more communication time.

The thesis is organized as follows.

In Chapter 1, I present the theoretical background necessary to deal with the problem of moving interfaces. I begin by introducing the Hamilton-Jacobi equations and viscosity solution, emphasizing the Eikonal equation and its application. In the second part of this chapter, I explain the numerical approximation scheme and the numerical methods used to solve the Eikonal equation over the past years. Specifically, I talk about the main features of the Rouy-Tourin algorithm [21] and the Fast Sweeping algorithm [28].

Chapter 2 is devoted to the sequential Fast Marching Methods, which "are the optimal way to solve Hamilton-Jacobi equations" [23]. I begin by explaining the idea of classifying the nodes as *accepted*, *narrow band* and *far away*. I follow with the description of the algorithm, pointing out how the upwind nature of the numerical scheme is preserved. I end up presenting how the numerical solution built by the Fast Marching Methods converges to the viscosity solution of the Eikonal equation. To prove this, I first show how the solution of the discrete Eikonal equation converges to the viscosity solution [3]. Secondly, I show that the sequence

built by the Fast Marching Methods converges to the solution of discrete Eikonal equation.

Chapter 3 deals with the parallel Fast Marching Methods. First of all, I focus on formulating the problem in terms of parallel programing. I define the necessary notions, such as sub-domains, neighbors, ghost-nodes, ghost-zones. After that, I present the convergence results for the parallel Fast Marching algorithm.

Chapter 4 focuses on the aspect of implementation and on numerical experiments. The chapter starts with a brief presentation of the sequential implementation and elaborates the main problems through numerical experiments. Then, it gives a short background on parallel computing before focusing on the actual parallel implementation of the algorithm. I bring to one's attention parallel programming concepts, such as parallel architectures, programming models, and the issues that differentiate it from sequential programming. I also focus on the obstacles encountered during parallel implementation and how to get over them. I illustrate the strengths of the parallel approach with a series of benchmarks, which include the study of convergence, error estimates. In addition, I show the algorithm is monotone and stable.

Chapter 1
Background

Let us consider a boundary (a closed curve in two dimensions or a surface in three dimensions), separating two regions. Let this curve or surface evolve with a known normal velocity F as shown in Figure 1.1. The function F may depend on factors such as curvature, normal direction, shape and position of the front, or shape independent properties [23].

Assume that the curve moves outwards from the domain (i.e. $F > 0$) and the tangential direction of the motions are ignored. In all that follow, we will consider that F depends on the position of the front and not on curvature.

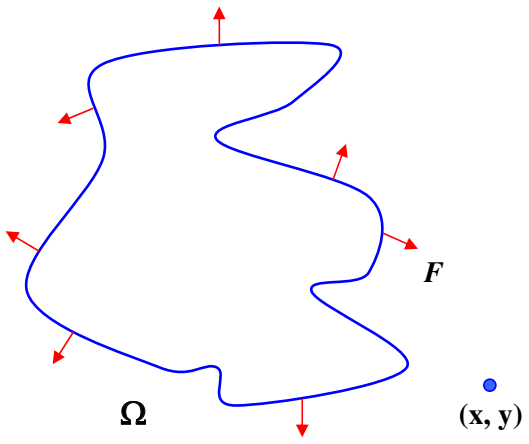

FIGURE 1.1. Curve propagation with speed F in normal direction

In order to characterize the position of the expanding front, we can compute its first arrival time T as it crosses each point *(x,y)* in the domain. Therefore, we define $T(x, y) = \inf_{t>0} \Gamma_t,\ (x, y) \in \Gamma_t$.

Formally, in one dimension we have *distance* = *rate* × *time*, so we can write the equation for the arrival function T:

$$1 = F\frac{dT}{dx}.$$

In higher dimensions, the time T of first arrival is the solution of a boundary value problem, known as the *Eikonal equation*:

$$\begin{cases} F(x)|\nabla T(x)| &= 1, \quad x \in \Omega \\ T(x) &= 0, \quad x \in \Gamma, \end{cases} \tag{1.1}$$

where Ω is a domain in $\mathbb{R}^n$, Γ is the initial position of a curve evolving with normal velocity F, ∇ denotes the gradient, and $|\cdot|$ is the Euclidean norm.

We want to show how the time of first arrival is different from the curve evolution. For illustration purposes consider the propagation of a curve, with normal velocity $F = 1$, as presented in Figure 1.2.

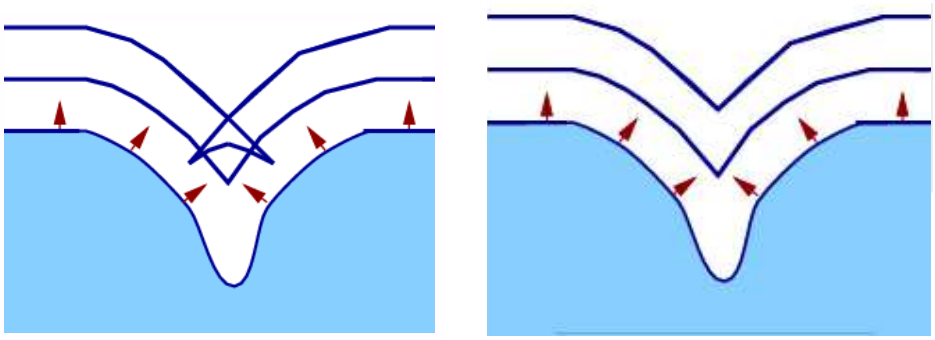

(a) Swallowtail (b) Physically Correct Evolution

FIGURE 1.2. Curve propagating with $F = 1$

In Figure 1.2(a), the curve passes through itself developing the so-called *swallowtail*. Analyzing the swallowtail from the geometric point at view, at a time t, we have a multivalued solution. Since "the solution should consist of only the set of all points located a distance t from the initial curve" [22], we need to remove the "tail" from "swallowtail". In [23], Sethian described this situation as: "if the

front is viewed as a burning flame, then once a particle burnt it stayed burnt". Therefore, from the family of solutions, we pick the physically reasonable solution, with the shape presented in Figure 1.2(b).

Equation (1.1) is a particular form of first-order *Hamilton-Jacobi equation.*

The *Dirichlet problem* for a static Hamilton-Jacobi equation can be written in the form:

$$\begin{cases} H(x, Du) = 0 & \text{on } \mathbb{R}^n \times (0, \infty) \\ u = \phi & \text{on } \mathbb{R}^n \times \{t = 0\}, \end{cases} \tag{1.2}$$

where the Hamiltonian $H = H(x, Du)$ is a continuous real valued function on $\mathbb{R}^n \times \mathbb{R}^n$ ([8], pg. 539), and $\phi : \mathbb{R}^n \to \mathbb{R}$ is a given initial function.

In general, this equation does not have classical solutions, i.e. solutions which are C^1. The problem does have generalized solutions, which are continuous and satisfy the partial differential equation almost everywhere. Using the notion of viscosity solution, introduced by Crandall and Lions [4, 5] for first-order problems, one can choose the correct "physical" solution from the multitude of solutions.

1.1 Viscosity Solutions

1.1.1 Motivation

Let us consider the unidimensional Eikonal equation with homogeneous Dirichlet boundary condition:

$$\begin{cases} |u'(x)| = 1 \ \text{ in } (-1, 1) \\ u(x) = 0, \quad x = \pm 1. \end{cases} \tag{1.3}$$

The general solution of the differential equation is $u = \pm x + c$. We cannot choose a sign for x and a constant of integration to satisfy both boundary conditions, but there are weak solutions that satisfy the differential equation almost everywhere.

The function:

$$u(x) = 1 - |x|$$

satisfies the boundary conditions and satisfies the differential equation everywhere except $x = 0$. This solution gives the distance to the boundary of the domain, but is not unique. As shown in Figure 1.3, there exists infinitely many weak solution: continuous function with slope ± 1, satisfying almost everywhere the boundary conditions.

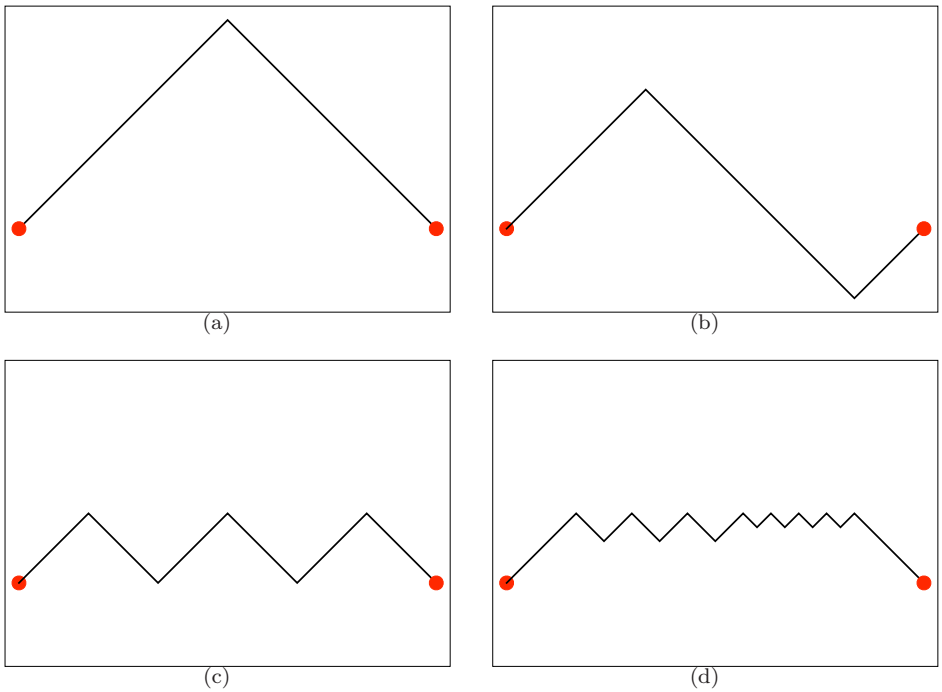

FIGURE 1.3. Weak solutions of $|u'| = 1, u(-1) = u(1) = 0$

By adding a small viscosity term to Equation (1.3), one can obtain a second-order equation for $u_\varepsilon(x)$:

$$\begin{cases} -\varepsilon u_\varepsilon'' + |u_\varepsilon'| = 1 \ \text{ in } (-1,1) \\ u_\varepsilon(-1) = u_\varepsilon(1) = 0, \ \ \varepsilon \geq 0. \end{cases} \tag{1.4}$$

It is well known that equation (1.4) has a unique solution of the form:

$$u_\varepsilon(x) = 1 - |x| + \varepsilon e^{-1/\varepsilon}(1 - e^{(1-|x|)/\varepsilon}).$$

In Figure 1.4 we graph the solution of equation (1.4) for $\varepsilon = 1/5, 1/10, 1/20, 1/40, 1/100$. For small ε, the viscosity term smooths out part of the solution $u_\varepsilon(x)$. In fact, it will smooth out the corners to make the solution C^2. In this example we choose $\varepsilon > 0$ to smooth the solution at its relative maximum. By choosing $\varepsilon < 0$, one would obtain an approximation of $u(x) = |x| - 1$, which smooths the solution at relative minimum point. As $\varepsilon \to 0$, u_ε converges to the *viscosity solution* of (1.3), which is introduced in more details in the following section.

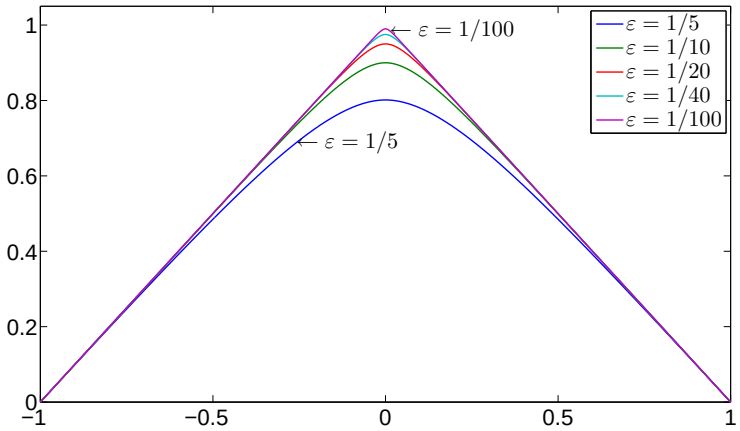

FIGURE 1.4. Solution of Equation (1.4) for $\varepsilon = 1/5, 1/10, 1/20, 1/40, 1/100$

1.1.2 The General Case

Let Ω be an open bounded domain in $\mathbb{R}^n$, $\Gamma \subset \partial\Omega$ and consider the general static Hamilton-Jacobi equation:

$$\begin{cases} H(x, Du) = 0 & \text{on } \Omega \\ u = \phi & \text{on } \Gamma \subseteq \partial\Omega, \end{cases} \tag{1.5}$$

where H is convex, u and ϕ are continuous.

As Crandall, Evans and Lions pointed out in [4] and [5], problem (1.5) does not have, in general, a C^1 solution. It admits generalized (weak) solutions. Hence, we

can approximate the problem by adding a viscosity term to (1.5):

$$\begin{cases} H(x, Du_\varepsilon) - \varepsilon \Delta u_\varepsilon = 0 & \text{on } \Omega \\ u_\varepsilon = \phi & \text{on } \Gamma \subseteq \partial\Omega, \end{cases} \tag{1.6}$$

for $\varepsilon > 0$. Problem (1.6) admits a smooth solution u_ε [4, 5, 8].

We want to prove that as $\varepsilon \to 0$, the solution $u_\varepsilon(x)$ of (1.6) converges locally uniformly to a weak solution u of (1.5). In order to do that, we follow Evans's arguments, presented in [8]. This method is known as the method of *vanishing viscosity*. When $\varepsilon \to 0$, we can find a family of functions $\{u_\varepsilon\}_{\varepsilon>0}$, which is uniformly bounded and equicontinuous on a compact subset of $\Omega \subset \mathbb{R}^n$. Applying the Arzela-Ascoli compactness criterion, there exists a subsequence $u_{\varepsilon_j} \subseteq u_\varepsilon$ such that

$$u_{\varepsilon_j} \to u \ \text{ locally uniformly in } \Omega \subset \mathbb{R}^n. \tag{1.7}$$

At this point, we can expect u to be some kind of solution of our initial-value problem (1.5), but we only know that u is continuous and we do not have any information on the derivatives of u. As $\varepsilon \to 0$, we do not have a uniform bound on Du_ε, which would allow us to show that $Du_\varepsilon \to Du$ in some sense. To prove that, we introduce a smooth test function $v \in C^\infty(\Omega), v|_\Gamma = 0$, and suppose that

$$u - v \text{ has a } \textit{strict} \text{ local maximum at } x = x_0 \in \Omega. \tag{1.8}$$

This means $u(x_0) - v(x_0) > u(x) - v(x)$ in some neighborhood of x_0, with $x \neq x_0$. Recalling (1.7) we claim that for each $\varepsilon_j > 0$ sufficiently small enough, there exists a point x_{ε_j} such that

$$u_{\varepsilon_j} - v \text{ has a local maximum at } x_{\varepsilon_j}, \text{ and } x_{\varepsilon_j} \to x_0 \text{ as } j \to \infty. \tag{1.9}$$

To confirm this, note that for each sufficient small $r > 0$, equation (1.8) implies $\max_{\partial B}(u - v) < (u - v)(x_0)$, where $B(x_0, r)$ is the closed ball in $\Omega \subset \mathbb{R}^n$ with center

at x_0 and radius r. Applying Arzela-Ascoli compactness criterion, we claim that for ε_j small enough, $u_{\varepsilon_j} \to u$ uniformly on B and $\max_{\partial B}(u_{\varepsilon_j} - v) < (u_{\varepsilon_j} - v)(x_0)$. Consequently $u_\varepsilon - v$ attains a local maximum at some point in the interior of B. Considering now a radii sequence r_j such that $r_j \to 0$, we obtain (1.9).

Using the second derivative test and relation (1.9) we can relate the derivatives of u_{ε_j} and v:

$$\begin{aligned} Du_{\varepsilon_j}(x_{\varepsilon_j}) &= Dv(x_{\varepsilon_j}) \\ -\Delta u_{\varepsilon_j}(x_{\varepsilon_j}) &\geq -\Delta v(x_{\varepsilon_j}) \end{aligned} \tag{1.10}$$

We show that $H(x_0, Dv(x_0)) \leq 0$:

$$\begin{aligned} H(x_{\varepsilon_j}, Dv(x_{\varepsilon_j})) &= H(x_{\varepsilon_j}, Du_{\varepsilon_j}(x_{\varepsilon_j})) \text{ (using 1.10)} \\ &= \varepsilon_j \Delta u_{\varepsilon_j}(x_{\varepsilon_j}) \text{ (using 1.6)} \\ &\leq \varepsilon_j \Delta v(x_{\varepsilon_j}) \text{ (using 1.10).} \end{aligned}$$

Since v is smooth, H is continuous, $x_{\varepsilon_j} \to x_0$ as $j \to \infty$ and letting $\varepsilon_j \to 0$, the previous inequality becomes

$$H(x_0, Dv(x_0)) \leq 0. \tag{1.11}$$

Similarly, we deduce the inverse inequality:

$$H(x_0, Dv(x_0)) \geq 0, \tag{1.12}$$

provided that

$$u - v \text{ has a local minimum at } x_0. \tag{1.13}$$

Equations (1.8), (1.11), (1.13) and (1.12) define the concept of weak solution of (1.5) as:

Definition 1.1 (version I)**.** *A bounded, uniformly continuous function u is a* ***viscosity solution*** *of the initial-value problem (1.5) for the Hamilton-Jacobi equation*

provided that the function satisfies the boundary condition: $u = \phi$ *on* $\partial\Omega$ *and for all* $v \in C^\infty(\Omega)$*:*

$$\begin{aligned} &\textit{if } u - v \textit{ has a local maximum at } x_0, \textit{ then } \; H(x_0, Dv(x_0)) \leq 0, \\ &\textit{(u is called a viscosity sub-solution)} \end{aligned} \tag{1.14}$$

and

$$\begin{aligned} &\textit{if } u - v \textit{ has a local minimum at } x_0, \textit{ then } \; H(x_0, Dv(x_0)) \geq 0 \\ &\textit{(u is called a viscosity supra-solution).} \end{aligned} \tag{1.15}$$

Remark 1.2. *In the light of Definition 1.1,* u *defined in (1.7) and solution of (1.6) converges to the viscosity solution of (1.5).*
To verify that a given function u *is a viscosity solution of the Hamilton-Jacobi equation* $H(x, Du) = 0$*, equations (1.14) and (1.15) must hold for all smooth functions* v*. Evans noted in [8] that if we used the vanishing viscosity method to construct* u*, then it would indeed be a viscosity solution.*

Viscosity solutions can be seen as the limit function $u = \lim_{\varepsilon \to 0} u_\varepsilon$, where $u_\varepsilon \in C^2(\Omega)$ is the classical solution of the perturbed problem (1.6), if u_ε exists and converges locally uniformly to some continuous function u.
If ϕ is bounded and uniformly continuous, then u is the unique viscosity solution of (1.5). One can extend the notion of viscosity solution of (1.5) for ϕ discontinuous, using the lower semi-continuous (l.s.c) and the upper semi-continuous (u.s.c) envelopes of the solution [2].

Definition 1.3. *For any* $x \in \Omega$*, define the upper semi-continuous envelope of* u *as:*

$$\bar{u}(x) = \limsup_{y \to x} u(y),$$

and the lower semi-continuous envelope of u *as:*

$$\underline{u}(x) = \liminf_{y \to x} u(y).$$

Therefore, we can rewrite the definition of the *viscosity solution*:

Definition 1.4 (version II)**.** *A locally bounded function u is a viscosity sub-solution of the Hamilton Jacobi equation (1.5) if*

$$\forall\, v \in C^1(\mathbb{R}^n), \quad \textit{at each maximum point } x_0 \textit{ of } \bar{u} - v, \quad \textit{we have:}$$
$$\max\{H(x_0, Dv(x_0)),\, \bar{u} - \phi\} \leq 0$$

and a viscosity super-solution of the Hamilton Jacobi equation (1.5) if

$$\forall\, v \in C^1(\mathbb{R}^n), \quad \textit{at each minimum point } x_0 \textit{ of } \underline{u} - v, \quad \textit{we have:}$$
$$\max\{H(x_0, Dv(x_0)),\, \underline{u} - \phi\} \geq 0.$$

Remark 1.5. *Then u is a viscosity solution of (1.5) if u is both a sub-solution and super-solution.*

Remark 1.6. *Definition (1.4) is an extension of Crandall-Lions or Ishii definition of viscosity solution for continuous Hamiltonians (see [2] pg. 558-577, [5, 13]). Definition (1.1) is a particular case of Definition (1.4) for continuous Hamiltonians.*

Viscosity solutions have the following properties: consistency, existence, uniqueness and stability. One can show that the viscosity solution satisfies the partial differential equation (1.5) whenever it is differentiable, that it exists, and furthermore it is unique and stable.

Theorem 1.7 (Consistency of a viscosity solution)**.** *Let u be a viscosity solution of problem(1.5) and suppose u is differentiable at some point $x_0 \in \Omega \subset \mathbb{R}^n$. Then $H(x_0, Du(x_0)) = 0$.*

The proof of this theorem can be found in [8], section 10.1.2, page 545.

Proposition 1.8. *If $u \in C^1(\Omega)$ solves (1.5) and if u is bounded and uniformly continuous, then u is a viscosity solution.*

Proof. If v is smooth and $u-v$ has a local maximum at x_0, then $Du(x_0) = Dv(x_0)$. This implies that $H(x_0, Dv(x_0)) = H(x_0, Du(x_0)) = 0$, since u solves (1.5). Similar equality holds for $u - v$ having a local minimum at x_0. □

Theorem 1.9 (Existence and uniqueness)**.** *Let Ω be a bounded open subset of $\mathbb{R}^n$, H convex on Ω, $H \geq 0$; also let $F : \Omega \to \mathbb{R}$ such that $F > 0$ is continuous on $\bar{\Omega}$. Then there exists a unique viscosity solution u of the problem:*

$$\begin{cases} F(x)H(x, \nabla u) = 0, & x \in \Omega \\ u(x) = 0, & x \in \Gamma \subseteq \partial\Omega, \end{cases} \tag{1.16}$$

Crandall and Lions proved this theorem in [5], pages 24-25, and pointed out assumptions that can cause the uniqueness of the viscosity solution to fail.

Remark 1.10. *If the function F vanishes at at least a single point in Ω, then the uniqueness result does not hold. It can be proved that in this case many viscosity solutions or even classical solutions may exist.*

Theorem 1.11. *Assume $u_1, u_2 \in C(\bar{\Omega})$, where $\Omega \subset \mathbb{R}^n$ is open and bounded, are a viscosity sub-solution and a super-solution of $H(x, \nabla u(x)) = 0, x \in \Omega$ and $u_1 \leq u_2$ on $\partial\Omega$. Assume also that H satisfies the conditions of Lipschitz continuity:*

$$|H(x, p) - H(y, q)| \leq C(|p - q|)$$

and

$$|H(x, p) - H(y, q)| \leq C(|x - y|(1 + |p|)) \tag{1.17}$$

for $x, y \in \Omega$, $p, q \in \mathbb{R}^n$, and some constant $C \geq 0$.

Then $u_1 \leq u_2 \in \bar{\Omega}$.

Remark 1.12. *Assuming that the Hamiltonian H satisfies the conditions of Lipschitz continuity, Evans proves that there exists at most one viscosity solution of (1.5) ([8], Theorem 1, pg. 547).*

We need to assume that H is convex with respect to the variable p, in order to apply this theorem to more general cases. This assumption is the key point in many theoretical results.

Proposition 1.13 (Stability Property)**.** *Let $\{u_n\}_{n\in\mathbb{N}} \in C^0(\Omega)$ be a sequence of functions such that u_n is the viscosity solution of the problem*

$$H_n(x, \nabla u_n) = 0, \quad x \in \Omega, \quad n \in \mathbb{N}.$$

Assume that u_n converges locally uniformly to u and H_n converges locally uniformly to H. Then u is the viscosity solution of

$$H(x, \nabla u) = 0, \quad x \in \Omega.$$

Theorem 1.14. *Let Ω be a bounded and open subset of $\mathbb{R}^n$. Assume that $u_1, u_2 \in C(\bar{\Omega})$ are the viscosity sub-solution and super-solution of equation (1.5), with $u_1 < u_2$ on $\partial\Omega$. Assume also that $H = H(x, p)$ is convex with respect to the variable p on $\mathbb{R}^n$ for each $x \in \Omega$, and satisfies (1.17) and the following conditions:*

$$\begin{cases} \exists\ \phi \in C(\bar{\Omega}) \cap C^1(\Omega) \qquad \text{such that } \phi \le u_1 \text{ in } \bar{\Omega} \text{ and} \\ \sup\limits_{x\in\Omega'} H(x, \nabla\phi(x)) < 0, \quad \text{for all } \Omega' \subset \Omega. \end{cases} \tag{1.18}$$

Then $u_1 \le u_2$ in Ω.

This theorem can be applied to the Eikonal equation whenever $F(x)$ is Lipschitz in Ω and it is strictly positive [6]. Conditions (1.18) are satisfied by taking

$$\phi(x) = \min_{x\in\bar{\Omega}} u_1.$$

1.1.3 Application to the Eikonal Equation

Proposition 1.15. *Let Ω be bounded open subset of $\mathbb{R}^n$. Set $u(x) = \text{distance}(x, \partial\Omega)$, $x \in \Omega$. Then u is Lipschitz continuous and is a solution of the Eikonal equation: $|Du| = 1$ in Ω.*

This means that for each $v \in C^\infty(\Omega)$, if $u - v$ has a maximum (minimum) at a point $x_0 \in \Omega$, then $|Dv(x_0)| \leq 1$ ($|Dv(x_0)| \geq 1$).

In the initial model problem (1.5), we can obtain the Eikonal equation, by considering the Hamiltonian $H(x, Du) = F|\nabla u| - 1$.

For a general set Ω, we have the following corollary.

Corollary 1.16. *If $F(x) > 0$ for all $x \in \Omega \subset \mathbb{R}^n$, then the equation*

$$\begin{cases} F(x)|\nabla T(x)| = 1, & x \in \Omega \subset \mathbb{R}^n \\ T(x) = 0, & x \in \Gamma, \end{cases} \tag{1.19}$$

admits a unique viscosity solution T.

Remark 1.17. *In [9] it is proved that if F is Lipschitz in $\mathbb{R}^n \cap L^\infty(\mathbb{R}^n)$, then the unique viscosity solution T is locally Lipschitz in Ω.*

For the front propagation problems, we want to have an Eulerian formulation for the motion of the initial curve $\Gamma_{t=0} \subset \Omega$, under the influence of normal velocity $F > 0$. We interpret the solution $T(x, y)$ of the Eikonal equation as the time needed by the curve Γ_t to evolve and reach the point (x, y) for the first time. We consider the t-level set of $T(x, y)$ as the zero-level set of the viscosity solution of the Eikonal equation at time t: $\Gamma_0(t) = \{(x, y)|T(x, y) = t\}$.

Remark 1.18. *When $F = 1$, T is also interpreted as the distance to Γ_0.*

The gradient flow of T gives the trajectories of each point.

Property 1.19 (Optimality Property)**.** *Let curve Γ propagate in the domain Ω with normal velocity $F > 0$ and $T(x, y)$ be the viscosity solution of (1.19). Let $\Gamma_0(t) = \{(x, y)|T(x, y) = t\}$ be the zero-level set of the solution T. The trajectory of a point (x, y) of the front coincides with the trajectory starting at $(x_0, y_0) \in \Gamma_0$ and reaching (x, y) in time t.*

The way of interpreting T, in the light of the last property, is very important for the construction of all numerical schemes. Since T is the viscosity solution, the trajectory of a point (x, y) is the "physically" correct trajectory from all the possible ones starting from (x, y).

1.2 Numerical Approximations

In this section we present a numerical scheme to compute the viscosity solution of the Eikonal equation (1.1), under the assumption that $F(x) > 0$ on Ω.
It is shown in [26] that the first-arrival travel-time field is a viscosity solution of the Eikonal equation. Numerical methods utilizing *upwind finite differences* schemes manage to produce viscosity solutions of the Eikonal equation. If we consider the numerical methods to approximate the partial differential equation, then we distinguish the following methods: the algorithm introduced by Rouy and Tourin [21], the Fast Sweeping algorithm [28], the Fast Marching Methods proposed by Osher and Sethian [18]. They all compute an approximation of the same solution.

1.2.1 Motivation

Let $\Omega = (0, 1)$ and consider the one-dimensional Eikonal equation given by:

$$\sqrt{u_x^2} = F(x), \quad u(-1) = u(1) = 0.$$

Given the speed function $F(x) > 0$, we want to construct $u(x)$ away from the boundary and we observe that the solution is not unique (for instance, if $v(x)$ solves the problem, then so does $-v(x)$). We will deal only with nonnegative solutions of the function u.
Consider the following ordinary differential equations and try to solve each problem

separately:

$$\begin{cases} \dfrac{du}{dx} = \begin{cases} F(x), & if\ x \geq 0, \\ -F(x), & if\ x \leq 0, \end{cases} \\ u(-1) = u(1) = 0. \end{cases}$$

In order to do the numerical approximation, we partition the x-axis into a collection of grid points $x_i = i\Delta x$ and define $u_i = u(i\Delta x)$ and $F_i = F(i\Delta x)$, where Δx is the discretization step, and $i = -n, \cdots, n$. Using a Taylor expansion and neglecting the remainder we obtain the discrete system:

$$\begin{cases} u_n = 0, \\ \dfrac{u_{i+1} - u_i}{\Delta x} = F_i, \quad i > 0, \\ \dfrac{u_i - u_{i-1}}{\Delta x} = -F_i, \quad i \leq 0, \\ u_{-n} = 0. \end{cases}$$

Notice that

u_{n-1} can be computed exactly from u_n

u_{n-2} can be computed exactly from u_{n-1}

$\cdots$

u_1 can be computed exactly from u_2

u_0 can be computed exactly from u_1

$\cdots$

u_{-n+1} can be computed exactly from u_{-n}

u_{-n+2} can be computed exactly from u_{-n+1}

$\cdots$

u_{-1} can be computed exactly from u_{-2}

u_0 can be computed exactly from u_{-1}.

This is an upwind scheme: we compute derivatives using points "upwind" or toward the boundary condition (i.e., each ordinary differential equation is solved

away from the boundary condition).

Modeling numerically the Eikonal equation, we consider that the information is propagating like waves, with certain speeds, along the gradient directions. The **upwind** discretization methods compute the values of the variables using the direction(s) from which the information should be coming. More precisely, the discretization of the partial differential equations uses a finite differences stencil, biased on the direction determined by the sign of the gradient [16]. The upwind scheme uses backward differences scheme if the velocity is in the positive x direction, and forward differences scheme for negative velocities. Thus, in a one-dimensional domain, for any point i we have only two direction: left $(i-1)$ and right $(i+1)$. If the velocity is positive, the left side of the axis is called **upwind side** and the right side is called **downwind side**, and vice versa for negative velocities.

Let u_i^n be the computed solution at the point i at iteration n. We have the following schemes:

1. *Forward scheme*: $u_i^{n+1} = u_i^n - \Delta x D_i^{+x} u_i^n$,

2. *Backward scheme*: $u_i^{n+1} = u_i^n - \Delta x D_i^{-x} u_i^n$.

Similarly to the one dimensional case, using forward, backward or centered Taylor series expansions in x and y for the value u around the point (x, y), with $(x_i, y_j) = (i\Delta x, j\Delta y)$ and $u_{ij} = u(x_i, y_j)$ we can define four differentiation operators for the two-dimensional case:

$$\begin{aligned} D_{i,j}^{-x} u(x_i, y_j) &= \frac{u_{i,j} - u_{i-1,j}}{\Delta x} \qquad & D_{i,j}^{+x} u(x_i, y_j) &= \frac{u_{i+1,j} - u_{i,j}}{\Delta x} \\ D_{i,j}^{-y} u(x_i, y_j) &= \frac{u_{i,j} - u_{i,j-1}}{\Delta y} \qquad & D_{i,j}^{+y} u(x_i, y_j) &= \frac{u_{i,j+1} - u_{i,j}}{\Delta y} \end{aligned} \tag{1.20}$$

where

- D^{+x} computes the new value at (i, j) using information at i and $i + 1$; thus information for the solution propagates from right to left.

- D^{-x} computes the new value at (i, j) using information at i and $i - 1$; thus information for the solution propagates from left to right.

- D^{+y} computes the new value at (i, j) using information at j and $j + 1$; thus information for the solution propagates from top to bottom.

- D^{-y} computes the new value at (i, j) using information at j and $j - 1$; thus information for the solution propagates from bottom to top.

For two-dimensional domains, the upwind method uses the gradient direction in order to select which differentiation operator to use. In Figure 1.5 we illustrate only two possible situations, all the other cases being similar up to a rotation in the system of coordinates. In case 1.5(a) we use the backward differences scheme in x and y and define the third quadrant as the upwind side. In case 1.5(b) we use backward differences in x and forward differences in y and the upwind side is quadrant two.

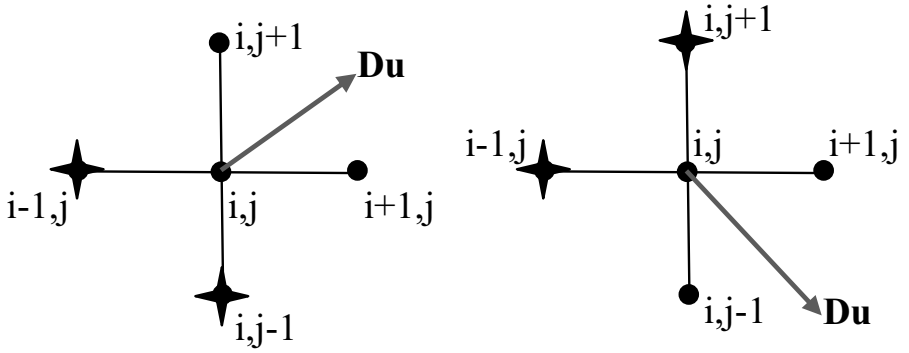

FIGURE 1.5. Upwind Discretization - 2D case

1.2.2 Approximations of the Eikonal Equation

Crandall and Lions [5] proved that consistent, monotone schemes converge to the correct viscosity solution. Starting from equation (1.1), in order to construct a numerical scheme which guarantees a correct *upwind* direction and a correct approximation of the *viscosity solution*, it is necessary to have a good approximation of the derivative. Extending the ideas of upwind approximations for the gradient to multiple dimensions, we have the following schemes:

- Godunov's scheme [16]

$$\begin{aligned} &[max\left(D_{ij}^{-x}T, -D_{ij}^{+x}T, 0\right)^2 \quad + \\ &max\left(D_{ij}^{-y}T, -D_{ij}^{+y}T, 0\right)^2]^{1/2} \quad = \quad \frac{1}{F_{ij}}, \end{aligned} \tag{1.21}$$

- Osher and Sethian's scheme [18]

$$\begin{aligned} &[max(D_{ij}^{-x}T, 0)^2 \quad + \quad min(D_{ij}^{+x}T, 0)^2 \quad + \\ &max(D_{ij}^{-y}T, 0)^2 \quad + \quad min(D_{ij}^{+y}T, 0)^2]^{1/2} \quad = \quad \frac{1}{F_{ij}}, \end{aligned}$$

  where the forward and backward operators D_{ij}^{-x}, D_{ij}^{+x} are those defined earlier in equation (1.20) for the x and y directions.

Remark 1.20. *Rewriting Godunov's scheme, we obtain the so called Rouy-Tourin's scheme [21]:*

$$\begin{aligned} &[max[max\left(D_{ij}^{-x}T, 0\right), -min\left(D_{ij}^{+x}T, 0\right)]^2 \quad + \\ &max[max\left(D_{ij}^{-y}T, 0\right), -min\left(D_{ij}^{+y}T, 0\right)]^2]^{1/2} \quad = \quad \frac{1}{F_{ij}}. \end{aligned} \tag{1.22}$$

Recall the boundary value problem $F|\nabla T| = 1$ can be written in the form of general Hamilton Jacobi equation:

$$H(x, y, D^x T, D^y T) = 0,$$

where the Hamiltonian is given by:

$$H(x, y, D^x T, D^y T) = F\sqrt{(D^x T)^2 + (D^y T)^2} - 1. \tag{1.23}$$

To solve numerically the Eikonal equation, we need a correct approximation of the *viscosity solution* [18, 22, 24]. A smart way to do this is to consider only numerical schemes which satisfy the upwind condition. These schemes ensure that, out of all possible T such that $F|\nabla T| = 1$ almost everywhere, only the correct "physical" solution from the family of solutions of (1.22) is picked. Since T solves equation (1.22), T cannot be locally convex. In Figure 1.6 we consider a stencil with $\Delta x = 1$ and $F(x) = 1$, $1 < i < n$ and show how it selects only concave solutions:

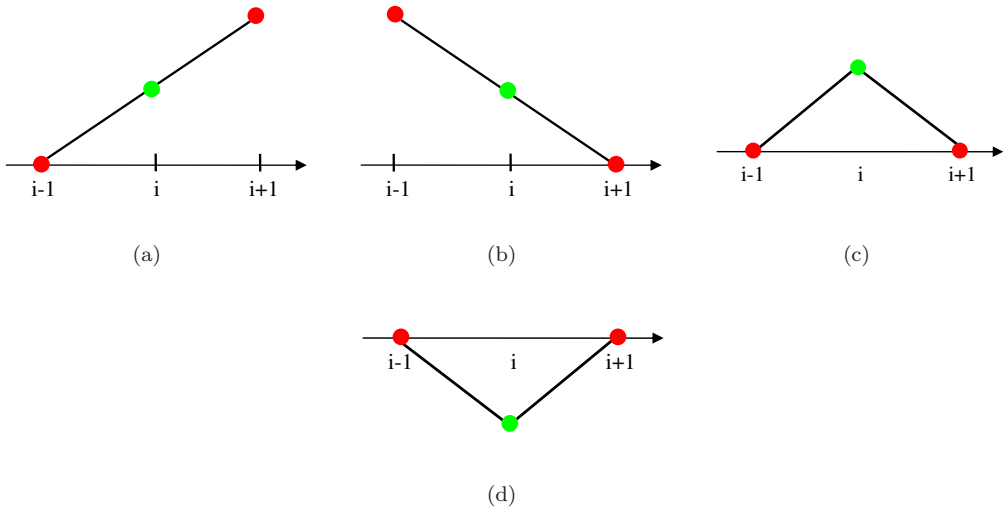

FIGURE 1.6. Discretization for the 1-D case

Case a : If $T_{i,j} = T_{i-1,j} + 1$ and $T_{i+1,j} = T_{i,j} + 1$, then $D^{-x}_{i,j} T = 1$ and $D^{+x}_{i,j} T = 1$.

Equation (1.22) becomes:

$\max\left[\max(D^{-x}_{i,j} T, 0), -\min(D^{+x}_{i,j} T, 0)\right]^2 = [\max(1, 0)]^2 = 1.$

Case b : If $T_{i-1,j} = T_{i,j} + 1$ and $T_{i,j} = T_{i+1,j} + 1$, then $D^{-x}_{i,j}T = -1$ and $D^{+x}_{i,j}T = -1$.

Equation (1.22) becomes:

$$\max\left[\max(D^{-x}_{i,j}T, 0), -\min(D^{+x}_{i,j}T, 0)\right]^2 = [\max(0,1)]^2 = 1.$$

Case c : If $T_{i,j} = T_{i-1,j} + 1$ and $T_{i,j} = T_{i+1,j} + 1$, then $D^{-x}_{i,j}T = 1$ and $D^{+x}_{i,j}T = -1$.

Equation (1.22) becomes:

$$\max\left[\max(D^{-x}_{i,j}T, 0), -\min(D^{+x}_{i,j}T, 0)\right]^2 = [\max(1,1)]^2 = 1.$$

Case d : If $T_{i-1,j} = T_{i,j} + 1$ and $T_{i+1,j} = T_{i,j} + 1$, then $D^{-x}_{i,j}T = -1$ and $D^{+x}_{i,j}T = 1$.

Equation (1.22) becomes:

$$\max\left[\max(D^{-x}_{i,j}T, 0), -\min(D^{+x}_{i,j}T, 0)\right]^2 = [\max(0,0)]^2 = 0.$$

Thus, this case is not feasible and it is clear that the scheme selects only the concave solution.

Remark 1.21. *At this point we need to choose which discretization scheme to use in the following steps of the numerical implementation. We settled for Rouy-Tourin discretization scheme (1.22), since it is the easiest one to implement.*

1.2.3 Numerical Methods

There have been lots of trials to solve the Eikonal equation directly: starting from upwinding schemes [26], Jacobi-iterations [21], semi-Lagrangian schemes [11], fast marching type methods [18, 24], fast sweeping methods [28] and many others methods. In the following subsections we briefly present the Rouy-Tourin and Fast Sweeping algorithms.

1.2.3.1 Rouy-Tourin Algorithm

An iterative algorithm for computing the solution of Eikonal equation was introduced by Rouy and Tourin in [21]. The idea of this algorithm is to solve the quadratic equation (1.22) at each point of the grid, and iterate until convergence.

In Figure 1.7 we present the stencil structure for Rouy-Tourin algorithm and the algorithm is presented in Algorithm 1.

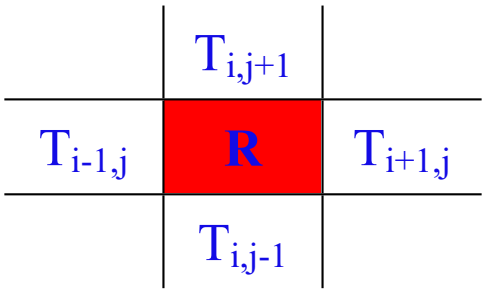

FIGURE 1.7. Grid points for Rouy-Tourin algorithm

Algorithm 1 The Rouy-Tourin algorithm

Consider $S > diam(\Omega)$.
Initialization:
$T_{i,j} = 0$ on $\partial\Omega$
$T_{i,j} = S$, otherwise
Iteration:
repeat
  for $i = 0$ **to** n **do**
    for $j = 0$ **to** n **do**
      compute R solution of local Eikonal equation at $X_{i,j}$
    end
  end
  $\tilde{T_{i,j}} = \min(T_{i,j}, R)$
  $T = \tilde{T}$
until $\|T - \tilde{T}\| \leq \varepsilon$;

For any node (i, j) in the domain we should solve the equation:

$$\begin{aligned} [\max\left[\max(D_{i,j}^{-x}T, 0), -\min(D_{i,j}^{+x}T, 0)\right]^2 \quad &+ \\ \max\left[\max(D_{i,j}^{-y}T, 0), -\min(D_{i,j}^{+y}T, 0)\right]^2]^{1/2} \quad &= \quad \frac{1}{F_{i,j}}, \end{aligned} \tag{1.24}$$

in order to compute its $T_{i,j}$.

Let us consider the case presented in the previous section, in Figure 1.5(a), where the third quadrant is the upwind side of our domain and show how the Rouy-Tourin algorithm satisfies the upwind-ing. All the other possible situations can be reduced

to this case, based on rotation and symmetry of the domain. By evaluating:

$$\begin{aligned} D_{i,j}^{-x}T_{i,j} &= \frac{T_{i,j}-T_{i-1,j}}{\Delta x} \geq 0 \quad & D_{i,j}^{+x}T_{i,j} &= \frac{T_{i+1,j}-T_{i,j}}{\Delta x} \geq 0 \\ D_{i,j}^{-y}T_{i,j} &= \frac{T_{i,j}-T_{i,j-1}}{\Delta y} \geq 0 \quad & D_{i,j}^{+y}T_{i,j} &= \frac{T_{i,j+1}-T_{i,j}}{\Delta y} \geq 0, \end{aligned}$$

and plugging them in equation (1.24), we obtain:

$$\sqrt{\max\left(D_{i,j}^{-x}T,0\right)^2+\max\left(D_{i,j}^{-y}T,0\right)^2} = \sqrt{D_{i,j}^{-x}T^2+D_{i,j}^{-y}T^2} = \frac{1}{F_{i,j}},$$

which is the quadratic equation that we need to solve:

$$\sqrt{\left(\frac{T_{i,j}-T_{i-1,j}}{\Delta x}\right)^2+\left(\frac{T_{i,j}-T_{i,j-1}}{\Delta y}\right)^2} = \frac{1}{F_{i,j}}.$$

During the algorithm execution, this computation is done many times for each node in the domain, until convergence is achieved. Basically, the value at the grid point $T_{i,j}$ can be computed exactly using only T at its neighbors, i.e. $T_{i\pm1,j}$ and $T_{i,j\pm1}$. We consider T to be computed exactly, if and only if the new T is smaller than the old one.

Remark 1.22. *Since during the algorithm execution, at each iteration, we recompute T at every point of the domain, we have a lot of useless computations (T is changing only at a few grid points). The algorithm is not taking this shortcut into consideration.*

To illustrate the Rouy-Tourin algorithm, we consider a rectangular domain, with the boundary condition imposed in two opposite corners. In the initialization step, if $X_{i,j} \in \Gamma$ (a point where we can approximate the initial curve), then $T(X_{i,j}) = 0$, otherwise $T(X_{i,j}) = \infty$. For exemplification purposes, Figure 1.8 shows the stages of the algorithm for a particular case. At each iteration of the algorithm, we solve the local Eikonal equation at all the points of the domain. Note how T changes

only at a few grid points. In Figure 1.8, these points are shown in green, while the points with exactly computed T are represented by red cells, and the points where

Iteration 0

0	∞	∞	∞	∞	∞
∞	∞	∞	∞	∞	∞
∞	∞	∞	∞	∞	∞
∞	∞	∞	∞	∞	∞
∞	∞	∞	∞	∞	∞
∞	∞	∞	∞	∞	0

Iteration 1

0	1	∞	∞	∞	∞
1	∞	∞	∞	∞	∞
∞	∞	∞	∞	∞	∞
∞	∞	∞	∞	∞	∞
∞	∞	∞	∞	∞	1
∞	∞	∞	∞	1	0

Iteration 2

0	1	2	∞	∞	∞
1	1.71	∞	∞	∞	∞
2	∞	∞	∞	∞	∞
∞	∞	∞	∞	∞	2
∞	∞	∞	∞	1.71	1
∞	∞	∞	2	1	0

Iteration 3

0	1	2	3	∞	∞
1	1.71	2.55	∞	∞	∞
2	2.55	∞	∞	∞	3
3	∞	∞	∞	2.55	2
∞	∞	∞	2.55	1.71	1
∞	∞	3	2	1	0

Iteration 4

0	1	2	3	4	∞
1	1.71	2.55	3.44	∞	4
2	2.55	3.25	∞	3.44	3
3	3.44	∞	3.25	2.55	2
4	∞	3.44	2.55	1.71	1
∞	4	3	2	1	0

Iteration 5

0	1	2	3	4	5
1	1.71	2.55	3.44	4.36	4
2	2.55	3.25	4.04	3.44	3
3	3.44	4.04	3.25	2.55	2
4	4.36	3.44	2.55	1.71	1
5	4	3	2	1	0

Iteration 6

0	1	2	3	4	5
1	1.71	2.55	3.44	4.36	4
2	2.55	3.25	4.04	3.44	3
3	3.44	4.04	3.25	2.55	2
4	4.36	3.44	2.55	1.71	1
5	4	3	2	1	0

FIGURE 1.8. Rouy-Tourin Iterations

$T = \infty$ are the white cells. At each iteration, the area of the nodes where T is computed exactly, starting from the corners, extends until convergence.

1.2.3.2 Fast Sweeping Method

The Fast Sweeping Method is an efficient iterative method which uses upwind difference for discretization to solve the Eikonal equation [28]. The idea behind Fast Sweeping is to "sweep" through the grid in certain directions, computing the distance value for each grid point. The sweeping ordering follows a family of characteristics of the corresponding Eikonal equation in a certain direction simultaneously. For example, in a two-dimensional domain, T at a grid point depends on its neighbors in the following four ways:

- left and bottom neighbors,
- left and top neighbors,
- right and bottom neighbors,
- right and top neighbors.

Thus, for any point $X_{i,j}$ in a domain, we compute the solution as being the minimum between the local discrete Eikonal equations solutions based on its neighbors $X_{i\pm1,j}$, $X_{i,j\pm1}$. Repeatedly, we sweep the whole domain along the diagonal and anti-diagonal from top to bottom and from bottom to top. This sweeping idea is illustrated by solving the Eikonal equation in (-1,1):

$$\left|\frac{dT}{dx}\right| = 1, \quad T(-1) = T(1) = 0. \tag{1.25}$$

From this point on, by a "sweep" we mean a computation in a certain direction and by an "iteration" we mean a completed set of sweeps, i.e. four-direction sweeps

in 2D problems.

Let $T_i = T(x_i)$ denote the values for the grid points $-1 = x_0 < x_1 < \ldots < x_n = 1$. We solve (1.25) in different directions, using the discretized nonlinear system, based on Godunov scheme (1.21):

$$max\left(D_{ij}^{-x}T, -D_{ij}^{+x}T, 0\right) = 1, \quad T_0 = T_n = 0. \tag{1.26}$$

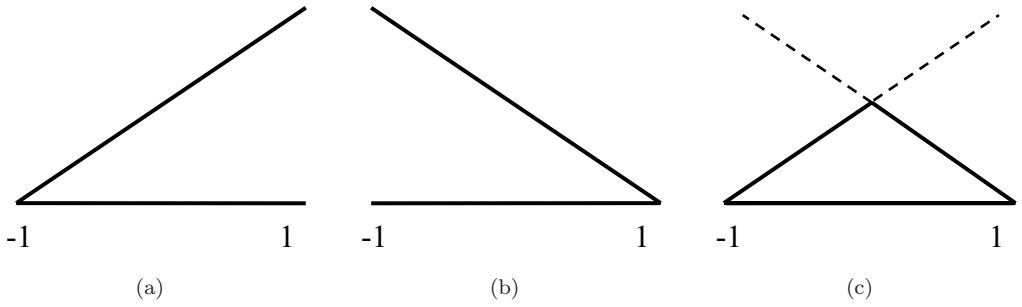

FIGURE 1.9. Sweeping in 2 directions

First, we have a sweep from left to right, enforcing the boundary condition at $x = 0$. This is equivalent to following the directions emanating from x_0 as shown in Figure 1.9(a). We obtain the solution $T_i = x_i$.

Secondly, we sweep from right to left, which means following the directions emanating from x_n, as shown in Figure 1.9(b). We obtain the solution $T_i = 1 - x_i$.

Since in 1-D there are only two directions of sweeping, i.e. left to right and right to left, two sweeps are enough to compute the solution correctly. Thus, T at a grid point X_i can be computed exactly from either its left or right neighbor, $T(X_i) = \min(T_{i-1}, T_{i+1}) + h$. Using the Godunov discretization scheme (1.26), we obtain the continuous viscosity solution drawn in Figure 1.9(c):

$$T_i = \begin{cases} x_i, & -1 \le x_i < 0 \\ 1 - x_i, & 0 \le x_i \le 1. \end{cases}$$

Notice that, for $i \leq \frac{n}{2}$, T_i is correctly computed based on its left neighbors during the first sweep, while for $i \geq \frac{n}{2}$, T_i is correctly computed based on its right neighbors during the second sweep. The Fast Sweeping algorithm is illustrated in Algorithm 2.

Remark 1.23. *The first sweep satisfies the upwind-ing condition for* $0 \leq i \leq \frac{n}{2}$ *and the second sweep for* $\frac{n}{2} < i < n$.

The most important point in the algorithm is that the upwind difference scheme used in the discretization enforces that "the solution at a grid point be determined by its neighboring values that are smaller" [28].

Algorithm 2 Fast Sweeping Algorithm

Consider $S > diam(\Omega)$;
Initialization:
$T_i = 0$ on Γ;
$T_i = S$, otherwise;
Iteration:
for $i = 1$ **to** $n/2$ **do**
  Compute R_i solution of local Eikonal equation ;
end
for $i = n - 1$ **to** $n/2$ **do**
  Compute P_i solution of local Eikonal equation ;
end
$\tilde{T}_i = \min(P_i, R_i)$;
$T = \tilde{T}$;

Chapter 2
Sequential Fast Marching Methods

2.1 General Idea

The Fast Marching Method is very closely related to Dijkstra's algorithm, a well-known algorithm from the 1950's for computing the shortest path on a network. Dijkstra's algorithm is widespread, from Internet routing applications to navigation system applications. To explain the connection, consider a network with a cost assigned to each node as in Figure 2.1:

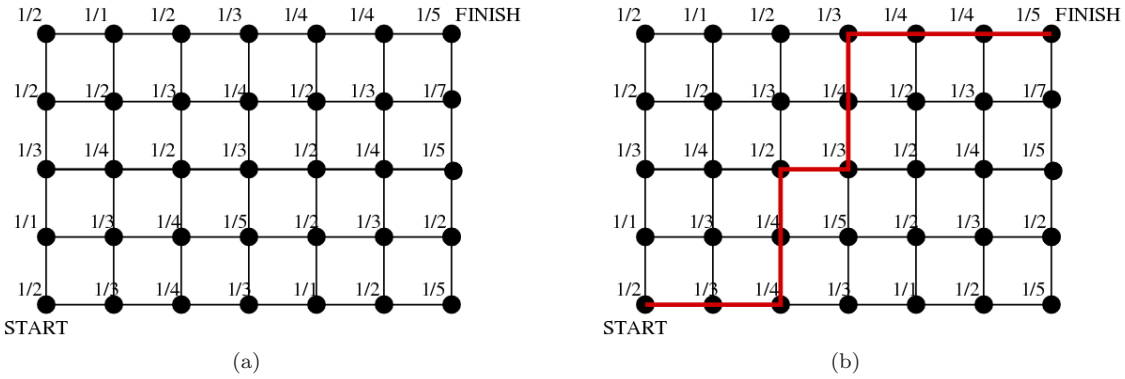

FIGURE 2.1. Dijkstra algorithm for finding the shortest path from Start to Finish

The basic idea of Dijkstra's method [7] is as follows:

1. Put the starting point in a set called "Accepted".

2. Call the grid points which are one link away from the Start "Neighbors".

3. Compute the cost of reaching each of these "Neighbors".

4. The smallest cost of these Neighbors must be the correct cost. Remove it from "Neighbors", call it "Accepted" and return to step 2, until all points are labeled "Accepted".

The algorithm orders the way in which the points are accepted, from the known costs (the starting point) all the way to the finish. The method is a one-pass method, each point being touched essentially only once. Note that it is not guaranteed that the method converges to the optimal solution.

The Fast Marching Methods use upwind difference operators to approximate the gradient, but retains the Dijkstra idea of a one-pass algorithm.

Tsitsiklis was the first to develop a Dijkstra-like method for solving the Eikonal equation. Addressing a trajectory optimization problem, he presented a first-order accurate *Dijkstra-like algorithm* in [27]. Later Sethian and Osher [18, 22, 23, 24] developed the idea and produced the Fast Marching Methods.

For solving equation (1.1), assume that $n = 2$ and $F(x) > 0$. All the results obtained in this case can be generalized to the 3-dimensional case.

The central idea behind the Fast Marching Methods is to systematically construct the solution of (1.1) outward from the smallest values of T to its largest ones, stepping away from the boundary condition in a downwind direction. The algorithm is initialized by tagging the points of the domain as:

- *far away* nodes: $T_{i,j} = +\infty$ - T has never been calculated,
- *accepted* nodes: $T_{i,j} = 0$ is given,
- *narrow band* nodes: these are the neighbors of the *accepted* points.

As it can be seen in Figure 2.2, the yellow-orange region, representing the *narrow band* points, separates the *accepted* nodes from the *far away* nodes. The algorithm is *mimicking* the front evolution step by step:

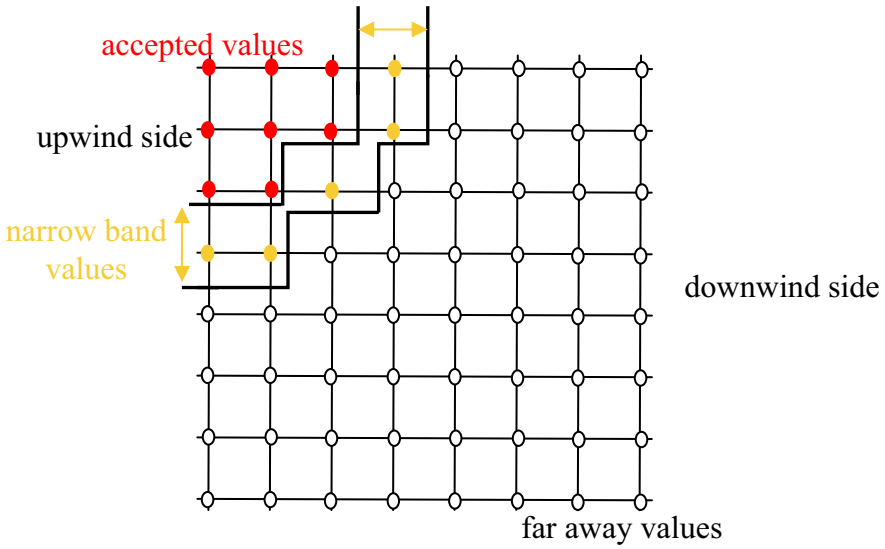

FIGURE 2.2. Far away, narrow band and accepted nodes

- sweep the front ahead by considering the narrow band points,
- march this narrow band forward, freezing the values of existing points and bringing new points into the narrow band.

The key is in selecting *which* grid point in the narrow band to update. The algorithm will stop when all the nodes become *accepted*.

2.2 Fast Marching Algorithm Description

Let Ω be the rectangular domain $(0,1)\times(0,1)$ of $\mathbb{R}^2$. Given the discretization steps $\Delta x = \frac{1}{N}, \Delta y = \frac{1}{M} > 0$, we denote by T_{ij} the value of our numerical approximation of the solution at $(x_i, y_j) = (i\Delta x, j\Delta y), i = 0,\ldots,N, j = 0,\ldots,M$. Similarly, $F_{i,j}$ represents the value of F at node (x_i, y_j).

We define the neighbors of a grid point (x_i, y_j):

Definition 2.1. *The set of neighboring nodes of a grid point $X = (x_i, y_j)$ is:*

$$V(X) = \{(x_{i+1}, y_j), (x_{i-1}, y_j), (x_i, y_{j+1}), (x_i, y_{j-1})\},$$

for $1 \leq i \leq N-1$ *and* $1 \leq j \leq M-1$.

Remark 2.2. *The definition of* $V(X)$ *has to be adapted for* $i = 0$ *or* $j = 0$ *and* $i = N$ *or* $j = M$*, by eliminating the appropriate points.*

These are the nodes appearing in the stencil of the finite difference discretization.

The Fast Marching algorithm is presented in Algorithm 3.

Algorithm 3 Fast Marching algorithm

Initialization:
Set $T = 0$ for *accepted* nodes.
Tag all neighbors of *accepted* nodes, that are not *accepted* as *narrow band*.
Compute T for all *narrow band* nodes.
Set $T = +\infty$ for the rest of the nodes.
Main Cycle:
repeat
  Let A be the smallest T from all *narrow band* nodes
  Add node A to *accepted*
  Remove A from *narrow band*
  Tag as *narrow band* all neighbors of A that are not *accepted*
  for *all* $y \in V(A)$ **do**
    if *y is in far away* **then**
      Remove neighbor from *far away*
      Add it to *narrow band* set.
    end
    if *y is in narrow band* **then**
      Update $T_{i,j}$ by solving the local Eikonal equation (1.22) at $X_{i,j}$.
    end
  end
until *all nodes are accepted* ;

In Figure 2.3, the Fast Marching algorithm is graphically illustrated. In order to have a better understanding of the algorithm, we consider the case of an isolated *accepted* node in the domain and we replace the network grid representation with the table format. The algorithm steps are:

- start from the *accepted* node X, shown as a red cell in Figure 2.3(a)

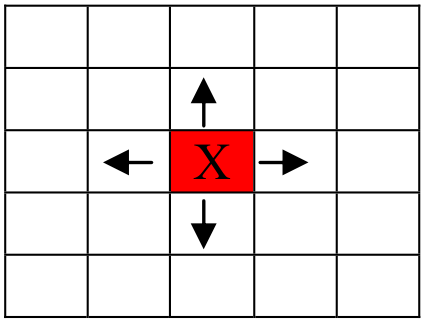

(a) Start with an accepted point

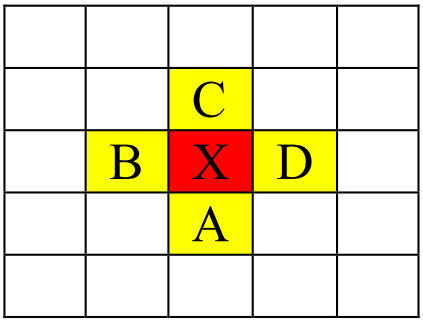

(b) Update neighbors values

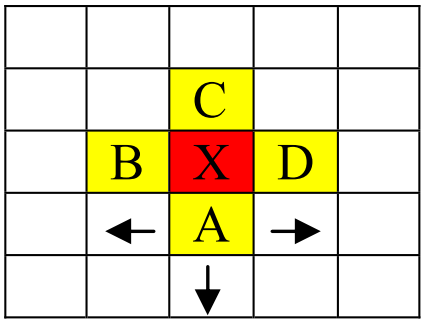

(c) Choose the smallest value (i.e. A)

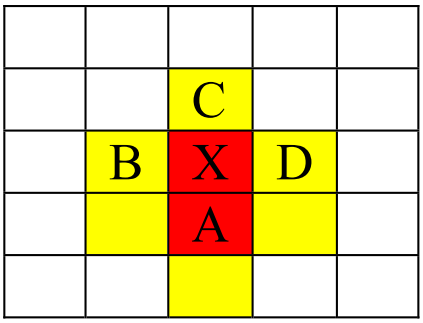

(d) Freeze value of A, update its neighbors

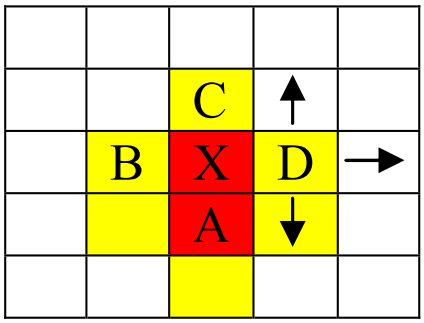

(e) Choose the smallest value (i.e. D)

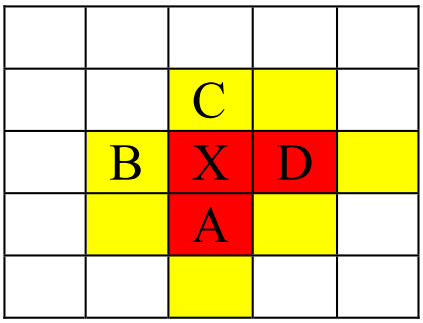

(f) Freeze value of D, update its neighbors

FIGURE 2.3. Update procedure for Fast Marching Method

- march "downwind" from X, solve the local Eikonal equation (1.22) at all neighbors $Y \in V(X)$. $T(Y)$ for all $Y \in V(X)$, represented by yellow-orange cells in Figure 2.3(b), are *narrow band* points.

- consider the neighbor A of X with the smallest T and tag it as *accepted* (see Figure 2.3(c) and 2.3(d)). Due to the upwinding property of the difference operator used in equation (1.22), $T(A)$ is now correct (up to the discretization error).

- tag the neighbors of A as *narrow band* points (yellow-orange cells in Figure 2.3(d)).

- choose the *narrow band* point with the smallest T, i.e. D (see Figure 2.3(e) and 2.3(f))

- repeat the algorithm until all the nodes become *accepted*.

Remark 2.3. *$T_{i,j}$ is determined only by those neighboring nodes of smaller T.*

2.3 Convergence

Theorem 2.4. *As the mesh size goes to zero, i.e. $\Delta x \to 0$ and $\Delta y \to 0$, the numerical solution built by the Fast Marching Methods converges to the viscosity solution of (1.1).*

Proof. The proof is performed in two steps, through the following lemmas.

Lemma 2.5. *The solution of the discrete Eikonal equation converges toward the viscosity solution, as the mesh sizes go to zero [3].*

Lemma 2.6. *The sequence built by Fast Marching Methods converges to the solution of discrete Eikonal equation.*

□

2.3.1 Proof of Lemma 2.5

The proof is borrowed from Barles and Souganidis [3].

Consider an approximation scheme of the form:

$$S(\rho, x, u^\rho) = 0 \ \ in \ \ \bar{\Omega}, \tag{2.1}$$

where $S : \mathbb{R}^+ \times \bar{\Omega} \times L^\infty(\bar{\Omega}) \to \mathbb{R}$ is locally bounded, $L^\infty(\bar{\Omega})$ is the space of bounded functions defined on $\bar{\Omega}$ and u^ρ is the solution of (2.1).

Let u be the viscosity solution of the Hamilton Jacobi equation: $H(x, Du) = 0$ on Ω and $u = \phi$ on $\partial\Omega$.

If this scheme is monotone, stable and consistent with the Hamilton-Jacobi equations, it converges to the solution of (1.1). For this, we need to recall some results from [3].

Definition 2.7 (Monotonicity)**.** *The scheme S is monotone if and only if it satisfies:*

$$S(\rho, x, u) \leq S(\rho, x, v), \ \textit{if}\, u \geq v, \ \forall\ \rho \geq 0, \ x \in \bar{\Omega} \ \textit{and}\, u, v \in L^\infty(\bar{\Omega}) \tag{2.2}$$

The purpose of the scheme S is to approximate the Hamilton-Jacobi equations and thus the monotonicity condition for S is equivalent to the ellipticity condition for H for the Hamilton-Jacobi equation $H(x, \nabla u) = 0$ in $\bar{\Omega}$. That is, for all M, N, if for all $x \in \bar{\Omega}$, $H(x, M) \leq H(x, N)$, then $M \geq N$. This property assures some maximum principle type property for the scheme.

Definition 2.8 (Stability)**.** *The scheme S is stable if and only if:*

$$\forall\ \rho > 0, \ \exists\ \textit{a uniformly bounded solution}\, u^\rho \in L^\infty(\bar{\Omega})\, \textit{such that}\, (2.1)\, \textit{holds.} \tag{2.3}$$

The bound is independent of ρ.

The scheme is stable in the sense that for all points of space discretization, the solution exists and has a (lower and upper) bound. Moreover, it is independent of discretization step (the information propagates from the smaller value of T to larger values).

Definition 2.9 (Consistency)**.** *The scheme S, defined in (2.1), is consistent, i.e.* $\forall\, x \in \bar{\Omega}$ *and* $\phi \in C^{\infty}(\bar{\Omega})$

$$\limsup_{\substack{\rho\to 0\\ y\to x\\ \xi\to 0}} \frac{S(\rho, y, \phi+\xi)}{\rho} \leq \limsup_{y\to x} H(x, D^2\phi(x)) \tag{2.4}$$

and

$$\liminf_{\substack{\rho\to 0\\ y\to x\\ \xi\to 0}} \frac{S(\rho, y, \phi+\xi)}{\rho} \geq \liminf_{y\to x} H(x, D^2\phi(x)) \tag{2.5}$$

Definition 2.10 (Strong Uniqueness)**.** *Consider the solution $u \in L^{\infty}(\bar{\Omega})$ of the Hamilton-Jacobi equation:*

$$H(x, \nabla u) = 0 \ \ in \ \ \bar{\Omega} \tag{2.6}$$

If for any $x \in \Omega$, one has that $u(x) = \limsup_{y\to x} u(y)$, then u is the upper semi-continuous envelope of the solution of equation (2.6). Similarly, $v(x) = \liminf_{y\to x} v(y)$ is the lower-semi-continuous envelope of the solution of equation (2.6)

Lemma 2.11 (Strong Uniqueness Property)**.** *In the setting of the previous definition, if u and v are the upper-semi-continuous envelope, and the lower-semi-continuous envelope of the solution of (2.6), respectively, then*

$$u \leq v \ \ on \ \ \bar{\Omega}. \tag{2.7}$$

The following theorem is the Barles and Souganidis convergence result published in [3] pg. 275-276.

Theorem 2.12. *Assume that (2.2), (2.3), (2.4), (2.5) and the hypothesis of Lemma (2.11) hold. Then, as $\rho \to 0$, the solution u^ρ of (2.1) converges locally uniformly to the unique continuous viscosity solution u of (2.6).*

Proof. The proof follows the steps and arguments presented in [3], pg. 275-276, [2], pg. 576-577 and [5].

Consider u^ρ satisfying (2.1) and let $\bar{u}, \underline{u} \in L^\infty(\bar{\Omega})$ be defined as:

$$\begin{aligned} \bar{u} &= \limsup_{\substack{y \to x \\ \rho \to 0}} u^\rho(y) \\ \underline{u} &= \liminf_{\substack{y \to x \\ \rho \to 0}} u^\rho(y) \quad . \end{aligned} \tag{2.8}$$

Assume that $\bar{u}$, $\underline{u}$ are sub and super viscosity solutions of (2.6). Then, based on their definitions, $\bar{u} \geq \underline{u}$. Since $\bar{u}$ is the upper-semi-continuous (usc) and $\underline{u}$ is the lower-semi-continuous (lsc) envelope of solution of (2.1), Lemma (2.11) implies that $\bar{u} \leq \underline{u}$. Hence, we can write that $\bar{u} = \underline{u} \equiv u$.

Since the upper semi-continuous solution $\bar{u}$ and lower semi-continuous solution $\underline{u}$ are equal, Lemma (2.11) assures that u is the unique continuous solution of Hamilton-Jacobi equation (2.6). Using (2.8), one gets that u^ρ converges locally uniformly to u.

Now let us prove that $\bar{u}$, $\underline{u}$ are the viscosity sub-solution and super-solution of (2.6). We only present the case of $\bar{u}$ being the sub-solution of (2.6).

Let x_0 be a local maximum of $\bar{u} - \phi$ on $\bar{\Omega}$, for some $\phi \in C^\infty(\bar{\Omega})$. We assume that x_0 is the *unique* maximum point of $\bar{u} - \phi$ in $B(x_0, r)$, for some $r > 0$, such that $\bar{u}(x_0) = \phi(x_0)$ inside the ball $B(x_0, r)$ and $\phi \geq 2 \sup_\rho \|u^\rho\|_\infty$ outside the ball $B(x_0, r)$. In some neighborhood of x_0, with $x \neq x_0$, we have:

$$\bar{u}(x) - \phi(x) \leq 0 = \bar{u}(x_0) - \phi(x_0) \ \text{ in } \ B(x_0, r), \text{ for some } r > 0.$$

By Lemma A.3, pg. 577 of Barles and Perthame in [2], there exist sequences $y_n \in \bar{\Omega}$ and $\rho_n \in \mathbb{R}^+$ such that for $n \to \infty$

$$\begin{aligned} &y_n \to x_0, \quad \rho_n \to 0, \quad u^{\rho_n}(y_n) \to \bar{u}(x_0) \ \text{ and} \\ &y_n \ \text{ is a global maximum point of } \ u^{\rho_n}(.) - \phi(.). \end{aligned} \tag{2.9}$$

Hence for $y_n \to x_0$ and all $x \in B(x_0, r)$ we have

$$u^{\rho_n}(y_n) - \phi(y_n) \leq 0 = u^{\rho_n}(x_0) - \phi(x_0). \tag{2.10}$$

In [5], Crandall and Lions remarked that by replacing $\phi(y_n)$ with $\phi(y_n) + \xi_n$, where $\xi_n \to 0$, there exists a sequence still denoted y_n of local maximum points of $u^{\rho_n} - \phi$ converging to x_0. Thus, relation (2.10) becomes:

$$u^{\rho_n}(y_n) \leq \phi(y_n) + \xi_n, \text{ for all } x \in \bar{\Omega}.$$

Applying the monotonicity property (2.2) of scheme S to $u^{\rho_n}(y_n) \leq \phi(y_n) + \xi_n$ one gets:

$$S(\rho_n, y_n, \phi + \xi_n) \leq S(\rho_n, x, u^{\rho_n}).$$

By definition of the u^{ρ_n}, $S(\rho_n, x, u^{\rho_n}) = 0$, and so:

$$S(\rho_n, y_n, \phi + \xi_n) \leq 0. \tag{2.11}$$

Taking the limit of (2.11) and using the consistency property (2.5) of S, one gets:

$$\begin{aligned} 0 \ &\geq \ \liminf_n \frac{S(\rho_n, y_n, \phi + \xi_n)}{\rho_n} \\ &\geq \ \liminf_{\substack{y \to x_0 \\ \rho \to 0 \\ \xi \to 0}} \frac{S(\rho, y, \phi + \xi)}{\rho} \\ &\geq \ \liminf_{y \to x_0} H(x_0, D^2(\phi(x_0))). \end{aligned}$$

Since $\bar{u}(x_0) = \phi(x_0)$, $\liminf_{y \to x_0} H(x_0, D^2(\phi(x_0))) \leq 0$ and $\bar{u}$ is the sub-solution of (2.6). $\square$

Now, we have all the tools to prove Lemma 2.5 for our numerical scheme.

In our case, the numerical approximation scheme will satisfy:

$$\begin{cases} g_{ij}(D^{-x}T_{i,j}, D^{+x}T_{i,j}, D^{-y}T_{i,j}, D^{+y}T_{i,j}) = 0, & x \in \Omega \\ T(x) = 0, & x \in \Gamma, \end{cases} \tag{2.12}$$

where $g_{ij}(D^{-x}T_{i,j}, D^{+x}T_{i,j}, D^{-y}T_{i,j}, D^{+y}T_{i,j})$ is computed as

$$\sqrt{\max(D^{-x}T_{i,j}, D^{+x}T_{i,j})^2 + \max(D^{-y}T_{i,j}, D^{+y}T_{i,j})^2} - \frac{1}{F_{i,j}}.$$

The discretization ρ represents a pair $(\Delta x,\ \Delta y)$ of space discretization steps, $u^\rho = T_{i,j}$ is a function defined on $\Delta_\rho = \{(x_i, y_i), i = 0, \ldots, N,\ j = 0, \ldots, M\} \cap \bar{\Omega}$ and for all $x \in \bar{\Omega}$, we define $\underline{u}$ and $\bar{u}$ as:

$$\underline{u} = \liminf_{\substack{\eta \to 0 \\ 0<\rho<\eta}} \inf_{y \in B(x,\eta) \cap \Delta_\rho} u^\rho(y)$$

and

$$\bar{u} = \limsup_{\substack{\eta \to 0 \\ 0<\rho<\eta}} \sup_{y \in B(x,\eta) \cap \Delta_\rho} u^\rho(y).$$

Our scheme is *monotone*, i.e. if $U \geq V$, then for all i, j we have

$$g_{ij}(D^{-x}U_{i,j}, D^{+x}U_{i,j}, D^{-y}U_{i,j}, D^{+y}U_{i,j}) \leq g_{ij}(D^{-x}V_{i,j}, D^{+x}V_{i,j}, D^{-y}V_{i,j}, D^{+y}V_{i,j}).$$

The scheme is *stable* since u^ρ has its minima in $\partial\Omega$ and is bounded below by a constant independent of ρ, which is the minimum value on $\partial\Omega$.

The scheme is *consistent* with the Hamilton-Jacobi equation (2.6) as, for each i, j,

$$g_{ij}(a, a, b, b) = \sqrt{a^2 + b^2} - \frac{1}{F_{ij}}, \text{ for all } a, b \in \mathbb{R}.$$

We can also prove, as in [3], that $\bar{u}$ and $\underline{u}$ are the sub-solution and the super-solution of equation (2.6) respectively and that $\underline{u} \leq \bar{u}$ on $\partial\Omega$.

Since our approximation scheme satisfies all the assumptions made in the hypothesis of Theorem 2.12, we can apply Theorem 2.12 to prove that the solution of the discrete Eikonal equation converges toward the viscosity solution, as the mesh sizes go to zero.

2.3.2 Proof of Lemma 2.6

To prove convergence Lemma 2.6 we need to demonstrate that the field computed by the Fast Marching Methods solves the discrete Eikonal equation.

Since T is built by marching forward from the smallest value to largest, we need to show that whenever a *narrow band* node $X_{i,j}$ is converted into an *accepted* one, none of its neighbors has a T less than $T(X_{i,j})$. Thus, the solution of the local Eikonal equation at node $X_{i,j}$ can be considered as exact and there is no need to go back and readjust previously set values. This way, the *upwind* nature of the algorithm will be satisfied.

Consider a two dimensional grid like in Figure 2.4. For simplicity, we assume that in our domain $N = M$ and $\Delta x = \Delta y$.

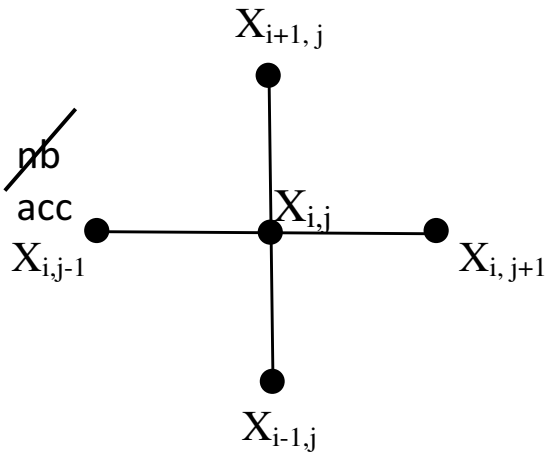

FIGURE 2.4. Matrix of neighboring nodes of $X_{i,j}$

Theorem 2.13. *Assume that the nodes in the domain Ω are partitioned into accepted, narrow band and far away nodes. By construction, we have that for any two nodes Y and Z, if Y has become accepted before Z, then $T(Y) \leq T(Z)$.*

Assume that $X_{i,j-1}$ is the narrow band point with the smallest T. The algorithm will label $X_{i,j-1}$ as accepted and start to compute the neighboring nodes that are

not accepted.

Furthermore, assume that:

- $F \in Lip(\mathbb{R}^n) \cap L^\infty(\mathbb{R}^n)$*, with Lipschitz constant* L_f*.*
- $F(x) > 0$*, for* $x \in \Omega$ *and* $F_{min} = \min_{\Omega} F(x) > 0$*,*
- *the Courant Friedrichs Lewy-like (CFL) condition holds true [6]:*

$$\Delta x \leq (\sqrt{2} - 1)\frac{F_{min}}{L_f}. \tag{2.13}$$

Then we have the upwind condition satisfied:

$$T_{i,j-1} \leq T_{i,j} \leq T_{i,j-1} + \frac{\Delta x}{F_{i,j}}. \tag{2.14}$$

Remark 2.14. *The above theorem shows that the value of the smallest node in the narrow band can be computed exactly at the next iteration. An approximate value is considered to be exact, within the consistency error of the scheme, if at the next iterations of the algorithm we cannot obtain a lower value [6].*

Remark 2.15. *We can make the assumptions that* $T_{i+1,j} \leq T_{i-1,j}$ *and* $T_{i,j-1} \leq T_{i,j+1}$*, without loss of generality, up to two mirror symmetries of the domain.*

Proof. (Theorem 2.13) To compute T at $X_{i,j}$ we distinguish the following cases [22, 23, 6]:

Case 1: one of the $X_{i,j}$ neighbors is accepted,

Case 2: two of the $X_{i,j}$ neighbors are accepted,

Case 3: three of the $X_{i,j}$ neighbors are accepted.

Case 4: all the $X_{i,j}$ neighbors are accepted.

Case 1:

Suppose that only one of $X_{i,j}$'s neighbors is accepted. Up to a rotation, we can assume without loss of generality that this node is $X_{i,j-1}$. All the other possible situations will be treated in a similar way. This case is graphically illustrated in Figure 2.5.

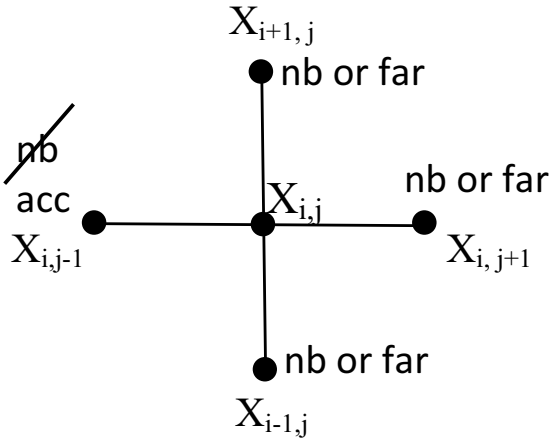

FIGURE 2.5. Node $X_{i,j}$ has only one accepted neighbor

Note also that $T_{i,j} < T_{i-1,j}$, $T_{i,j} < T_{i,j+1}$ and $T_{i,j} < T_{i+1,j}$, since these three neighbors are either *far away* or *narrow band* nodes and $X_{i,j}$ is the *narrow band* node with smallest T. Therefore we have that:

$$D^{-x}T_{i,j} \geq 0, \quad D^{+x}T_{i,j} \geq 0,$$
$$D^{-y}T_{i,j} \leq 0, \quad D^{+y}T_{i,j} \geq 0.$$

and equation (1.22) becomes:

$$\left(\max(D^{-x}T_{i,j}, 0)\right)^2 + \left(\max(0,0)\right)^2 = \frac{1}{F_{i,j}^2}$$
$$\left(D^{-x}T_{i,j}\right)^2 = \frac{1}{F_{i,j}^2}.$$

Using the definition (1.20) of the finite difference operator $D^{-x}T_{i,j}$, we obtain:

$$\left(\frac{T_{i,j} - T_{i,j-1}}{\Delta x}\right)^2 = \frac{1}{F_{i,j}^2}, \tag{2.15}$$

and

$$T_{i,j} = T_{i,j-1} \pm \frac{\Delta x}{F_{i,j}}.$$

Since we assumed that $X_{i,j-1}$ is the only accepted neighbor of $X_{i,j}$, we have that $T_{i,j} > T_{i,j-1}$. Therefore: $T_{i,j} = T_{i,j-1} + \frac{\Delta x}{F_{i,j}}$.
In the case of only one accepted node, we proved that $T_{i,j-1} \leq T_{i,j} = T_{i,j-1} + \frac{\Delta x}{F_{i,j}}$.

Case 2:

Suppose that two neighbors of $X_{i,j}$ are accepted. From hypothesis we know that node $X_{i,j-1}$ is one of the accepted neighbors. We have three ways of positioning the other accepted node: at the top, at the bottom or at the right of $X_{i,j}$. Let us study the case of top node and the case of right node.

2.1: Up to a rotation in the domain, we can assume without loss of generality that the accepted nodes are $X_{i+1,j}$ and $X_{i,j-1}$, with $T_{i+1,j} < T_{i,j-1}$. In this case the other two neighbors of $X_{i,j}$ are *narrow band* or *far away* nodes, as presented in Figure 2.6. We should remark that $T_{i,j} < T_{i,j+1}$, $T_{i,j} < T_{i-1,j}$, since $X_{i,j}$ is the *narrow band* node with the smallest T.

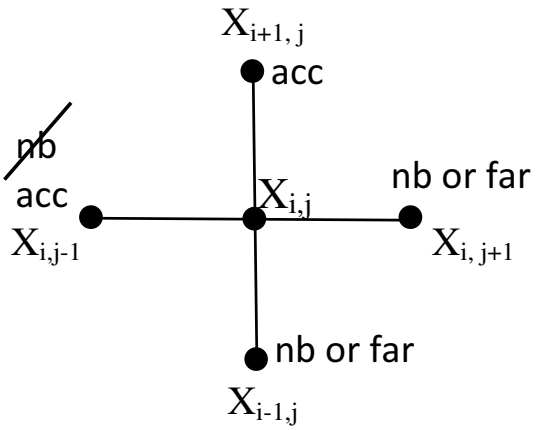

FIGURE 2.6. Node $X_{i,j}$ has the neighbors $X_{i,j-1}$ and $X_{i+1,j}$ accepted

In this case the finite difference operators are:

$$D^{-x}T_{i,j} \geq 0, \quad D^{+x}T_{i,j} \geq 0,$$
$$D^{-y}T_{i,j} \leq 0, \quad D^{+y}T_{i,j} \leq 0.$$

and equation (1.22) becomes:

$$\left(\max(D^{-x}T_{i,j}, 0)\right)^2 + \left(\max(0, D^{+y}T_{i,j})\right)^2 = \frac{1}{F_{i,j}^2}$$
$$\left(D^{-x}T_{i,j}\right)^2 + \left(D^{+y}T_{i,j}\right)^2 = \frac{1}{F_{i,j}^2}.$$

Using the finite difference operators $D^{-x}T_{i,j}$ and $D^{+y}T_{i,j}$, we get:

$$\left(\frac{T_{i,j} - T_{i,j-1}}{\Delta x}\right)^2 + \left(\frac{T_{i+1,j} - T_{i,j}}{\Delta y}\right)^2 = \frac{1}{F_{i,j}^2},$$

and

$$(T_{i,j} - T_{i,j-1})^2 + (T_{i+1,j} - T_{i,j})^2 = \frac{\Delta x^2}{F_{i,j}^2}, \tag{2.16}$$

Solving the quadratic equation in $T_{i,j}$ we get:

$$T_{i,j} = \frac{T_{i,j-1} + T_{i+1,j} \pm \sqrt{2\frac{\Delta x^2}{F_{i,j}^2} - (T_{i,j-1} - T_{i+1,j})^2}}{2}. \tag{2.17}$$

Since $X_{i,j-1}, X_{i+1,j} \in A(\Omega)$, $T_{i,j} > T_{i,j-1}$, $T_{i,j} > T_{i+1,j}$, and therefore $T_{i,j} > \frac{T_{i-1,j}+T_{i,j+1}}{2}$. Hence we consider only the solution of (2.17) involving the "+" sign:

$$T_{i,j} = \frac{T_{i,j-1} + T_{i+1,j} + \sqrt{2\frac{\Delta x^2}{F_{i,j}^2} - (T_{i,j-1} - T_{i+1,j})^2}}{2}. \tag{2.18}$$

Since $T_{i,j}$ is the solution of equation (2.16), we can rewrite it as:

$$(T_{i,j} - T_{i,j-1})^2 = \frac{\Delta x^2}{F_{i,j}^2} - (T_{i+1,j} - T_{i,j})^2,$$

and therefore

$$(T_{i,j} - T_{i,j-1})^2 \leq \frac{\Delta x^2}{F_{i,j}^2}.$$

Since both sides of the above inequality are positive, we can take the square root and get

$$T_{i,j} - T_{i,j-1} \leq \frac{\Delta x}{F_{i,j}}. \tag{2.19}$$

Now, we can conclude that:

$$T_{i,j-1} \leq T_{i,j} \leq T_{i,j-1} + \frac{\Delta x}{F_{i,j}}.$$

In order to complete the proof for this case, we need to show that the expression that appears under the square root in the calculation of $T_{i,j}$ as a function of two of its neighbors, in equation (2.18), can never be negative . Since node $X_{i+1,j}$ was accepted before node $X_{i,j-1}$, we know that $T_{i,j-1} \leq T_{i+1,j}$. In this setting, $T^*_{i,j}$ was first computed based on $X_{i+1,j}$ and following the arguments from case 1, we can say that:

$$T_{i+1,j} \leq T^*_{i,j} \leq T_{i+1,j} + \frac{\Delta x}{F_{i,j}}.$$

Since $X_{i,j-1}$ becomes accepted before $X_{i,j}$, we have that $T_{i,j-1} \leq T^*_{i,j}$.
From all of these, we deduce that:

$$T_{i+1,j} \leq T_{i,j-1} \leq T^*_{i,j} \leq T_{i+1,j} + \frac{\Delta x}{F_{i,j}},$$

which implies that

$$0 \leq T_{i,j-1} - T_{i+1,j} \leq \frac{\Delta x}{F_{i,j}}. \tag{2.20}$$

Therefore, when we compute $T_{i,j}$ at the current iteration, from equation (2.18), the quantity under the square root becomes:

$$\frac{2\Delta x^2}{F^2_{i,j}} - (T_{i,j-1} - T_{i+1,j})^2 \geq \frac{2\Delta x^2}{F^2_{i,j}} - \frac{\Delta x^2}{F^2_{i,j}} = \frac{\Delta x^2}{F^2_{i,j}} \geq 0.$$

2.2: Up to a rotation in the domain, we can assume without loss of generality that the accepted nodes are $X_{i,j+1}$ and $X_{i,j-1}$, with $T_{i,j+1} < T_{i,j-1}$. In this

case the other two neighbors of $X_{i,j}$ are *narrow band* or *far away* nodes, as presented in Figure 2.7. We should remark that $T_{i,j} < T_{i+1,j}$, $T_{i,j} < T_{i-1,j}$, since $X_{i,j}$ is the *narrow band* node with the smallest T.

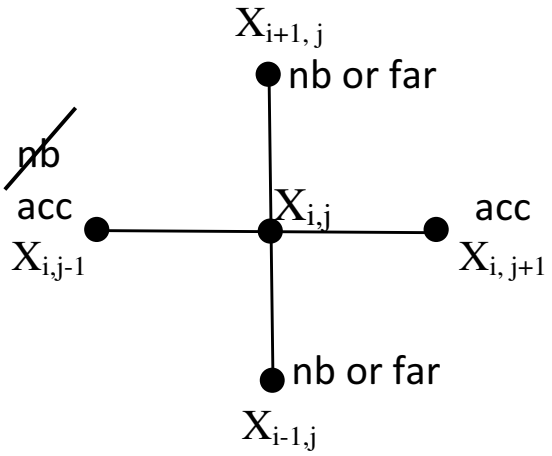

FIGURE 2.7. Node $X_{i,j}$ has the neighbors $X_{i,j-1}$ and $X_{i,j+1}$ accepted

For this situation, the finite difference operators are:

$$D^{-x}T_{i,j} \geq 0, \quad D^{+x}T_{i,j} \leq 0,$$
$$D^{-y}T_{i,j} \leq 0, \quad D^{+y}T_{i,j} \geq 0.$$

and equation (1.22) becomes:

$$\left(\max(D^{-x}T_{i,j}, -D^{+x}T_{i,j})\right)^2 + (\max(0,0))^2 = \frac{1}{F_{i,j}^2}$$
$$\left(\max(D^{-x}T_{i,j}, -D^{+x}T_{i,j})\right)^2 = \frac{1}{F_{i,j}^2}.$$

Using the finite difference operators $D^{-x}T_{i,j}$ and $D^{+x}T_{i,j}$, we get:

$$\left(\frac{T_{i,j} - T_{i,j-1}}{\Delta x}\right)^2 = \frac{1}{F_{i,j}^2}$$
$$\left(\frac{T_{i,j} - T_{i,j+1}}{\Delta x}\right)^2 = \frac{1}{F_{i,j}^2}.$$

Since $T_{i,j} \geq T_{i,j-1}$ and $T_{i,j} \geq T_{i,j+1}$, this case is equivalent to solving the local Eikonal equation for $T_{i,j}$ in first and in second quadrant, and taking the

minimum of the solutions:

$$T_{i,j} = \min\left(T_{i,j+1} + \frac{\Delta x}{F_{i,j}}, T_{i,j-1} + \frac{\Delta x}{F_{i,j}}\right).$$

Repeating the first case steps, we conclude that:

$$T_{i,j+1} \leq T_{i,j-1} \leq T_{i,j} \leq T_{i,j-1} + \frac{\Delta x}{F_{i,j}} \leq T_{i,j+1} + \frac{\Delta x}{F_{i,j}}.$$

Case 3 and **4**, where three or all the $X_{i,j}$'s neighbors are *accepted*, are similar to the previous cases, since the finite differences take the smallest values in each coordinate direction. □

Remark 2.16. *We should remark that the proof of Theorem 2.13 provides a constructive solution for the local Eikonal equation at $X_{i,j}$. In the implementation, we notice that it is more efficient to solve the four variants of equation (2.15) and (2.16) and take the minimum of these real solutions.*

Convergence of Fast Marching

At each step of the algorithm the size of the *accepted* nodes set grows by 1. We can apply Theorem 2.13 iteratively using induction on the number of iterations of the algorithm.

During first iteration, if node $X_{i,j-1}$ is *accepted*, then its value is known and initialized with $T_{i,j-1} = 0$ and we have $T_{i,j} \leq 0 + \frac{\Delta x}{F_{i,j}}$, which satisfies relation (2.14) and therefore Theorem 2.13 holds true.

At the n-th step of the algorithm, the induction hypothesis implies that, at each iteration, the T's at the nodes in the *narrow band* are greater than the ones at the nodes labeled as *accepted*. And thus Theorem 2.13 can be applied.

In conclusion, the *upwind* nature of the numerical scheme is satisfied since T at the node labeled as *accepted*, at every iteration, is exact, i.e. it cannot be improved on the same grid [22].

Chapter 3
Parallel Fast Marching Methods

In the previous sections we saw that Fast Marching Methods are inherently sequential and hence not straightforward to parallelize and implement on today's supercomputers. Parallelizing Fast Marching Methods is a step forward for employing the Level Set Methods on parallel supercomputers.

3.1 General Idea

The idea behind the distributed implementation of the Fast Marching Methods is to divide the whole computational grid between processors, giving each processor access to *only its own sub-domain*, and use message passing strategy to communicate between different processors (more details about parallel computing can be found in section 4.3). This approach has its own drawbacks:

- when the grid is simply split between processors, in some cases there is no longer enough data to update all the points in each sub-domain,
- we cannot preserve the upwind nature of the numerical scheme for the whole domain just in one pass,
- communication through message passing is really expensive, since it requires a lot of time for data transmissions.

The efficiency of the parallel algorithms depends on the required amount of communication between sub-domains, i.e. how often boundary nodes change status, and our ability to preserve the upwind structure during the algorithm execution.

All of the above are main obstacles for good scalability.

To overcome these problems, *ghost-zones* with *ghost points* are used. Ghost-zones are additional (duplicated) grid points which are added to each processor and they contain necessary data to advance to the next iteration. Hence, we expand each sub-domain by adding 1 layer of ghost nodes. All ghost-nodes of a sub-domain form the ghost-zone or overlap of that sub-domain. Figure 3.1 illustrates the particular decomposition of a two dimensional 10×10 grid into four sub-domains.

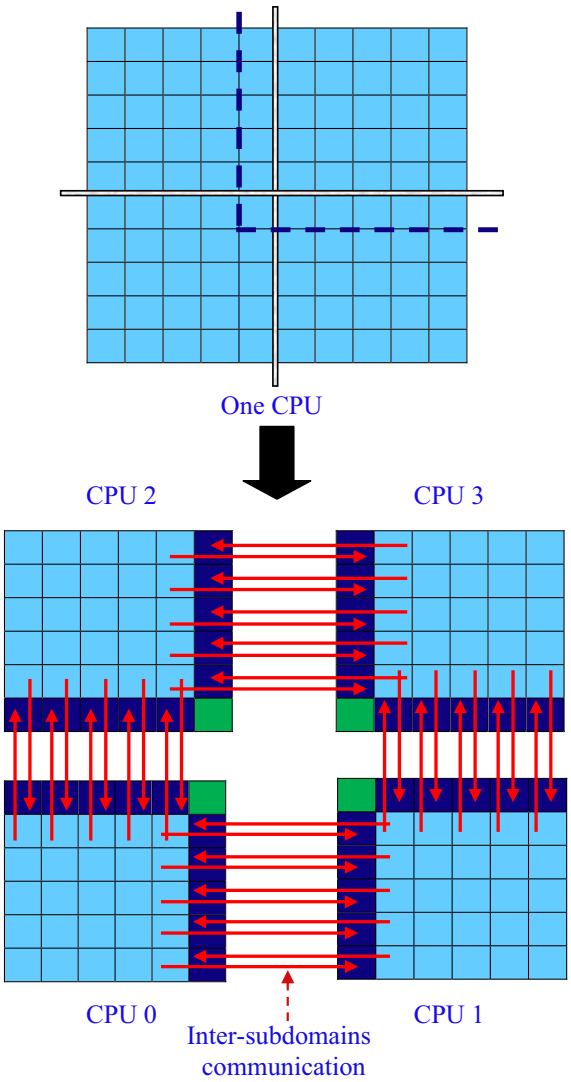

FIGURE 3.1. Domain decomposition in sub-domains, the dark blue cells are the ghost cells, the dashed line delimits the ghost-zone for the top right sub-domain

The dashed line shows how the ghost-zone is formed for the top-right sub-domain. In the same manner, we formed the ghost-zones for the other sub-domains. The second part of the picture presents the sub-domain decomposition and indicates in dark blue the ghost-zone for each sub-domain. After decomposition, each sub-domain has dimension 6×6, because there are an extra row and column for the ghost points to make sub-domains interaction possible.

In two-dimension, a sub-domain can have at most four neighbor sub-domains, and also at most four ghost-regions, depending on the position on the global grid. Figure 3.2 (reproduced from PETSc User Manual [19]) illustrates the ghost points for process six of a two-dimensional, regular parallel grid. Each box represents a process; the ghost points for the sixth process are shown in gray.

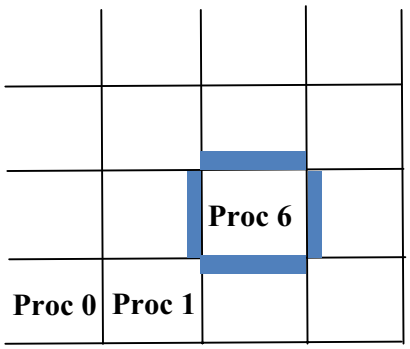

FIGURE 3.2. Ghost points for a particular process

In the following sections, we address the above issues and the way that we chose to implement the parallel Fast Marching algorithm in more details.

3.2 Notations

We partition our initial domain Ω in N_s sub-domains. In order to keep the notation simple, we commit the following abuse of notation: by Ω, we denote both

the domain and the discretized domain, i.e $(0,1) \times (0,1)$ and $\{0,\, 1, \ldots, N\} \times \{0,\, 1, \ldots, M\}$.

We use k, $1 \leq k \leq N_s$, to denote the sub-domain index and by Ω_k we refer to the sub-domain k.

Definition 3.1. *For a sub-domain Ω_k we denote its boundary by $\partial\Omega_k$.*
The sub-domain Ω_k together with its ghost-points form the so called extended sub-domain, denoted by $\tilde{\Omega}_k$.

Any point in the domain is denoted by $X_{i,j}$, where $0 \leq i \leq N$ and $0 \leq j \leq M$ are the row and column indexes. When decomposing the domain in sub-domains, it is necessary to distinguish between neighbors in the sub-domain and neighbors that are ghost-points.

Definition 3.2. *Consider a sub-domain Ω_k and a node $X_{i,j} \in \Omega_k$, we define*

- *the **set of neighbors of** $X_{i,j}$ **in** Ω_k as:*

$$D(X_{i,j}) = \{Y \in \{X_{i+1,j},\, X_{i-1,j},\, X_{i,j+1},\, X_{i,j-1}\} \bigcap \Omega_k\},$$

- *the **set of ghost neighbors of** $X_{i,j}$ as:*

$$G(X_{i,j}) = \{Y \in \{X_{i+1,j},\, X_{i-1,j},\, X_{i,j+1},\, X_{i,j-1}\} \backslash \Omega_k\}.$$

Definition 3.3. *The ghost-zone of a sub-domain contains all the ghost-nodes of that sub-domain and it is denoted $G(\Omega_k)$, $k = 1, \ldots, N_s$, where N_s is the number of sub-domains.*

Definition 3.4. *For any node $X_{i,j}$ of the grid, we define the neighbors set as*

$$V(X_{i,j}) = D(X_{i,j}) \cup G(X_{i,j}).$$

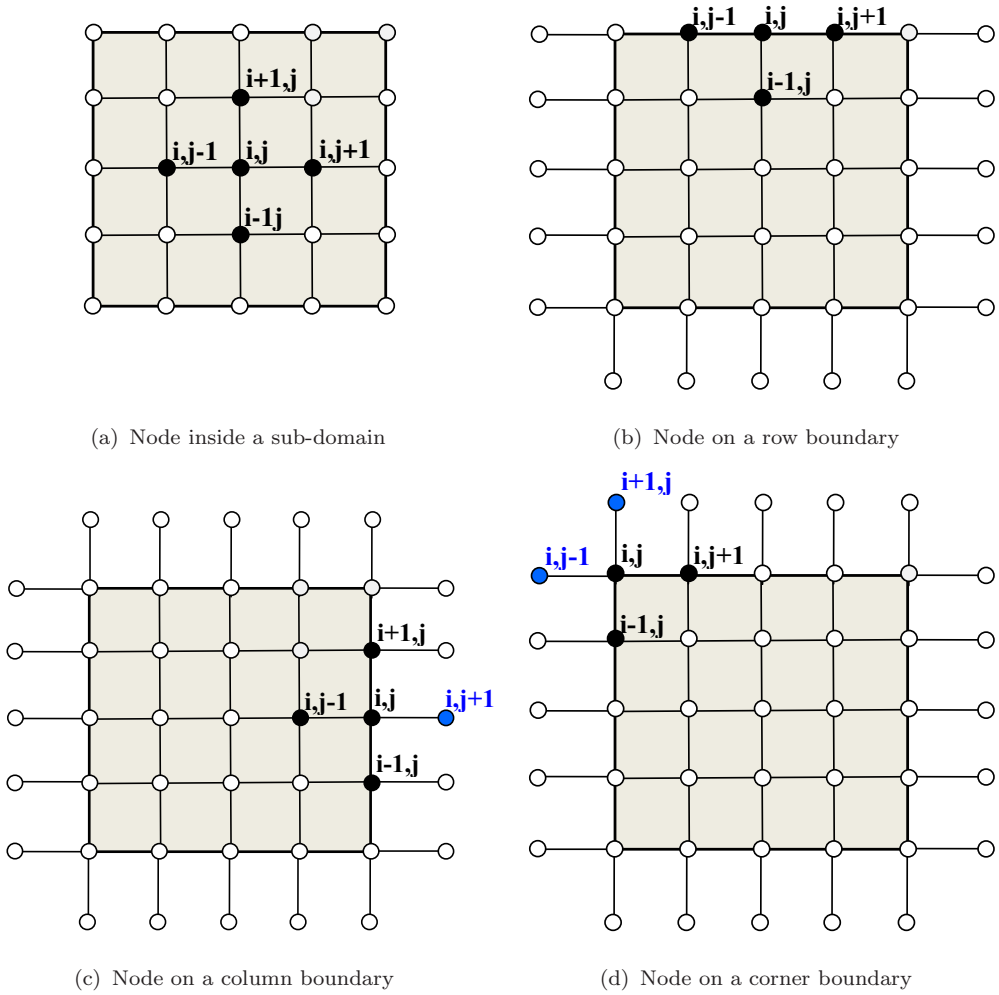

(a) Node inside a sub-domain

(b) Node on a row boundary

(c) Node on a column boundary

(d) Node on a corner boundary

FIGURE 3.3. Neighbors of $X_{i,j}$

In Figure 3.3, the sub-figures illustrate the difference between the neighbors and the ghost neighbors, based on a typical situation.

Thus, the sets of neighbors and ghost neighbors of $X_{i,j}$ are:

- figure 3.3(a): $D(X_{i,j}) = \{X_{i+1,j},\ X_{i-1,j},\ X_{i,j+1},\ X_{i,j-1}\}$ and $G(X_{i,j}) = \{0\}$,
- figure 3.3(b): $D(X_{i,j}) = \{X_{i-1,j},\ X_{i,j-1},\ X_{i,j+1}\}$ and $G(X_{i,j}) = \{0\}$,
- figure 3.3(c): $D(X_{i,j}) = \{X_{i+1,j},\ X_{i-1,j},\ X_{i,j-1}\}$ and $G(X_{i,j}) = \{X_{i,j+1}\}$,
- figure 3.3(d): $D(X_{i,j}) = \{X_{i,j+1}, X_{i-1,j}\}$ and $G(X_{i,j}) = \{X_{i,j-1},\ X_{i+1,j}\}$.

Remark 3.5. *Again, we commit an abuse of notation, since special care has to be applied when $X_{i,j}$ is at the boundary of Ω_k. We let the reader distinguish between the indices of a ghost node and a node in the domain ($X_{0,0} \in \partial\Omega_k$ and $X_{-1,0} \in G(X_{0,0})$, but $0 \leq i \leq N$).*

Definition 3.6. *By $\boldsymbol{A}(\Omega_k)$, $\boldsymbol{NB}(\Omega_k)$ and $\boldsymbol{FA}(\Omega_k)$ we denote the sets of **accepted**, **narrow band**, and **far away** nodes over the sub-domain Ω_k.*
We also define:

- *the set of **accepted nodes over the boundary** of domain Ω_k as:*
  $\boldsymbol{A}(\partial\Omega_k) = \boldsymbol{A}(\Omega_k) \cap \partial\Omega_k$,

- *the set of **narrow band nodes over the boundary** of domain Ω_k as:*
  $\boldsymbol{NB}(\partial\Omega_k) = \boldsymbol{NB}(\Omega_k) \cap \partial\Omega_k$,

- *the set of **far away nodes over the boundary** of domain Ω_k as:*
  $\boldsymbol{FA}(\partial\Omega_k) = \boldsymbol{FA}(\Omega_k) \cap \partial\Omega_k$.

3.3 Parallel Fast Marching Algorithm

The main idea of the parallel algorithm is to perform Fast Marching on the sub-domains, update the boundary values at the interfaces and restart the algorithm until convergence is achieved. To update the boundary values at the interfaces we need to preserve the upwind structure of the numerical scheme and to synchronize the ghost-zones at each iteration.
The parallel Fast Marching algorithm performs iteratively, the steps presented in Algorithm 4, until convergence is achieved.

Algorithm 4 Parallel Fast Marching algorithm

repeat

Compute $T_k^n(X_{i,j})$, $\forall \Omega_k$, $\forall X_{i,j} \in \Omega_k$, $k = 0, \ldots, N_s$ using Fast Marching on the sub-domains (local FM)

Ghost points synchronization

(`/* Exchange and update the boundary data at the interfaces */`)

until *convergence conditions are satisfied* ;

3.3.1 Ghost Points

The ghost-zones synchronization is not trivial, since it should preserve the upwind nature of the discretization scheme. The steps of the ghost-zones synchronization procedure are presented in Algorithm 5.

Algorithm 5 Ghost-zones Synchronization procedure

begin

1. $\forall \Omega_k, X_{i,j} \in \partial\Omega_k$, compute $T_k^{n+\frac{1}{2}}(X_{i,j})$ as the solution of the local Eikonal equation at $X_{i,j} \in \tilde{\Omega}_k$

2. reassign the flags

3. save the minimum of all $T_k^{n+\frac{1}{2}}$ for $X_{i,j} \in \partial\Omega_k$ and use it to update the flags in Ω_k.

end

Remark 3.7. *To avoid confusions in the parallel implementation, when we refer to the value of a certain point, we need to specify its sub-domain and also the iteration during which it was computed. Therefore, let $T_k^n(X_{i,j})$ be the T at node $X_{i,j}$, obtained during n^{th} iteration, at the end of local Fast Marching algorithm, in sub-domain Ω_k, and $T_k^{n+\frac{1}{2}}(X_{i,j})$ be the T at node $X_{i,j}$ in sub-domain Ω_k, obtained after the ghost-points synchronization.*

Consider a domain with the starting nodes in opposite corners. These nodes are initialized as *accepted* nodes at the beginning of the Fast Marching algorithm. Let us consider the particular decomposition of the domain in two sub-domains, each including one of the accepted nodes, as illustrated in Figure 3.4. In the following,

for this particular case, we describe how the synchronization procedure works step by step for each sub-domain.

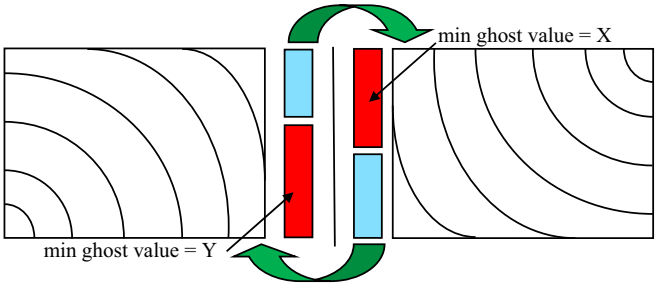

(a) After Local FM

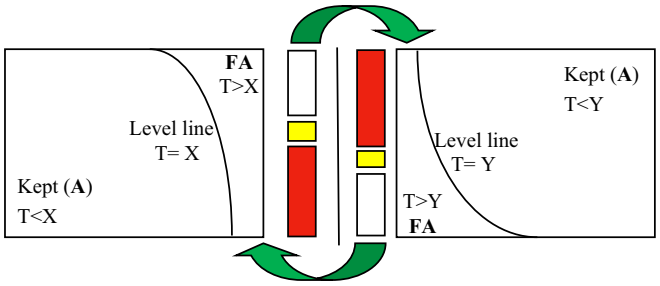

(b) After Ghost Update

FIGURE 3.4. Ghost points update

Step 1: for all Ω_k and all $X \in \partial\Omega_k$, let $T_k^{n+\frac{1}{2}}$ be the solution of the local Eikonal equation at X in $\tilde{\Omega}_k$. If $T_k^{n+\frac{1}{2}}(X_{i,j})_k < T_k^n(X_{i,j})$, we say that $X_{i,j}$ is a node with **ghost point influence** in Ω_k (colored in blue in Figure 3.4(a)). If $T_k^{n+\frac{1}{2}}(X_{i,j}) = T_k^n(X_{i,j})$, we say that $X_{i,j}$ is an *accepted* node, and its T will not change in Ω_k (colored in red in Figure 3.4(a)).

Step 2: for all Ω_k and for any node $X_{i,j} \in \partial\Omega_k$, we do a comparison so that we can **reassign the flags** and reconstruct the accepted and narrow band sets:

$$\begin{aligned} \text{if } T_k^{n+\frac{1}{2}}(X_{i,j}) \leq T_k^n(X_{i,j}) \quad & \text{then tag } X_{i,j} \in \mathbf{NB}(\Omega_k) \\ & \text{otherwise tag } X_{i,j} \in \mathbf{A}(\Omega_k). \end{aligned}$$

Step 3: let $\mathbf{T}_k^{n+\frac{1}{2}} = \min_{Y \in \mathbf{NB}(\partial\Omega_k)} T_k^{n+\frac{1}{2}}(Y)$ be **the minimum T on the narrow band**. We use $T_k^{n+\frac{1}{2}}$ to **update the flags of the whole sub-domain**, i.e. for all

$X_{i,j} \in \Omega_k$:

$$\begin{aligned}
&\text{if } T_k^{n+\frac{1}{2}}(X_{i,j}) < \mathbf{T}_k^{n+\frac{1}{2}}, \quad \text{then } X_{i,j} \in \mathbf{A}(\Omega_k) \\
&\text{if } T_k^{n+\frac{1}{2}}(X_{i,j}) = \mathbf{T}_k^{n+\frac{1}{2}}, \quad \text{then } X_{i,j} \in \mathbf{NB}(\Omega_k) \\
&\text{if } T_k^{n+\frac{1}{2}}(X_{i,j}) > \mathbf{T}_k^{n+\frac{1}{2}}, \quad \text{then } X_{i,j} \in \mathbf{FA}(\Omega_k).
\end{aligned}$$

In Figure 3.4(b), $\mathbf{T}_k^{n+\frac{1}{2}} = X$ for the left sub-domain and $\mathbf{T}_{k+1}^{n+\frac{1}{2}} = Y$ for the right sub-domain. The red region represents the accepted nodes , the yellow region represents the narrow band and the white one is for the far away nodes.

As presented in Algorithm 4 the ghost point synchronization procedure is the part where we can apply different strategies in order to restart the Fast Marching algorithm. The purpose of such strategies is to assure the monotonicity and upwind nature of the scheme even when we have inter-domain communications. The difference between strategies is in the way the boundary is computed using the ghost-points. We will describe these strategies in detail in Chapter 4.

3.4 Convergence

First let us remark that:

Remark 3.8. *For any iteration n, the following hold true:*

- *for any two nodes* $X_{i,j} \in \boldsymbol{NB}(\Omega_k)$ *and* $X_{r,c} \in \boldsymbol{A}(\Omega_k)$*, we have* $T_k^n(X_{i,j}) > T_k^n(X_{r,c})$*, for* $0 \leq r,\ i \leq M$ *and* $0 \leq c,\ j \leq N$*,*
- *if* $X_{i,j} \in \boldsymbol{NB}(\Omega_k)$ *with* $T_k^n(X_{i,j}) = \min_{Y \in \boldsymbol{NB}(\Omega_k)} T_k^n(Y)$*, then, at the next iteration,* $X_{i,j} \notin \boldsymbol{NB}(\Omega_k)$ *and* $X_{i,j} \in \boldsymbol{A}(\Omega_k)$ *(it will be the next node labeled as accepted).*

In the ghost-zone synchronization procedure, we reconstruct the narrow band of each sub-domain as a function of minimum/maximum values of the boundary

nodes. We have to prove that the minimum T over the *narrow band* cannot be decreased if we do not have ghost-nodes influence.

Proposition 3.9. *For all sub-domains Ω_k and Ω_l, consider a node $X_{i,j} \in \partial\Omega_k$ with $T_k^n(X_{i,j})$ and a node $X_{a,b} \in \partial\Omega_l$ with $T_l^n(X_{a,b})$, such that $X_{a,b} \in G(X_{i,j})$. Let $T_k^{n+\frac{1}{2}}(X_{i,j})$ be the solution of the local Eikonal equation at $X_{i,j}$ in $\tilde{\Omega}_k$.*

$$\begin{aligned} &\text{If } T_k^n(X_{i,j}) > T_l^n(X_{a,b}), \quad \text{then } T_k^{n+\frac{1}{2}}(X_{i,j}) < T_k^n(X_{i,j}) \\ &\qquad\qquad\qquad\qquad\quad \text{otherwise } T_k^{n+\frac{1}{2}}(X_{i,j}) = T_k^n(X_{i,j}). \end{aligned}$$

Proof. As we saw in the previous sections, in all the computations, a lower T for a node can be obtained only using a stencil that contains nodes already accepted in the previous iterations.

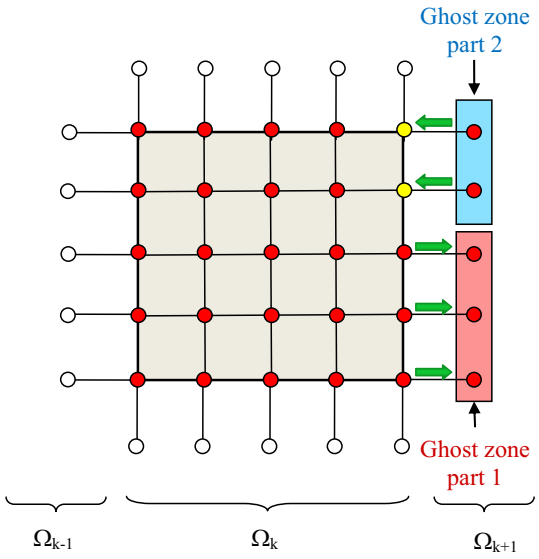

FIGURE 3.5. Ghost-zone influence on sub-domains

For illustration purposes, suppose that the sub-domain Ω_l is on the right of Ω_k (i.e. $\Omega_l = \Omega_{k+1}$), as drawn in Figure 3.5. Up to a symmetry or rotation in the domain, all possible configurations of sub-domains can be reduced to this case. Depending on the position of $X_{i,j}$ on the grid we have the cases:

- if $X_{i,j}$ is a corner node, then it has two ghost-nodes and one local Eikonal equation to solve in sub-domain $\tilde{\Omega}_k$,
- if $X_{i,j}$ is located at the edge of Ω_k, but it is not a corner node, then it has one ghost-node and two local Eikonal equations to solve in sub-domain $\tilde{\Omega}_k$.

We need to solve the local Eikonal equations on the extended domain $\tilde{\Omega}_k$ and take the minimum over all such solutions:

$$T_k^{n+\frac{1}{2}}(X_{i,j}) = \min\left\{\min_{\tilde{\Omega}_k}(T_k(X_{i,j})), T_k^n(X_{i,j})\right\}.$$

If $T_k^n(X_{i,j}) \leq T_l^n(X_{a,b})$, for $X_{i,j} \in \partial\Omega_k$ and $X_{a,b} \in G(X_{i,j})$ (see red region (part 1) of Figure 3.5), then $T_k^{n+\frac{1}{2}}(X_{i,j})$ is influenced more by the accepted neighbors from its sub-domain than by its ghost-neighbors:

$$\min\left\{\min_{\tilde{\Omega}_k}(T_k(X_{i,j})), T_k^n(X_{i,j})\right\} = T_k^n(X_{i,j}).$$

Then, for any such $X_{i,j} \in \partial\Omega_k$, if we do not have ghost point influence, we get

$$T_k^{n+\frac{1}{2}}(X_{i,j}) = T_k^n(X_{i,j}).$$

If $T_k^n(X_{i,j}) \geq T_l^n(X_{a,b})$, for $X_{i,j} \in \partial\Omega_k$ and $X_{a,b} \in G(X_{i,j})$, then the computation of $T_k^{n+\frac{1}{2}}(X_{i,j})$ is influenced mostly by its ghost-nodes (see blue region (part 2) of Figure 3.5). Solving the local Eikonal equation at $X_{i,j}$ in $\tilde{\Omega}_k$, we get that:

$$T_k^{n+\frac{1}{2}}(X_{i,j}) = \min\left\{\min_{\tilde{\Omega}_k}(T_k(X_{i,j})), T_k^n(X_{i,j})\right\} = \min_{\tilde{\Omega}_k}(T_k(X_{i,j})).$$

Therefore, we can decrease $T_k^n(X_{i,j})$, where $X_{i,j} \in \partial\Omega_k$ only if we have ghost points influence. □

Theorem 3.10 (Reconstruction of the **A**, **NB**, **FA** sets)**.** *Consider Ω_k and Ω defined as before. Assume that $X_{i,j} \in \Omega_k$, $X_{i,j} \in \boldsymbol{NB}(\Omega_k)$, $Z \in \tilde{\Omega}_k$ and $Z \in V(X_{i,j})$. During the n-th iteration of local Fast Marching algorithm, node Z becomes accepted. Then we have $T(X_{i,j}) > T(Z)$.*

Proof. To prove the theorem we use induction on the number of iterations of the algorithm.

At the first step the theorem holds true by construction (initialization).

At the n-th step of the algorithm, the remarks from 3.8 hold true. Since we have an ordering relation between boundary nodes, we can apply Proposition 3.9 to complete the proof. When node Z becomes accepted, node $X_{i,j}$ can be in one of the following cases:

Case 1: only one of the neighbor of $X_{i,j}$ is *accepted*,

Case 2: two of the neighbors of $X_{i,j}$ are *accepted*,

Case 3: more than two neighbors of $X_{i,j}$ are *accepted*.

Consider the particular setting, where sub-domain Ω_{k-1} is to the left of sub-domain Ω_k, which is to the left of Ω_{k+1}.

Case 1: Only one of the neighbors of $X_{i,j}$ is *accepted* and this node is Z.

Up to a rotation in the domain, we can assume, without loss of generality, that node $Z \in \Omega_k$ or that $Z \in \tilde{\Omega}_k$.

1.1: Let node $Z \in \Omega_k$ and $Z \in D(X_{i,j})$ be the only *accepted* neighbor of $X_{i,j}$ (see Figure 3.6).

Since $Z \in \mathbf{A}(\Omega_k)$, by part 1 of remark (3.8), $X_{i,j} \in \mathbf{NB}(\Omega_k)$ and all the other neighbors of $X_{i,j}$ are *narrow band* or *far away*. Hence, there is no *accepted* ghost-node to influence $T_k^{n+\frac{1}{2}}(X_{i,j})$ and $T_k^n(X_{i,j}) = T_k^{n+\frac{1}{2}}(X_{i,j})$. Therefore $T_k^{n+\frac{1}{2}}(Z) < T_k^{n+\frac{1}{2}}(X_{i,j})$.

1.2: Let node $Z \in G(X_{i,j})$ and $Z \in \tilde{\Omega}_k$ (see Figure 3.7).

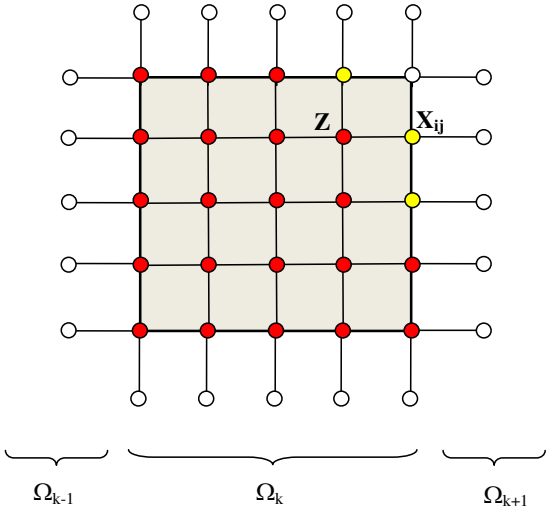

FIGURE 3.6. Node Z is in the same sub-domain as $X_{i,j}$

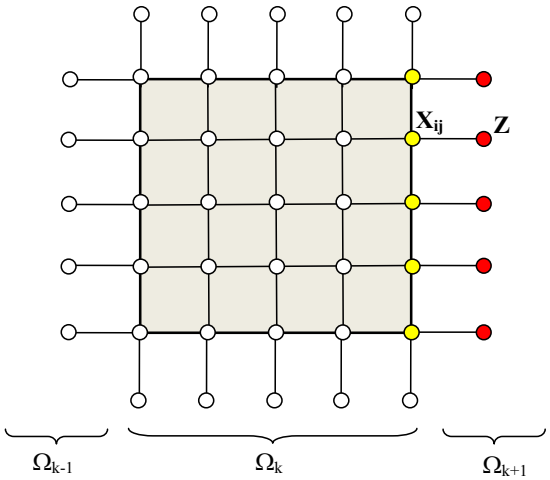

FIGURE 3.7. Node Z is a ghost-node of $X_{i,j}$

Since $Z \in \mathbf{A}(\tilde{\Omega}_k)$, $Z \in G(X_{i,j})$, $X_{i,j} \in \mathbf{NB}(\Omega_k)$ and $T_k^n(X_{i,j}) > T_k^n(Z)$. By Proposition 3.9, $T_k^n(X_{i,j}) \geq T_k^{n+\frac{1}{2}}(X_{i,j})$. For computing $T_k^{n+\frac{1}{2}}(X_{i,j})$ we used its accepted ghost-neighbor Z, and relation $T_k^{n+\frac{1}{2}}(Z) < T_k^{n+\frac{1}{2}}(X_{i,j})$ holds true.

Case 2: Two of the neighbors of $X_{i,j}$ are *accepted*. Assume that node A was accepted before node Z.

Let $A \in D(X_{i,j})$, $A \in \mathbf{A}(\Omega_k)$ and since A was the first accepted neighbor of $X_{i,j}$, $T_k^n(X_{i,j}) > T_k^n(A)$. When Z becomes accepted, $T_k^n(X_{i,j})$ needs to be recomputed.

Up to a rotation in the domain, we can assume, without loss of generality, that node $Z \in \Omega_k$ or that $Z \in \tilde{\Omega}_k$.

2.1: Let node $Z \in D(X_{i,j})$ and $Z \in \Omega_k$ (see Figure 3.8).

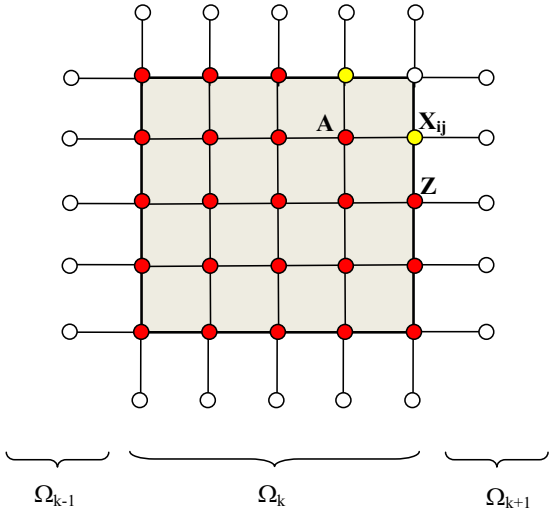

FIGURE 3.8. Node Z is in the same sub-domain as $X_{i,j}$

Since $A \in \mathbf{A}(\Omega_k)$, during n-th iteration, when Z becomes accepted, $X_{i,j} \in \mathbf{NB}(\Omega_k)$ with $T_k^n(X_{i,j}) > T_k^n(Z) > T_k^n(A)$. All other neighbors of $X_{i,j}$ are narrow band or far away nodes. Solving the local Eikonal equation at $X_{i,j}$ in $\tilde{\Omega}_k$, we do not have ghost point influence and applying Proposition 3.9 we get that $T_k^{n+\frac{1}{2}}(X_{i,j}) = T_k^n(X_{i,j})$. Thus relation $T_k^{n+\frac{1}{2}}(Z) < T_k^{n+\frac{1}{2}}(X_{i,j})$ holds true.

2.2: Let node $Z \in G(X_{i,j})$ and $Z \in \tilde{\Omega}_k$ (see Figure 3.9)

If $A \in \mathbf{A}(\Omega_k)$, then $X_{i,j}$ becomes a narrow band node and $T_k^n(A) < T_k^n(X_{i,j})$. When Z becomes accepted, $T_k^n(Z) < T_k^n(X_{i,j})$ and computing $T_k^{n+\frac{1}{2}}(X_{i,j})$ on the extended domain $\tilde{\Omega}_k$ we have ghost node influence. Therefore applying Proposition 3.9, we get that $T_k^{n+\frac{1}{2}}(Z) < T_k^{n+\frac{1}{2}}(X_{i,j}) < T_k^n(X_{i,j})$.

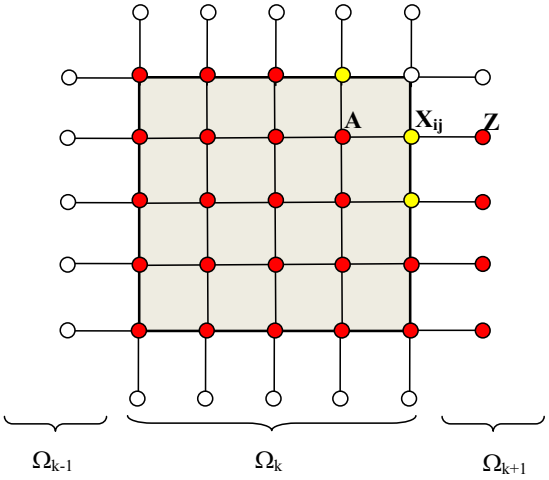

FIGURE 3.9. Node Z is a ghost-node of $X_{i,j}$

Case 3: More than two neighbors of $X_{i,j}$ were *accepted*, before Z was accepted. The proof for this case follows the arguments of the previous cases. □

In Chapter 2 we proved that the numerical solution built by the sequential Fast Marching methods converges to the viscosity solution of (1.1), as the mesh size is going to zero, i.e. $\Delta x \to 0$ and $\Delta y \to 0$ (see Theorem 2.4). Now, we need to prove that the solution computed by the parallel Fast Marching is the same as the solution computed by the sequential Fast Marching.

Theorem 3.11. *Consider $S_{i,j}$, $i = 0, \ldots, N$, $j = 0, \ldots, M$ be the solution computed using the sequential Fast Marching algorithm and $P_{i,j}$, $i = 0, \ldots, N$, $j = 0, \ldots, M$ be the solution computed using the parallel Fast Marching algorithm. Then for all i and j, $P_{i,j} = S_{i,j}$.*

Proof. Similar to the sequential case, we need to prove stability, consistency and monotonicity of the numerical scheme. Since both algorithms solve the problem based on the same scheme, i.e. (2.12), and since the parallel Fast Marching is based on the sequential Fast Marching, consistency and stability properties are inherited from the sequential algorithm. The only thing that we need to prove is

monotonicity. Precisely, we need to show that we preserve the upwind nature of the numerical scheme in the parallel version of the algorithm. This has already been proved in Theorem 3.10. □

Convergence to the same solution for both sequential and parallel Fast Marching is illustrated in the Chapter 4.

Chapter 4

Implementations and Numerical Experiments

4.1 Sequential Implementation

Since the solution of the Fast Marching is constructed by stepping away from the boundary condition in a downwind direction, we need to preserve the upwind nature of the numerical scheme. In order to arrange the nodes in increasing order, we use a double-chained sorted list. We consider the boundary conditions as the starting values for our list, and basically update the list one entry at a time. Each iteration, we (re)compute T at some of the nodes and insert those T at the right position in the sorted list. Since the list is double-chained, we can traverse the list forward or backward and insert T at the right place.

The structure of the double-chained list is presented in Figure 4.1. The list stores the following information in each element: pointers to the previous (graphically represented by the red link) and next (graphically represented by the blue link) elements of the list, position in the grid structure, i.e. row i, column j, value of $T_{i,j}$ and flag $Fl_{i,j}$ at each grid node to indicate its status. The first element in the list is called *head* and the last element of the list is called *tail*.

Initial Tagging

During the initialization phase of the algorithm, all nodes that approximate our initial curve are tagged as *accepted* with zero distance ($T_{i,j} = 0$) and zero flag ($Fl_{i,j} = 0$). All other nodes are tagged as *far away* nodes, with $T_{i,j} = S$, where S is a very large number ($S \gg N + M$) and flag two ($Fl_{i,j} = 2$).

The first *accepted* nodes represent the **starting** points in our algorithm: we use them to label all the adjacent neighbors. An *accepted* node labels an adjacent node by changing its status to *narrow band*, setting its flag to one ($Fl_{i,j} = 1$). An *accepted* node does not change the status of another accepted node.

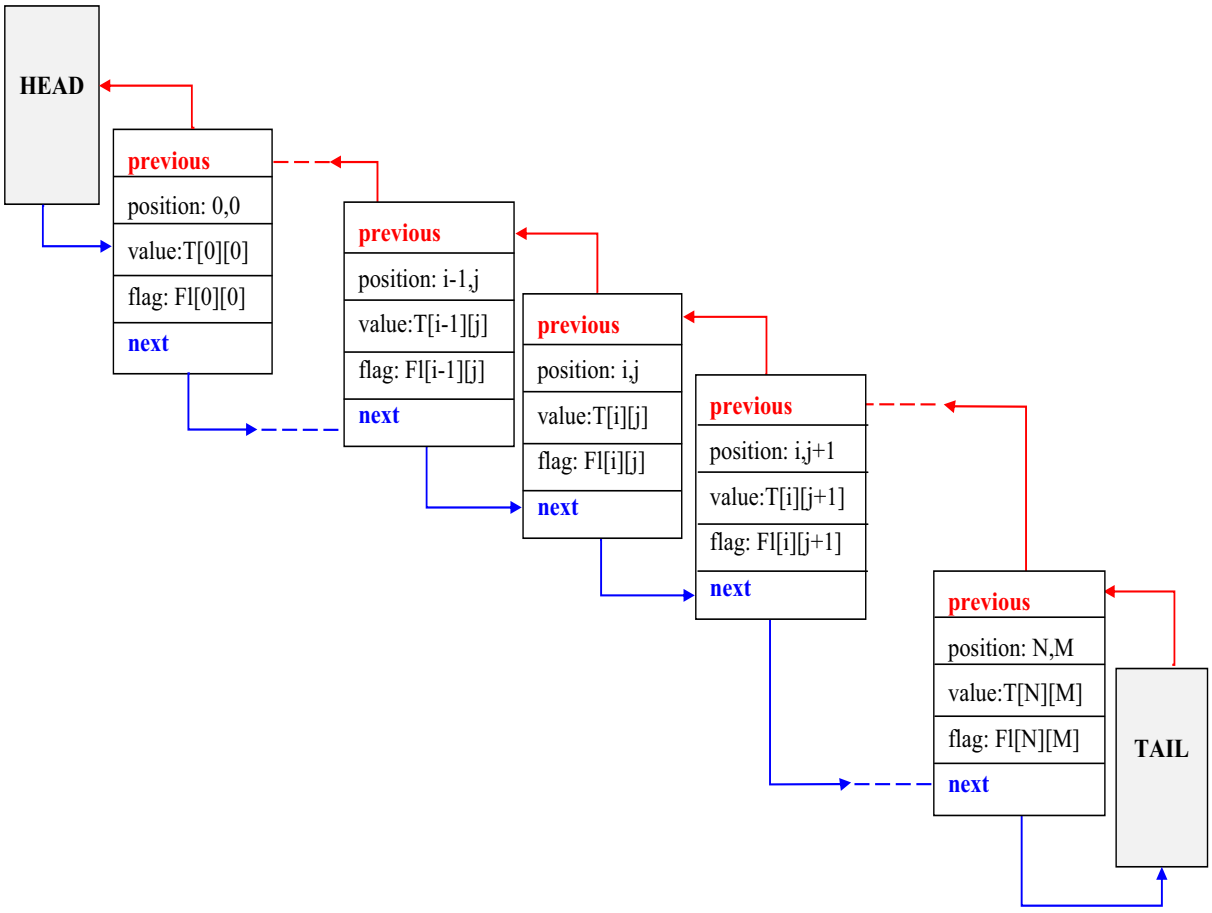

FIGURE 4.1. Double-chained list structure

Solving the Local Eikonal Equation

The way to solve the local Eikonal equation was presented during the proof of Theorem 2.13.

Algorithm 6 Solution of the quadratic equation

`Quadratic(`a,b`)`
Input: a and b real numbers
Output: d the solution of the quadratic eqaution
Calculate $\Delta = 4 \times [2 - (a-b)^2]$;
if $(\Delta \geq 0)$ **then**
  $d = (a + b + \sqrt{\Delta})/2$;
else
  $d = S$;
end
return d

The implementation of the first-order adjacent difference scheme for the Eikonal equation is presented in Algorithm 7, and uses Algorithm 6 to solve the quadratic equation.

Algorithm 7 Solution of the local Eikonal equation at $X_{i,j}$

`Distance(`*i, j, T[i][j]*`)`
Input: i, j, T[i][j]
Output: distance T
if *(i==row and j==col)* **then**
  $d1 \leftarrow 1 + min(min(T[i][j-1], T[i][j+1]), min(T[i+1][j], T[i-1][j]))$
  $d2 \leftarrow quadratic(T[i][j-1], T[i-1][j])$
  $d3 \leftarrow quadratic(T[i-1][j], T[i][j+1])$
  $d4 \leftarrow quadratic(T[i][j+1], T[i+1][j])$
  $d5 \leftarrow quadratic(T[i+1][j], T[i][j-1])$
  $T[i][j] \leftarrow min(val[i][j], min(d1, min(min(d2, d3), min(d4, d5))))$
end
return $T[i][j]$

Flag Assignment

To assign the flags, we check if there is any accepted node as neighbor. If there is, then our node is transformed from far away to a narrow band node. Otherwise, we leave it as a far away node. The function that assigns the flags to the nodes is called *UpdateFlag* and it is presented in Algorithm 8 for any generic grid point $X_{i,j}$.

Algorithm 8 Flag update

```
UpdateFlag(N,M, Fl)
Input: N,M, Fl
Output: updated flag list Fl
for i ← 0 to N do
    for j ← 0 to M do
        if (none of the neighbors of point (i, j) is accepted) then
            Fl[i][j] ← 2
        end
        else
            if Fl[i][j] !=0 then /* point is not accepted */
                Fl[i][j] ← 1
            end
        end
    end
end
return Fl
```

Sorting Algorithm

When node $X_{i,j}$ becomes *narrow band* or *accepted*, its $T_{i,j}$ is computed based on its neighbors. Therefore, we need to delete from the list the element with $T_k^n(X_{i,j})$ and insert, at the right position, the element with $T^{n+\frac{1}{2}}(X_{i,j})$. The algorithm of removing a node from the double-chained list is given in pseudo-code in Algorithm 9 and it is illustrated graphically in Figure 4.2. When removing node *current* from the list, the list connectivity needs to be preserved. Therefore, first we remove the forward and backward connections between current node and its preceding node, and replace them by a forward connection between previous and next element of current node (the dashed blue line in Figure 4.2(a)). Secondly, we do the same thing for the forward and backward connections between current node and its succeeding node, and replace them by a backward connection (the dashed red line in Figure 4.2(a)) between the following and the preceding nodes of the current node. The resulted list is one node shorter and has the backward and forward pointers correctly connected (see Figure 4.2(b)).

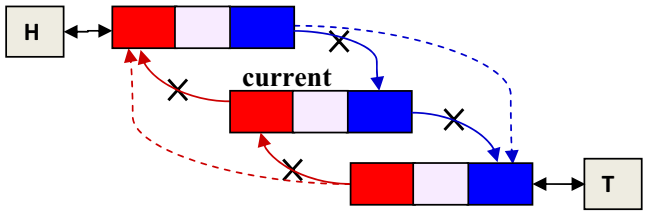

(a) Delete current node from list

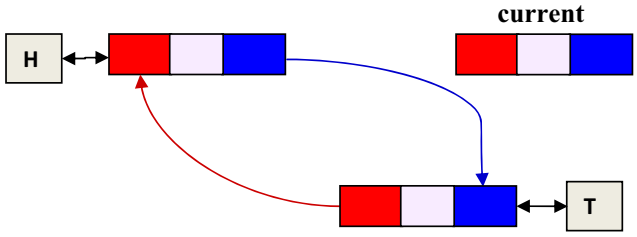

(b) List after deletion

FIGURE 4.2. Deletion from the double-chained list

Algorithm 9 Delete current node from the list

`DeleteList(`*node*`)`
Input: *node*
Output: delete node $X_{i,j}$ from the list
current->previous->next=current->next;
current->next->previous=current->previous;

The insertion operation can be performed in two ways:

- insert after the current node - described graphically in Figure 4.3 and in pseudo-code in Algorithm 10,
- insert before the the current node - described graphically in Figure 4.4 and in pseudo-code in Algorithm 11.

Since both procedures are similarly performed, we only explain how the insert-after-current-position works. First, we cut off the backward and forward links between the current node and its succeeder (see Figure 4.3(a)). Secondly, as presented in Figure 4.3(b) we follow the steps:

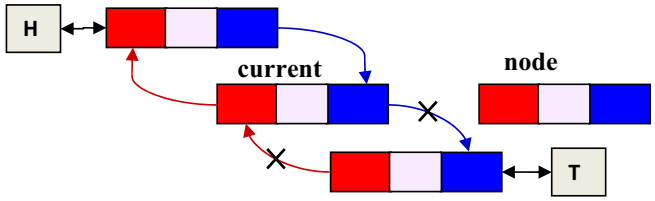

(a) Insert after current node in list

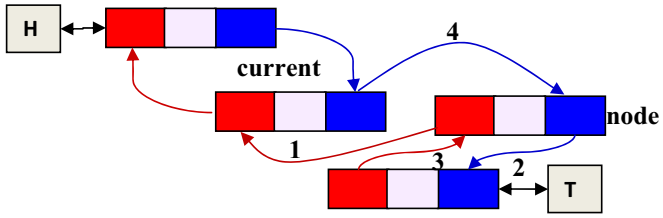

(b) Resulted list

FIGURE 4.3. Insertion after the current node in a double-chained list

Algorithm 10 Insert node $X_{i,j}$ after current node

`InsertAfter`(*node, current*)
Input: *node*, *current*
Output: insert node $X_{i,j}$ after current
node->previous=current;
node->next=current->next;
current->next->previous=node;
current->next=node;

1. using a backward connection (drawn in red), we link our new node to the current one

2. using a forward connection (blue color), we link our new node to the node succeeding the current node. At this step, we reconstructed half of the links and our new node is connected backward and forward in the list.

3. using a backward connection (red color), we link the the node succeeding the current node to our new node

4. using a forward connection (blue color), we link the current to our new node.

The resulted list is one element longer and it has all the links correctly established, as shown in Figure 4.3(b).

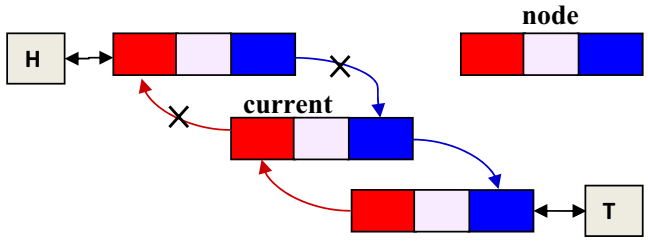

(a) Insert node before the current node in list

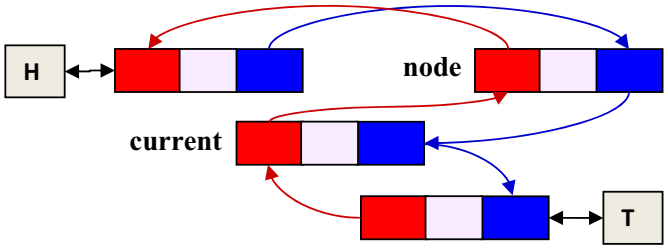

(b) Resulted list

FIGURE 4.4. Insertion before the current node in a double-chained list

Algorithm 11 Insert node $X_{i,j}$ before current node

`InsertBefore`(*node, current*) **Input**: *node*, *current*
Output: insert node $X_{i,j}$ before current
node->previous=current->previous;
current->previous->next=node;
node->next=current;
current->previous=node;

To organize the list elements in increasing order of T, we have to use a sorting algorithm. To insert new nodes into the list, an *insertion sort* algorithm could be used. To perform only the reordering of the elements in the list, a *comparison sort* algorithm could be employed. Our particular sorting algorithm is called *UpdateList* and combines both of them. Since our list is double chained, the algorithm has a forward and a backward sorting procedure. In Figure 4.5 we illustrate, on a numerical example, how the sorting procedure works. We respect the color code

Algorithm 12 UpdateList

```
UpdateList(node,T, head, tail)
Input: node,T, head, tail
Output: updated list of T values
v ← T[node.row][node.col]; crt ← node
if (crt.previous == head) then                    /* first element of the list */
    v_prev ← big number
else
    v_prev = T[(node.previous).row][(node.previous).col]
if (crt.next==tail) then                          /* last element of the list */
    v_next ← big number
else
    v_next = T[(node.next).row][(node.next).col]
if ((v_prev ≤ v) & (v ≤ v_next)) then do nothing;
else if ((v_prev > v) & (v_next < v)) then List messed up;
else
    if (v_prev > v) then                                  /* Going backward  */
        crt=node.previous;
        repeat
            if (crt.previous.previous==NULL) then
                RemoveNode(node); InsertBefore(node,crt);
            else
                crt=crt.previous
        until (v < T[crt.row][crt.col]) ;
        if (node==head) then
            RemoveNode(node); InsertBefore(node,crt);
        else
            RemoveNode(node); InsertAfter(node,crt);
    else                                          /* Going forward (v_prev ≤ v) */
        crt=node.next;
        repeat
            if (crt.next.next==NULL) then
                RemoveNode(node); InsertAfter(node,crt)
            else
                crt=crt.next
        until (v < T[crt.row][crt.col]) ;
        if (node==head) then
            RemoveNode(node); InsertAfter(node,crt);
        else
            RemoveNode(node); InsertBefore(node,crt);
```

defined in Chapter 2, in the introduction of Fast Marching algorithm: red for accepted node, orange for narrow band node and black for far away node. A pseudo-code version of the algorithm is presented in Algorithm 12.

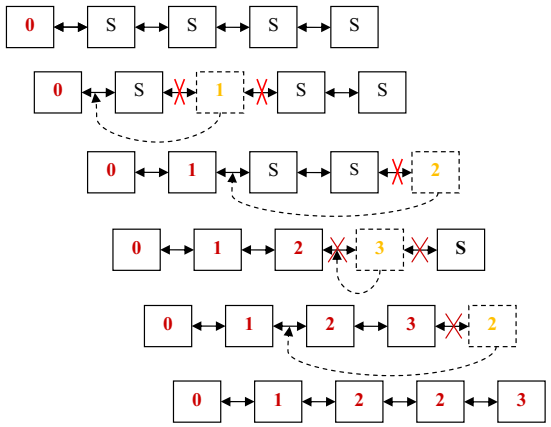

FIGURE 4.5. Sort algorithm

Our target is to do a parallel implementation. We know that by decomposing the domain in sub-domains, we do not deal with a huge amount of nodes per sub-domain. Therefore, sorting algorithms will not be compelled to use large lists. For our formulation, the algorithm is easy to implement and stable. Since our lists are not large, our sorting algorithm is more efficient than most of the other simple $\mathcal{O}(n^2)$ algorithms, such as *bubble sort*. The number of comparisons that a *comparison sort* algorithm requires increases as a function of $nlog(n)$. Thus, the algorithm time is in between $\mathcal{O}(nlog(n))$ and $\mathcal{O}(\frac{n^2}{4})$ [15]. By n we denote the number of elements to be sorted.

4.2 Sequential Numerical Experiments

We want to study the behavior of the Fast Marching algorithm on the following test grid sizes: 6×6, 10×10, 30×30, 60×60, 100×100, 120×120, 150×150, 164×164,

180×180, 200×200, 240×240, 256×256, 300×300, 600×600, with only one starting node in one of the corners.

4.2.1 Complexity of the Algorithm

Let N be the leading dimension of our grid size, i.e. for a grid of 300×300, N is 300. An efficient version of the Fast Marching depends on how quickly we manage to find the node with the smallest T in the *narrow band*. The main loop of the Fast Marching algorithm is characterized by:

- $\mathcal{O}(N^2)$ complexity for computing T at all the grid points;
- complexity in between $\mathcal{O}(N \log N)$ and $\mathcal{O}(N^2)$ for the sorting algorithm, due to the growth of narrow band size with $\mathcal{O}(N)$ complexity.

Therefore, the Fast Marching algorithm has a computational cost between $\mathcal{O}(N^3)$ and $\mathcal{O}(N^4)$, or actually $\mathcal{O}(N^3 \log N)$ and $\mathcal{O}(N^4)$. This is comparable with the complexity achieved by Sethian in [23], using a heap priority queue based on a tree.

To verify this assumption, let us analyze the time in the Fast Marching algorithm in terms of the image size, and graph this dependency. In Figure 4.6, the computing time in the Fast Marching algorithm versus the leading dimension of the grid size is drawn in red, while the green line represents a linear least square fitting. It is obvious that the approximation line is in between $\mathcal{O}(N^3)$ and $\mathcal{O}(N^4)$. Thus our theoretical estimation is confirmed experimentally.

4.2.2 Approximation Error

Based on the grid sizes listed above, we run some numerical experiments trying to approximate the solution of the modeled problem for which we know the exact

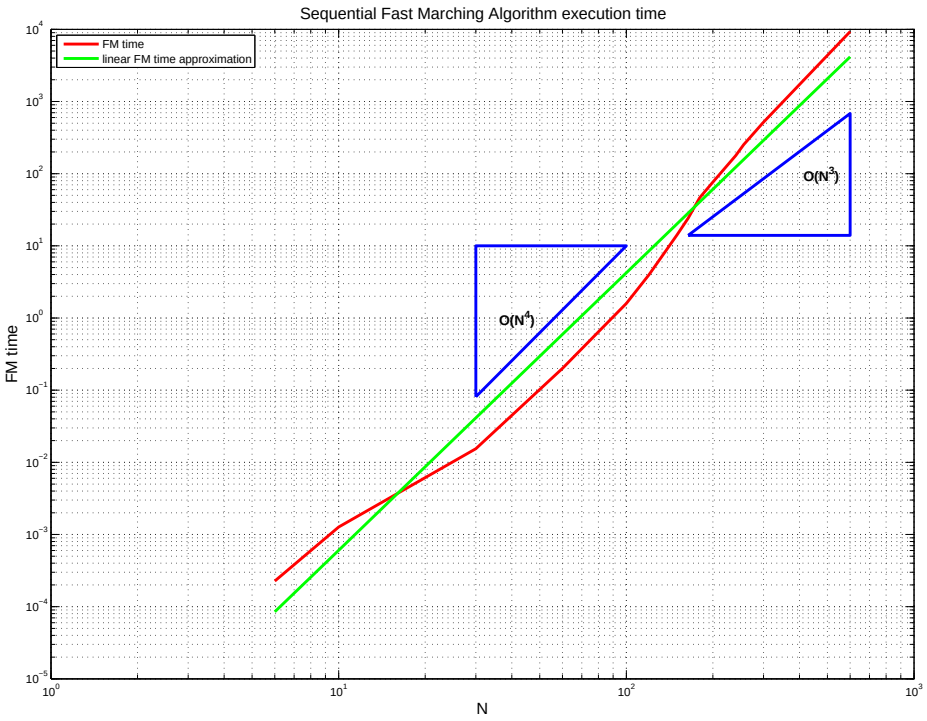

FIGURE 4.6. Sequential Fast Marching Algorithm Complexity

solution. Let T denote the exact solution and $\hat{T}$ the solution computed by the Fast Marching Method. We can express the error on the field as:

$$E_{\infty,\Delta x} = \max_{i,j} |T_{i,j} - \hat{T}_{i,j}|, \quad E_{1,\Delta x} = (\Delta x)^2 \sum_{i,j} |T_{i,j} - \hat{T}_{i,j}| \tag{4.1}$$

and the gradient error as:

$$G_{\infty,\Delta x} = \max_{i,j} \left| |\nabla T_{i,j}| - 1 \right|, \quad G_{1,\Delta x} = (\Delta x)^2 \sum_{i,j} \left| |\nabla T_{i,j}| - 1 \right| \tag{4.2}$$

In Figure 4.7 we present the $\| |\nabla T| - 1 \|_\infty$. The graph presents the gradient error versus the leading dimension N of the grid size. We can see that the gradient error is in $\mathcal{O}(N^{-\frac{3}{2}})$.

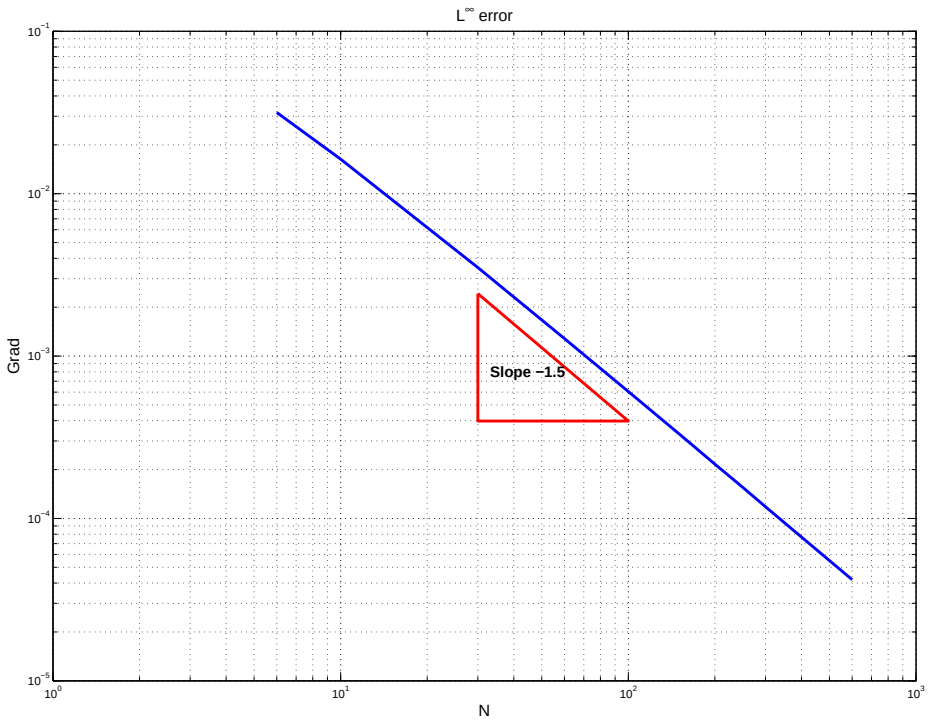

FIGURE 4.7. L^∞ error

4.2.3 Numerical Results

Consider an image with the size 100×100 and run the Fast Marching algorithm for one processor. Figure 4.8 and Figure 4.9 represent the numerical solutions of the Eikonal equation with initial conditions imposed at one node corner and at two opposite node-corners. In Figure 4.8(a) and Figure 4.9(a) we can follow the evolution of the level lines from the starting node(s) toward the boundary of the domain. For a better illustration of the solution's shape in both cases, we construct the elevated surface of the solution and plot it on the discretization grid (see Figure 4.8(b) and Figure 4.9(b)). The second case is relevant for the intersection of gradient directions of T, and how the solution is computed in this situation (see Figure 4.9(b)).

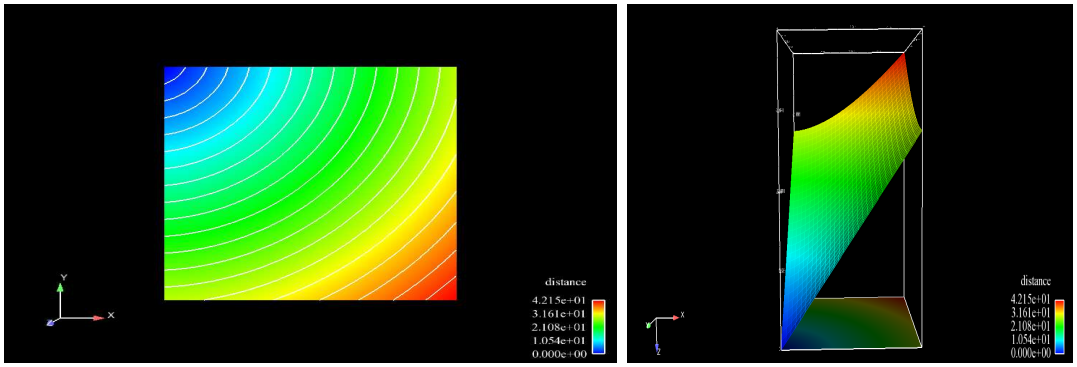

(a) (b)

FIGURE 4.8. Solution's shape for one processor - one starting node

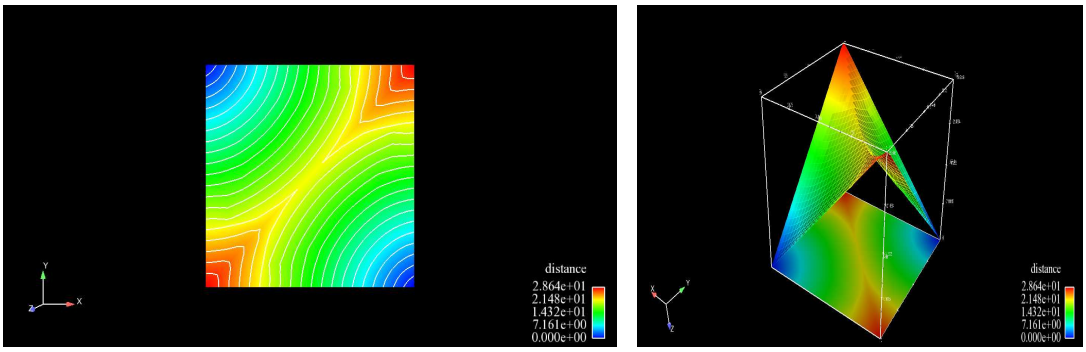

(a) (b)

FIGURE 4.9. Solution's shape for one processor - two starting nodes

4.3 Background on Parallel Computing

To solve a problem numerically, we construct an algorithm as a discrete series of instructions. Usually, an algorithm is implemented to be sequential, that is, instructions are executed one at a time, in order of appearance, on a single Central Processing Unit (CPU). For the parallel implementation, we use multiple processing units simultaneously. Our problem is divided into sub-problems, each sub-problem being assigned to a different processing unit. Furthermore, each sub-problem is divided into a series of instructions or tasks (a task is a program or program-like set of instructions that is executed by a processor). Thus, each CPU can execute

its part of the algorithm concurrently (in parallel) with the others. Resources that we can use as processing elements include a single computer with multiple processors, several networked computers, specialized hardware, or any combination of the above [20].

Parallel computing has its own advantages:

- we can solve large scale problems, since we can overcome memory constraints (single computers have finite memory resources),
- we can save time executing multiple things at the same time,
- we can save money by using available computing resources on a network or over Internet instead of buying the machines.

Nevertheless, some disadvantages are also worth mentioning:

- parallel computing programs are more difficult to write than sequential codes,
- communication and synchronization between the sub-problems is typically one of the greatest barriers to getting good performance.

From the architecture point of view, the parallel computers are classified as: shared memory, distributed memory and hybrid distributed-shared memory parallel computers.

In **shared memory architecture** multiple processors can operate independently, but share the same memory resources as shown in Figure 4.10 (picture reproduced from [20]). If one of the processors changes a location in memory, the change is visible to all the other processors.

In **distributed memory architecture** each processor has its own memory. To access the memory of another processor, a communication network is required as presented in Figure 4.11 (reproduced from [20]).

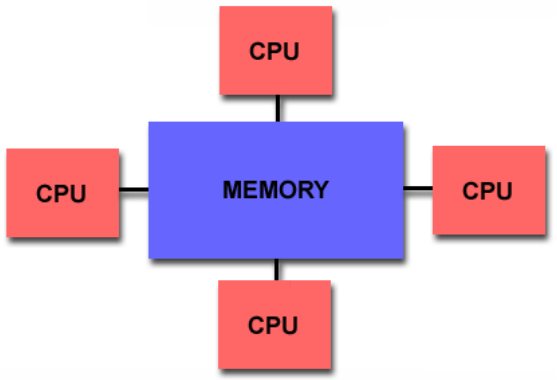

FIGURE 4.10. Shared memory architecture

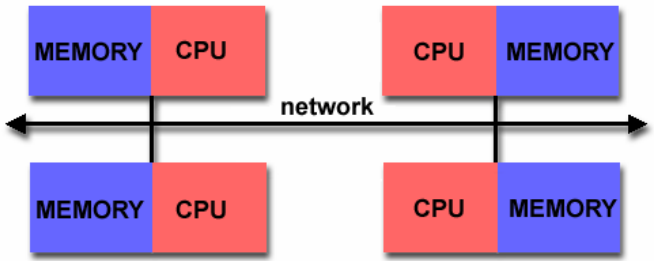

FIGURE 4.11. Distributed memory architecture

The **hybrid distributed-share memory architecture** is a combination of the previously presented approaches and is illustrated in Figure 4.12 (reproduced from [20]). Each processor has its own local memory and there is also a memory space shared by all processors. Accesses to local memory are typically faster than accesses to the shared memory [12].

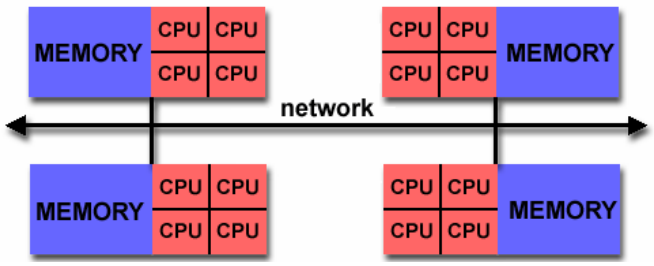

FIGURE 4.12. Hybrid shared-distributed memory architecture

Parallel programming models were created to program parallel computers. They represent an abstraction of real life hardware and memory architectures. They can generally be divided into: shared memory, threads, message passing,

data parallel, hybrid. Models are machine/architecture independent; each of them can be implemented on any hardware given appropriate operating system support. In the following paragraphs, we focus on two of the models: shared memory and message passing.

The **shared-memory programming model** inherited the properties of shared memory architecture, where tasks share a common address space, which they read and write asynchronously. From the programmer standpoint, in this model "it is not necessary to take care of the communication between tasks, but it is hard to understand and manage data locality" [20]. At the language level we find: shared variables, semaphores for synchronization, mutual exclusion, and monitors/locks.

The **message passing model** is defined as a set of processes having only local memory. Processes exchange data by sending and receiving messages. Data transfer usually requires cooperative operations to be performed by each process. For example, a send operation must have a matching receive operation. From the programming perspective, message passing implementations commonly comprise a library of subroutines embedded in source code. The programmer is responsible for determining all parallelism. **Message Passing Interface** (MPI) was created in 1994 from the necessity of a standard interface for message passing implementations. "The MPI is an industry standard developed by a consortium of corporations, government labs and universities. MPI is a message-passing library, a collection of routines for facilitating communication (exchange of data and synchronization of tasks) among the processors in a distributed-memory parallel program" [14].

Every MPI program must contain the preprocessor directive *#include "mpi.h"*, the initialization and termination of the MPI execution environment. We present all of this on a simple C-example (Algorithm 13):

Algorithm 13 Basic MPI example

```
#include “mpi.h”
#include <stdio.h>
int main( int argc, char *argv[])
{
MPI_Init(&argc, &argv);
printf(”Hello, World!”);
MPI_Finalize();
return 0;
}
```

MPI programs are made up of communicating processes. Each process has its own address space containing its own attributes such as *rank* and *size* (argc, argv and so on). The default communicator is *MPI_COMM_WORLD*. MPI provides functions to interact with it and the most used are those that give us the number of processors and the rank of each processor (see Example 14).

Algorithm 14 MPI functions

```
...
int size, rank;
MPI_Init(&argc,&argv);
...
MPI_Comm_size(MPI_COMM_WORLD, &size);
MPI_Comm_rank(MPI_COMM_WORLD, &rank);
...
MPI_Finalize();
```

When programming in MPI, we should be careful with the communications pattern to avoid getting into a **deadlock**. A **deadlock** is a situation where the dependencies between processors are cyclic: a processor cannot proceed because it is waiting on another processor, which is, itself, waiting on the first processor. Since MPI does not have timeouts, this job is killed only when our time in the queue runs out. For example, let us consider two processors that are trying to communicate through MPI, as shown in Figure 4.13 (reproduced from [20]).

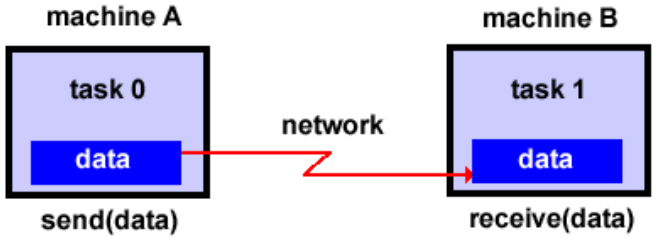

FIGURE 4.13. MPI communication between 2 processors

We can illustrate the deadlock by considering the pseudo-code example Algorithm 15.

Algorithm 15 Deadlock example

```
...
if (rank==0) then
    Recv(recvbuf, 1);
    Send(sendbuf,1);
else/* rank==1                                                    */
    Recv(recvbuf, 0);
    Send(sendbuf, 0);
...
```

For instance, deadlocks happen when each processor gets stuck during its receive operation while waiting for the corresponding send operation on the other processor to complete.

One possible solution to this problem would be to match each send operation to a corresponding receive operation before the other send operation starts, as shown in Algorithm 16.

Algorithm 16 Deadlock solution - version 1

```
...
if (rank==0) then
    Send(sendbuf,1);
    Recv(recvbuf, 1);
else
    Recv(recvbuf, 0);
    Send(sendbuf, 0);
...
```

Another solution consists in using non-blocking versions of the common send and receive operations. These versions are known in the MPI core as *ISend* and

IRecv. The Send/Receive pair does not block in this case, but we must check for completion of communications before using the buffers as shown in Algorithm 17.

Algorithm 17 Deadlock solution - version 2

```
...
if (rank==0) then
    ISend(sendbuf,1);
    IRecv(recvbuf, 1);
else
    IRecv(recvbuf, 0);
    ISend(sendbuf, 0);
Wait-all; ...
```

In combination with MPI, to create the parallel implementation of the Fast Marching algorithm, we use PETSC. **PETSc** (Portable, Extensible Toolkit for Scientific Computation) provides sets of tools for parallel (as well as serial) numerical solutions of partial differential equations that require solving large-scale, sparse nonlinear systems of equations. "PETSc provides many of the mechanisms needed within parallel application codes, such as simple parallel matrix and vector assembly routines that allow the overlap of communication and computation. In addition, PETSc includes support for parallel distributed arrays useful for finite difference methods" [19]. We discuss the parallel distributed arrays and all other PETSc related topics in the following sections.

4.4 Parallel Implementation

In many applications, we need both global and local representations of a vector. The difference between global and local vectors is illustrated graphically in Figure 4.14:

- in the global vector, each processor stores a local set of vertices and each vertex is owned by exactly one processor (see Figure 4.14(a)),
- in the local vector, each processor stores a local set of vertices as well as ghost nodes from neighboring processors (Figure 4.14(b)).

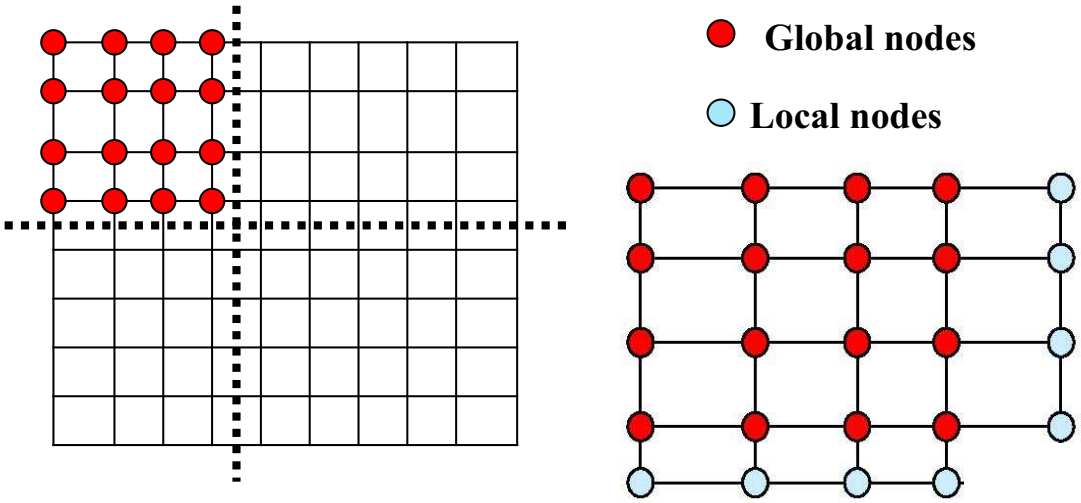

(a) Global vector (b) Local vector

FIGURE 4.14. Global and Local Vectors

PETSc provides routines to help map indices from a local numbering scheme to the PETSc global numbering scheme. We need this kind of mapping to read the initial mesh and write the final solution image. In PETSc User Manual the orderings for a two-dimensional distributed array, divided among four processors, is presented as in Figure 4.15 [19].

Distributed arrays (DAs) are intended for use with logically regular rectangular grids when communication of nonlocal data is needed before certain local computations can occur [19]. The PETSc DA object manages the parallel communication required, while working with data stored in regular arrays. The actual data is stored in appropriately sized vector objects; the DA object only contains the parallel data layout information and communication information; however it may be

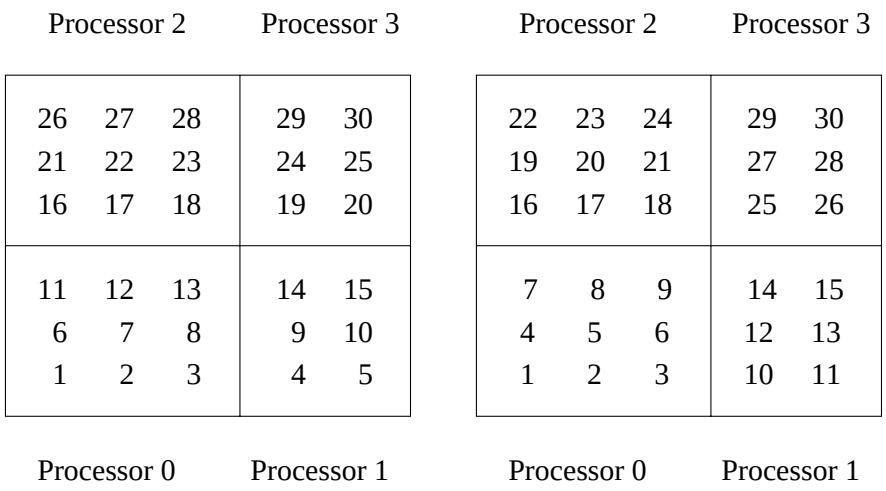

(a) Natural ordering (b) PETSC ordering

FIGURE 4.15. Natural and PETSC ordering for a Distributed Array

used to create vectors/matrices with the proper layout. Each DA object defines the layout of two vectors: a distributed global vector and a local vector that includes room for the appropriate ghost points. A distributed array communication data structure in two dimensions can be created using the command:

```
DACreate2d (MPI Comm comm, DAPeriodicType wrap,DAStencilType st,
    int M, int N, int m,int n,int dof,int s,int *lx,int *ly,DA *da),
```

where M and N are the global numbers of grid points in each direction, while m and n denote the process partition in each direction, $m \times n$ being the number of processes specified in the MPI communicator *comm* [19]. Instead of specifying the process layout, one may use PETSC DECIDE for m and n. Therefore, PETSc will determine the partition using MPI. The type of periodicity of the array is specified by *wrap*. dof indicates the number of degrees of freedom at each array point, and s is the stencil width (i.e., the width of the ghost point region). The optional arrays lx and ly may contain the number of nodes along the x and y axis for each cell; the dimension of lx is m and the dimension of ly is n. Rather than defining each argument, PETSC_NULL may be passed to the function, allowing the processor to

pick the appropriate values by itself. Two types of distributed array communication data structures can be created, as specified by *st*: DA_STENCIL_STAR, and DA_STENCIL_BOX. The type of stencil used is $DA\_STENCIL\_STAR$, which is the standard 5-points stencil, with width 1. We notice that this type of stencil will save us communication time, since some of the ghost-nodes are ignored.

We emphasize that a distributed array provides the information needed to communicate the ghost value information between processes. At certain stages of the applications, there is a need to work on a local portion of the vector, including the ghost points. For more information on how to make the connection between local and global vectors check Appendix B.

In the parallel Fast Marching Algorithm, we consider two distributed arrays: one for the $T_{i,j}$ and one for the flags $Fl_{i,j}$, for all $0 \leq i \leq N$ and $0 \leq j \leq M$. The structure used in the parallel implementation has the following format, and for clarity, consider the graphical representation in Figure 4.16:

```
typedef struct GeomStruct {
  int Nx, Ny;
  int xs, ys, xm, ym, ghostx, ghosty, ghostxw, ghostyw;
  int rank;
  struct neigh {
    int left, right, top, bottom;
      } Neighbor;
  DA Val_DA;
  DA Flg_DA;
} GeomStruct;
```

where Nx and Ny denote the global dimensions, and for each processor, we have the local dimensions limits xs, xm, and ys, ym, respectively. By $ghostx$, $ghosty$, $ghostxw$, $ghostyw$ we denote the ghost-zone rows and columns dimensions. Also for each processor we need to define its possible neighbors: left, right, top and bottom, as in structure *Neighbor*.

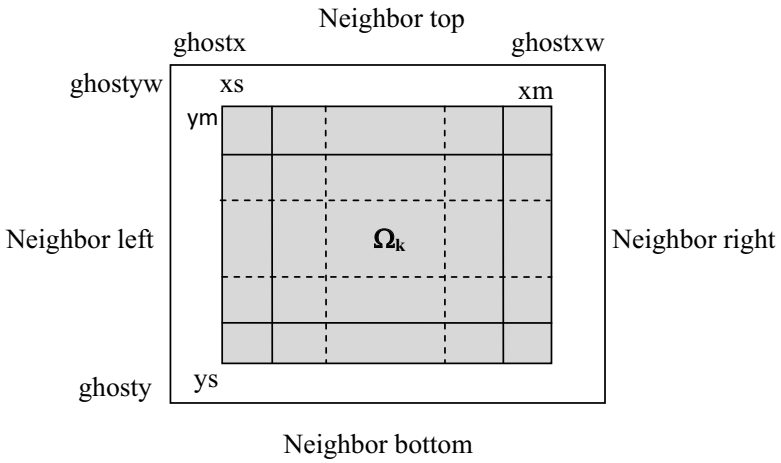

FIGURE 4.16. Domain structure with the points and ghost-points limits

As presented in Algorithm 4, the ghost point synchronization procedure is the part where we can apply different strategies in order to restart the Fast Marching algorithm. The purpose of such strategies is to assure the monotonicity and upwind nature of the algorithm even when we have inter-domain communications. The difference between these strategies is in the way the nodes in the boundary are computed using the ghost-points. We developed several strategies to accomplish this task, among which the following are the most viable:

1. Ordered Overlap strategy: group the overlapping nodes of each sub-domain in a sorted list and use this list to recompute the boundary values;

2. Fast Sweeping strategy: perform a Fast Sweeping [28] at the interfaces and update the overlapping regions of the sub-domains.

The advantage of these strategies is to not keep a distributed list for the *narrow band*, which would require much more communication time.

4.4.1 Ordered Overlap Strategy

The key observation for the implementation of this strategy is that, after the local Fast Marching, the algorithm satisfies the upwinding property on the whole domain. Taking advantage of this observation, we decided to process each edge after the other, in order to simplify our implementation:

- go through the ghost-nodes in increasing order of T and recompute T at each boundary node in Ω_k (solve the local Eikonal equations),
- reconstruct the sets of *accepted*, *narrow band* and *far away* points.

Let us consider the case presented in Figure 4.17, where we have a top row ghost-zone and focus on $T^{n+\frac{1}{2}}(X_{i,j})$. Up to a symmetry or rotation in the sub-domain all the other cases can be treated in the same way.

There is no need to solve the local Eikonal equations in the cases when internal sub-domain nodes are involved, because the solutions of the local Eikonal equations involving internal nodes are the same as the ones computed at the end of local Fast Marching algorithm. In order to avoid these unnecessary re-computations, we can use a special distance function, called *distanceNB*, to solve the local Eikonal equations only based on the ghost-nodes and the boundary of the sub-domain, ignoring the internal nodes. For example, in Figure 4.17, for node $X_{i,j}$, we consider only the local Eikonal equations in first quadrant and second quadrant, based on $X_{i\pm1,j}$, $X_{i,j+1}$, graphically drawn as the two up-right triangles.

Another important observation is that the Fast Marching preserves the upwind structure at all its nodes. Since the ghost-point update procedure is performed at

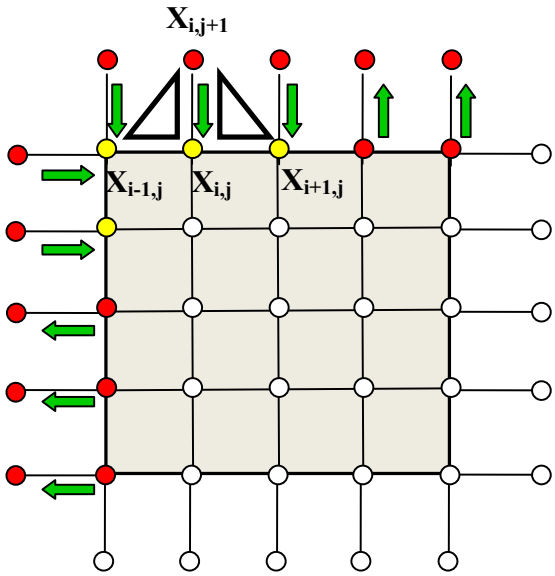

FIGURE 4.17. Possible situation in ordered overlap strategy

the end of local Fast Marching, the ghost-nodes of each sub-domain already satisfy the upwind condition and we can optimize the algorithm using the order of the ghost-nodes. At this point we need to distinguish between the ghost-points with or without influence on the neighbors. The ghost-nodes at which the gradient of T is pointing toward the sub-domain are called **sources**. More precisely:

Definition 4.1. *For $X_{i,j} \in \partial\Omega_k$, $X_{i,j+1} \in \tilde{\Omega}_k$ and $X_{i,j+1} \in G(X_{i,j})$, if $T(X_{i,j}) > T(X_{i,j+1})$, then $X_{i,j+1}$ is called a **source** node.*

Let N_b be the number of sources and let X_{i_l,j_l} be a source node, with $l = 0, \ldots, N_b$, such that for any $b < l$, we have $T(X_{i_b,j_b}) \leq T(X_{i_l,j_l})$.
Since our algorithm works edge by edge, using only the source nodes we can reduce the number of local Eikonal equations to solve. The optimized version of the ordered overlap algorithm is presented in Algorithm 18.

Remark 4.2. *For this strategy we remark that:*

Algorithm 18 Ordered Overlap Algorithm

begin

find the source nodes,
order sources in increasing order of T,
in sources's order, solve the local Eikonal equations at boundary node in Ω_k,
reconstruct **NB**, **A**, **FA** sets.

end

1. *The algorithm is equivalent to Fast Marching on a $N_b \times 2$ domain, where N_b is the number of sources. In this setting, the ghost-nodes represent the accepted nodes and the sub-domain boundary represents the narrow band nodes.*

2. *In the light of all the above observations, by applying the algorithm edge by edge we do not need to reconstruct narrow band for the whole boundary or order the sources of the whole boundary (four edges). The sources order is inherited from the previous steps of the algorithm. Thus, we save computational time.*

Basically $T^{n+\frac{1}{2}}(X_{i,j})$ is a function of $T^{n+\frac{1}{2}}(X_{i-1,j})$, $T^{n+\frac{1}{2}}(X_{i+1,j})$ and $T^{n}(G(X_{i,j}))$. Using the upwind condition, translated in the order of sources, we need to compute $T^{n+\frac{1}{2}}(X_{i,j})$ such that $T^{n+\frac{1}{2}}(X_{i,j})$ solves the local Eikonal equations in the $N_b \times 2$ domain. This way, we have the upwind condition satisfied inside the sub-domains and also between sub-domains. Since we apply the algorithm edge by edge, on each edge the type of overlap (row or column) and the order of sources are the things that make the implementation different. Therefore, we create a function for vertical processing (neighbor sub-domains located at the left or right of the sub-domain), and a function for horizontal processing (neighbor sub-domains located at the top or bottom of the sub-domain). In Algorithm 19 we present the steps for a row boundary c.

If, at the end of the Ordered Overlap algorithm, during reconstruction procedure,

we do not have any node added to the narrow band, then we set the minimum of the recomputed T on the narrow band to S. Similarly, the maximum of the recomputed T on the narrow band is set to -1.0.

Algorithm 19 Boundary recomputation based on ghost-points

```
UpdatedGhostH(geom, c, T, Fl, source, head, tail)
Input: geom, c, T, Fl, source, head, tail
Output: recomputed NB values
if (Fl[i][c]!=0) then
    if (source[i] >= T[i][c]) then
        if (Fl[i][c]!=1) then
            if (Fl[i][c]!=2) then
                Fl[a][c]=0;
    else
        Fl[i][c]=1;
        prt=FindPointer(i,c, head, tail);
        T[i][c]=distanceNB(i,c,T,geom);
        UpdateList(prt,T, head, tail);
if (no narrow band point) then
    minmax=-1;
else
    minmax= T[i][c];
return minmax;
```

4.4.2 Fast Sweeping Strategy

We want to apply the Fast Sweeping algorithm to update only the boundary of each sub-domain. Following Remark 4.2, part 1, we can update the boundary at each edge separately. Since the boundary is just a segment, i.e row or column, the 2D domain is reduced to a 1D domain. Thus, only two sweeps are necessary to compute the right values.

In general we need to do :

- 1^{st} sweep: for $i = 0$ to n, compute T at the boundary using the ghost-nodes and save the minimum between $T_k^n(X_{i,j})$ and $T_k^{n+\frac{1}{2}}(X_{i,j})$,

- 2^{nd} sweep: for $i = n$ to 0, compute T at the boundary using the ghost-nodes and save the minimum between $T_k^n(X_{i,j})$ and $T_k^{n+\frac{1}{2}}(X_{i,j})$,

- save the minimum between the T at 1^{st} and 2^{nd} sweep.

The pseudo-code of the algorithm is presented in Algorithm 20.

Algorithm 20 Fast Sweeping Boundary Update

```
FastSweepingUpdated(geom, n, c, T, Fl, ghost, head, tail)
Input: geom,n, c, T, Fl, ghost, head, tail
Output: recomputed NB
for i ← 0 to n do
    k[i]=FastSweep(geom,n,m c, T, Fl, ghost, head, tail);
end
for i ← n to 0 do
    l[i]=FastSweep(geom,n,m c, T, Fl, ghost, head, tail);
    sol[i]= min(k[i],l[i]);
    T[i][c]=sol[i];
    prt=FindPointer(i,c, head, tail);
    UpdateList(prt,T, head, tail);
end
return T;
```

4.4.3 Flags Reconstruction

In order to restart the Fast Marching algorithm, we need to reconstruct the **NB**, **A** and **FA** sets over the whole sub-domains. Thus, after applying one of the strategies for computing T at the boundary based on the ghost points, we need to:

- save the minimum/maximum of T over the boundaries (all four edges) of the sub-domain. The algorithm for this part is the one that finds the minimum and maximum in a vector. If the vector is empty (no narrow band nodes in that sub-domain), then the default value for the maximum is $max = -1.0$ and for the minimum is $min = S$.

- use the minimum/maximum of T over the boundaries to update the flags in the whole sub-domain as described in Algorithm 21.

Algorithm 21 Flag update on the sub-domains

```
UpdatedPtsFlag(n, m, min, max, T, Fl)
Input: n, m, min, max, T, Fl
Output: reconstructed flag list Fl
if ((min! = S) && (max! = −1)) then
    for i ← 0 to n do
        for j ← 0 to m do
            if (Fl[i][j]!=1) then
                if (T[i][j] < min) then
                    Fl[i][j]=0;
                else if (T[i][j] ≥ max) then
                    Fl[i][j]=2;
                else /* min ≤ T[i][j] < max                    */
                    Fl[i][j]=1;
        end
    end
end
return Fl;
```

4.4.4 Stopping Criteria

Modeling the problem numerically, we introduce **numerical error**. The numerical error is caused by the finite precision of computations involving floating-point values (round-off error) and by the difference between the exact mathematical solution and the approximate solution obtained through discretization (truncation error). We introduce the notion of **numerical stability**: an algorithm is numerically stable if an error, once it is generated, does not grow too much during the calculation. This is only possible if the problem is well-conditioned, meaning that the solution changes only a small amount if the problem data is modified by a small amount. Indeed, if a problem is ill-conditioned, then any error in the data will grow a substantially.

In iterative methods, we start from an initial guess, and form successive approximations that converge to the exact solution only in the limit. Let T^n and T^{n+1} denote the solution computed by the parallel Fast Marching algorithm at iteration

n and $n+1$. Then, the global error after each iteration is:

$$e_n = \sqrt{\int_\Omega (T^n - T^{n+1})^2} \cong \frac{1}{N * M} \sqrt{\sum_{i,j} (T^n_{i,j} - T^{n+1}_{i,j})^2}$$

Naively, we would iterate until $e_n = 0$. But this approach can bring us to an infinite number of iterations. Therefore, a **convergence criterion** needs to be specified in order to decide when a sufficiently accurate solution has been found. In this respect, we consider our solution approximation to be accurate when it changes within some imposed tolerance after two consecutive iterations, i.e. $error = mathop\max_{i,j} |T^n_{i,j} - T^{n+1}_{i,j}|_\infty$. We define tolerance, ϵ, as a function of number of rows and columns, i.e. N and M, more precisely a function of discretization step h.

If $error > \epsilon$, then we keep iterating, trying to decrease the error, otherwise we stop the algorithm and save and display the results.

Practically, we observe that even when T at all the nodes is computed, the algorithm is still iterating, trying to minimize as much as possible the global error. This means that only the condition for the error being less than a certain tolerance is not enough. Let us apply the algorithm for 9 CPU's on a 6×6 image with two starting points on the top edge corners and analyze what happens to the error after a certain iteration. The algorithm is reaching convergence after 4 iterations, but the iterative process continue 3 more iterations, until the error is zero. As Figure 4.18 shows, after the fourth iteration the error starts oscillating, and in fact the information starts propagating from the boundaries back into the domain. We call this process the *back-propagation of the error*.

For a better understanding of the error back-propagation let us consider a bigger image (see Figure 4.19). In Figure 4.19(a) we can see how the level line are intersecting. In Figure 4.19(b), remark the formation of the computational oscillations

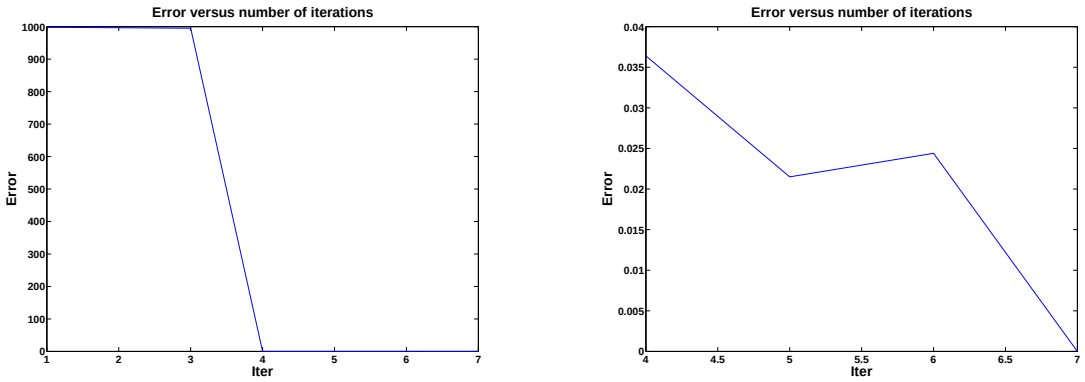

(a) Error (b) Error Zoom

FIGURE 4.18. Back-propagation of the error

at the intersection of the level lines and look how they are influencing the solution shape.

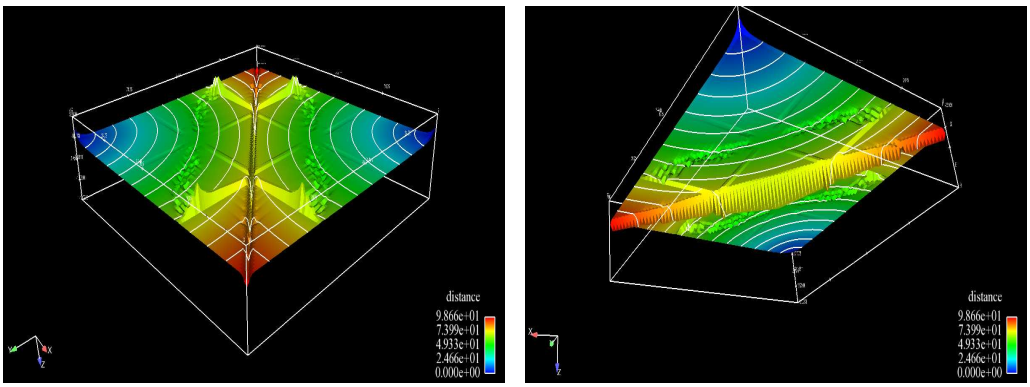

(a) Above view (b) Below view

FIGURE 4.19. Solution's shape for multiple processors case

To avoid the process of error back-propagation, we use the information covered in the gradient of error function for stopping the algorithm and define the residual error as:

$$r_n = \sqrt{\int_\Omega (|\nabla T^n| - 1)^2} \cong \frac{1}{h^2}\sqrt{\sum_{i,j}(|\nabla T^n_{i,j}| - 1)^2}.$$

We observe that after convergence, the residual error increases, as the error starts back-propagating.

In conclusion, convergence is decided based on the norm of the change in the

solution between successive iterations being less than some tolerance, or on the decrease of the residual norm, i.e. $e_n < \epsilon$ or $r_{n+1} < r_n$. Once the error is less than 1 (all the boundaries of all sub-domains are computed), we start monitoring the residual error and try to avoid its increase. If this is true we stop the algorithm and consider convergence reached.

When the parallel algorithm reaches convergence, the execution is stopped and all the information is saved in specific files. To read the initial image and write the final computations in a image format, we developed modules that perform the reading/writing in pgm format and also generate the files for visualization with EnSight. For a global view on the modules dependency and more implementation details, check Appendix A.

4.5 Parallel Numerical Experiments

All the simulations for the distributed memory implementations are performed on clusters:

- SCHUR: 64 CPUs, Dual 3.06 GHz Pentium IV Xeon Processors, Intel(R) C Compiler for 32-bit applications, Version 10.1, Gb Interconnect
- LONI machines - mostly on ERIC: 128 nodes, each node has two 2.33 GHz Dual Core Intel Xeon 64-bit Processors, 4 GB RAM per node, 4.77 TFlops Peak Performance, 10 Gb/sec Infniband network interface, Red Hat Enterprise Linux 4.

The implementations are MPI (MPICH2) based and PETSc based (PETSc version 2.3.3). The visualizations and post-processing are realized using EnSight Visualization Tool.

To make the parallel algorithms efficient, we mainly focus on minimizing the necessary time to reach the solution for our numeric implementation. Besides the algorithm's specific factors (the upwind nature of the numerical scheme, synchronization of the ghost-nodes), this minimization also depends on additional factors such as processor-memory communication and workload balancing, and input-output times. Communication between processors and memories takes time and influences the design of the algorithm; we are interested in an algorithm that minimizes the ratio of communication time to computation time for a given computer architecture.

To illustrate the efficiency of the parallel Fast Marching algorithm in the distributed memory implementations, we should analyze:

- the strong scalability - when the problem size is fixed and number of processors expands, and our goal is to minimize the time-to-solution;
- the weak scalability - when the problem size and the number of processors expand, and our goal is to achieve constant time-to-solution for larger problems.

We say that an algorithm is scalable, if its performance improves after adding hardware (CPU's), proportionally to the capacity added.

For this we need to define the test-cases that we use:

- **worst case scenario**: there is only one starting node in the whole domain (see Figure 4.20(a)). In this case, all the sub-domain computations depend on the ones from the starting sub-domain.
- **best case scenario**: there is a starting node in each sub-domain, i.e. number of starting nodes is (almost) equal to the number of sub-domains (see Figure

4.20(b)). In this case, each sub-domain influences and it is influenced by its neighbor sub-domain computations.

- **normal case scenario**: there are more than one starting nodes in the whole domain, but zero or one starting nodes per sub-domain. For illustration purposes, we consider the case with two starting nodes in opposite corners of the domain (see Figure 4.20(c)). All the sub-domain computations depend on the two starting sub-domains.

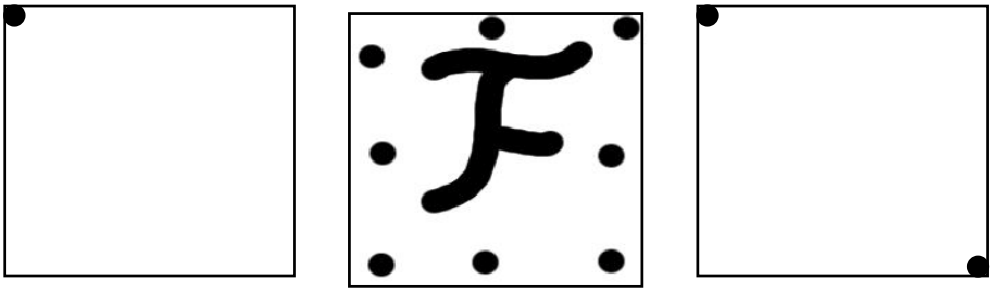

(a) Worst case (b) Best case (c) Normal case

FIGURE 4.20. Test cases

For the weak scalability, we choose to study the worst and normal case scenarios for the following grid sizes:

30×30	60×60	100×100	120×120	150×150	164×164
180×180	200×200	240×240	256×256	300×300	600×600

For the strong scalability we consider the best case scenario for an image size of 256×256.

The number of iterations on the parallel algorithm depends on the partition of CPU's along each direction. We come up with an estimate for the number of iterations.

Conjecture 4.3. *Let us consider that the initial domain is decomposed in $n \times m$ sub-domains (CPU's). The number of iterations iter is:*

$$iter < n + m.$$

Remark 4.4. *The number of iterations does not depend on the image size, but it depends on the processor decomposition. More precisely, the number of iterations is $n + m \pm 1$, where n and m represent the number of sub-domains in each direction; the $\pm$ allows us to take into account the stopping criteria.*

Of course the number of iterations can be estimated more precisely if we have a perfect square number of processors and if we know the type of image. For example, considering the grid sizes presented above, through simulations, we obtain the following number of iterations:

- in the worst case scenario the number of iterations is less or equal to $n+m-1$:

CPUs	Decomposition	Iterations
3	3×1	3
9	3×3	5
16	4×4	7
20	5×4	8
25	5×5	9
36	6×6	11

- in the normal case scenario: for perfect square number of processors ($n = m$), the number of iterations is close to $n + 1$ (in some cases the stopping criteria will bring us to n iterations):

CPUs	Decomposition	Iterations
4	2×2	2 (3)
9	3×3	3 (4)
16	4×4	4 (5)
25	5×5	5 (6)
36	6×6	6+1

4.5.1 Weak Scalability

In practice, weak scaling is really what we care the most, because the very reason we scale up the cluster size is to solve bigger problems (higher resolution models, more time steps).

We study weak scalability, we analyze our two strategies, Ordered Overlap and Fast Sweeping, in terms of time complexity, L^{∞} error and Fast Marching execution time with respect to number of CPU's.

We choose to study the worst and normal case scenarios for 50 CPU's for the following grid sizes:

30×30 60×60 100×100 120×120 150×150 164×164
180×180 200×200 240×240 256×256 300×300 600×600.

Fast Marching algorithm time complexity

For the Ordered Overlap strategy, the numerical results show that the time complexity is between $\mathcal{O}(N^2)$ and $\mathcal{O}(N^3)$, where N is the number of points in leading dimension, i.e. domain is $N \times N$. In Figure 4.21, we plot in red, on a logarithmic scale, the execution time of Fast Marching algorithm as a function of N, as resulted through simulations. The green line represents a linear least square fitting for our numerical data.

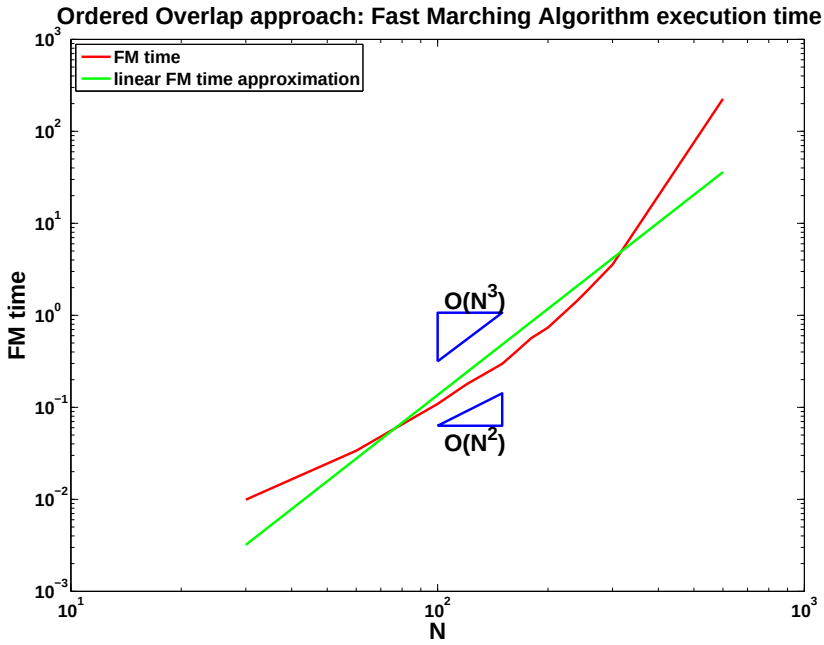

(a) Worst case

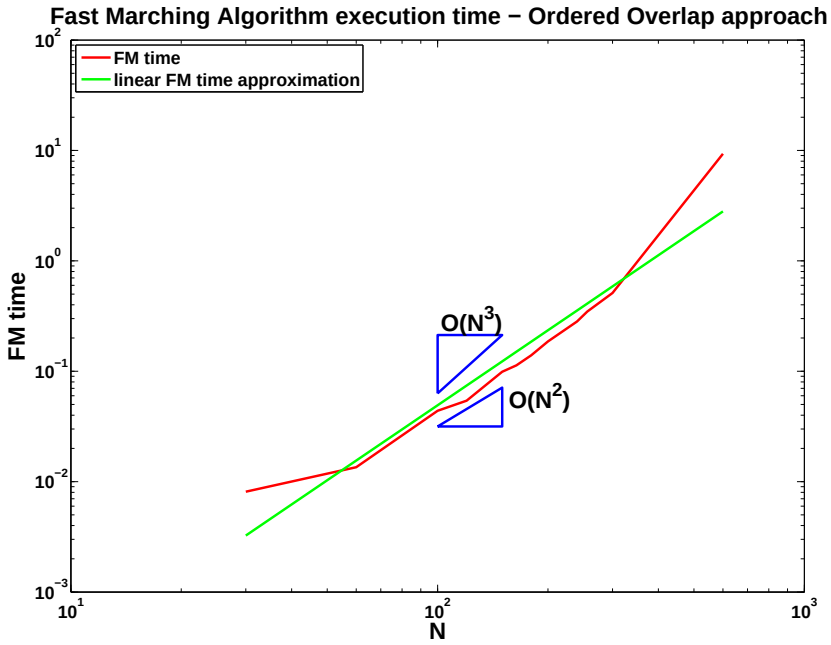

(b) Normal case

FIGURE 4.21. Time complexity for 50 CPU's - Ordered Overlap Strategy

For the **Fast Sweeping strategy**, we repeat the simulations on the same grid sizes for 50 CPU's and the results are presented in Figure 4.22. For the worst case

scenario (see Figure 4.22(a)), the time complexity of the Fast Marching algorithm in the Fast Sweeping strategy is almost $\mathcal{O}(N^2)$. For the best case scenario is between $\mathcal{O}(N^2)$ and $\mathcal{O}(N^3)$ (see Figure 4.22(b)).

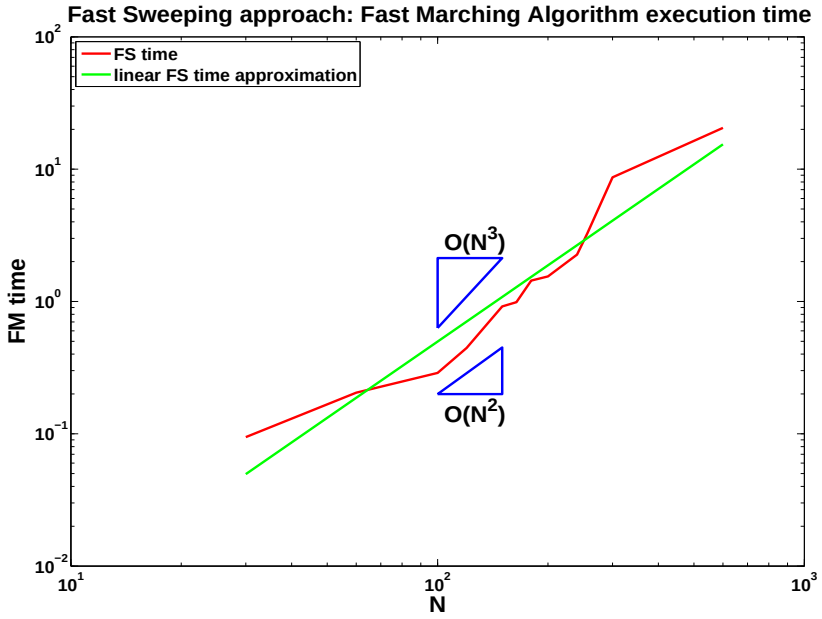

(a) Worst case

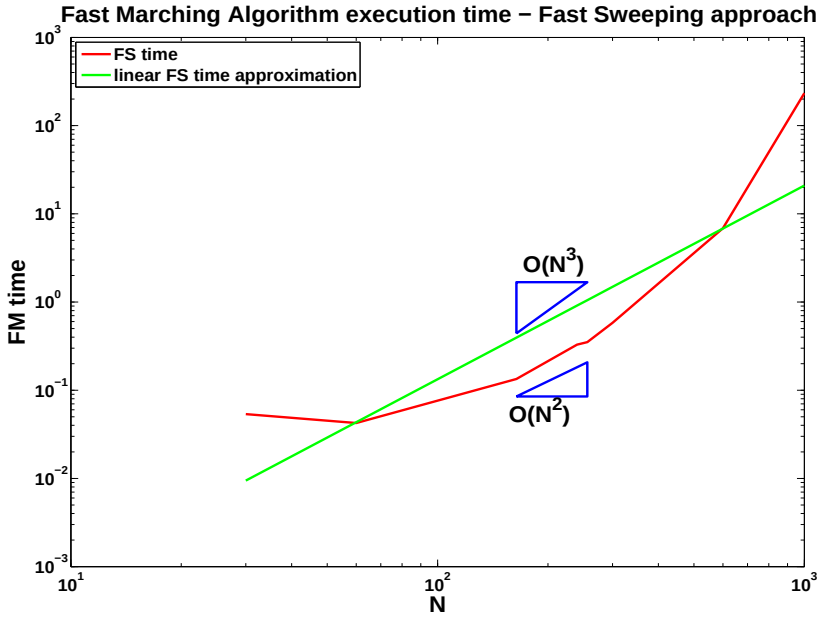

(b) Normal case

FIGURE 4.22. Time Complexity for 50 CPU's - Fast Sweeping Strategy

Comparing the Ordered Overlap strategy and Fast Sweeping strategy, we present the time complexity versus N, the number of points in leading dimension, in Figure 4.23. As we can see, for smaller images the Ordered Overlap strategy performs better (Figure 4.23(a)), but for large images the Fast Sweeping strategy gets better time (Figure 4.23(b)). The time complexity of Fast Sweeping strategy is closer to $\mathcal{O}(N^2)$ in the worst case scenario. Due to this fact, we can consider Fast Sweeping strategy better than Ordered Overlap strategy.

L^∞ error

In order to compute the L^∞ error we relate the gradient with N, the number of points in the leading dimension. In Figure 4.24 the blue line represents the gradient as a function of the leading dimension of the domain and the red line is the linear least square approximation of those simulations. We specify the value of the slope for each graph. We can see that the gradient is proportional to N^a, where a is the slope, $a < 0$. For the worst case scenario $a = -1.2661$ and for the normal case scenario $a = -1.0094$.

For the **Fast Sweeping strategy**, the results are presented in Figure 4.25 and in this case also the gradient is proportional to N^a, where $a < 0$ is the slope. For the worst case scenario $a = -0.4186$ and for the normal case scenario $a = -0.5745$.

Fast Marching execution time with respect to the number of processors

To study the execution time of the Fast Marching algorithm with respect to the number of CPU's, we consider the cases where the number of CPU's is a perfect square, i.e. 4, 9, 16, $\cdots$, and the image is a 256×256 with one and two starting nodes in the corners. Analyzing Figure 4.26 and Figure 4.27, we observe that the execution time of Fast Marching algorithm decreases with the number of proces-

sors, doubling the number of processors the time is reduced almost to half.

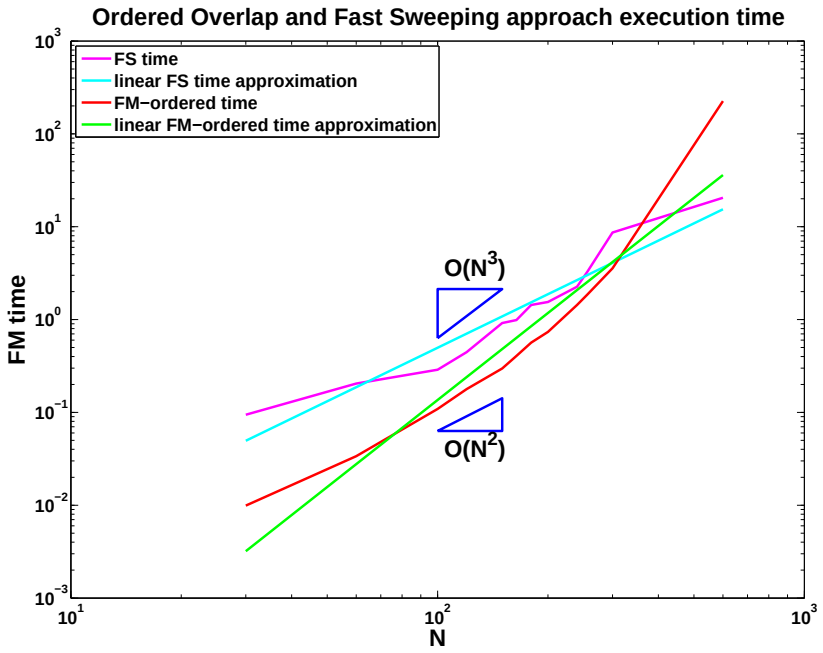

(a) Worst case

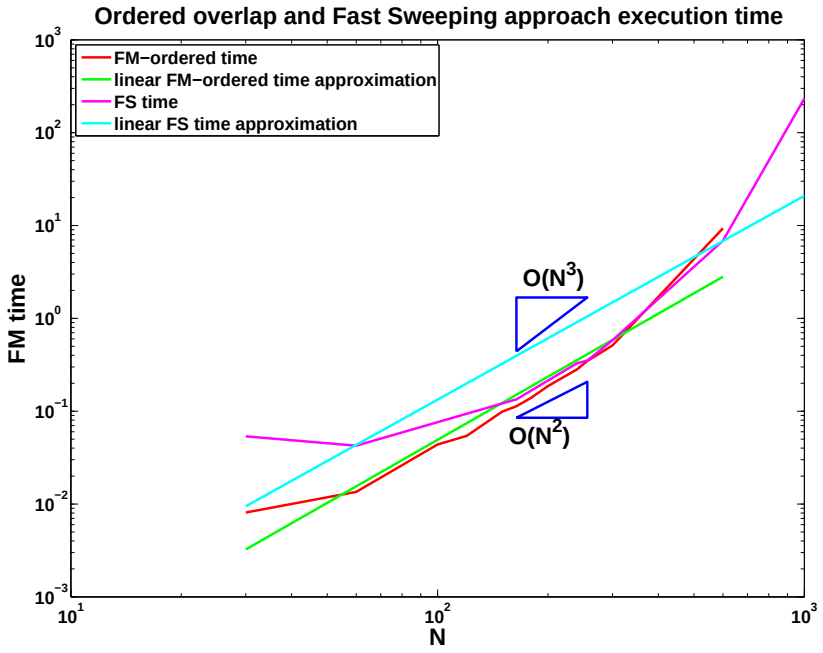

(b) Normal case

FIGURE 4.23. Time Complexity for 50 CPU's - Ordered Overlap and Fast Sweeping

4.5.2 Strong Scalability

Consider the best case scenario presented in Figure 4.20(b) for a grid of size 256×256. We expend the number of processors and analyze the execution time of the Fast Marching algorithm. We run the same simulation for our both strategies and present the results in Figure 4.28.

In both cases, we represent graphically the linear least square approximation for our data set with a green line. Analyzing the graphs, we can see how the execution time of Fast Marching algorithm decreases when we increase the number of CPUs. In oder words, if, for instance, we double the number of processors, we notice that the execution time is reduced to almost half of the initial one. This brings us to an almost linear scalability. To compare the Ordered Overlap approach with Fast Sweeping approach, we compute the slope of the linear least square approximation as shown in Figure 4.28. We conclude that the Fast Sweeping approach is faster than the Ordered Overlap approach. During the numerical experiments, for small number of processors we cannot say clearly which algorithm is faster. There are some factors, such as processors decomposition, number of CPU's (perfect square or not), type of the image (number of starting points), that will influence the output of the algorithm.

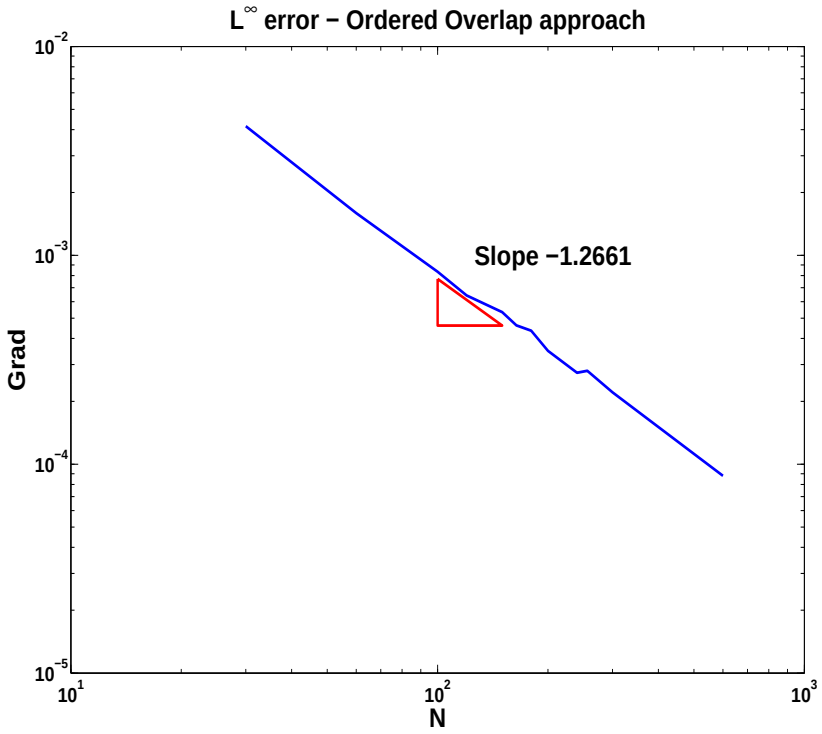

(a) Worst case

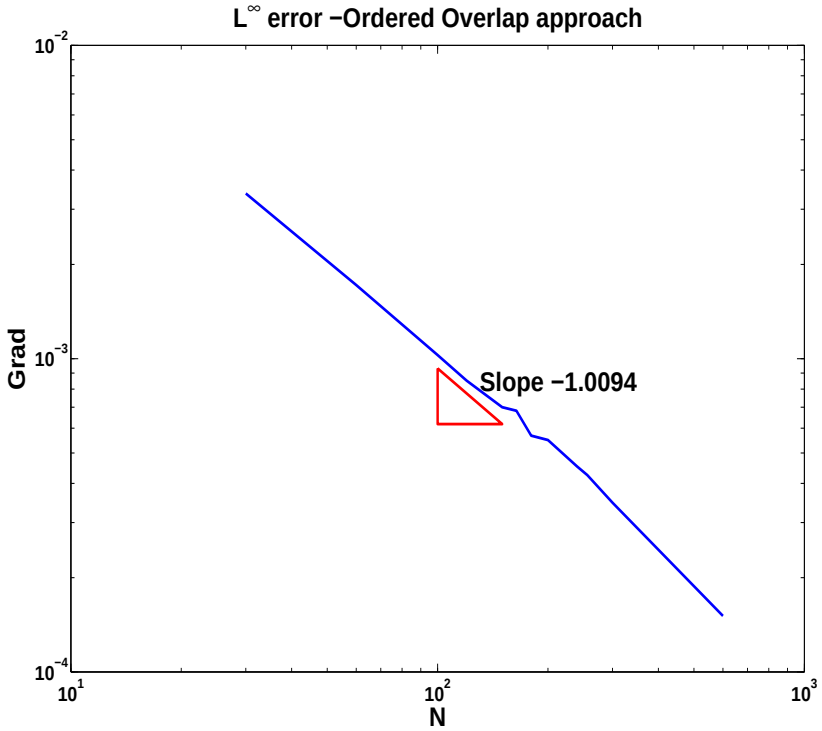

(b) Normal case

FIGURE 4.24. L^{∞} Error - Ordered Overlap Strategy

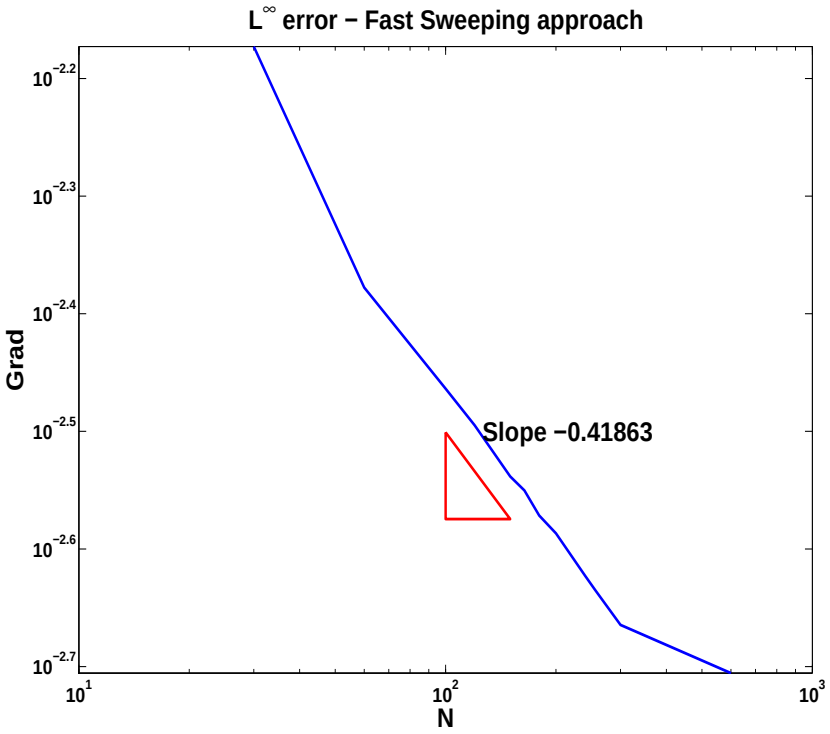

(a) Worst case

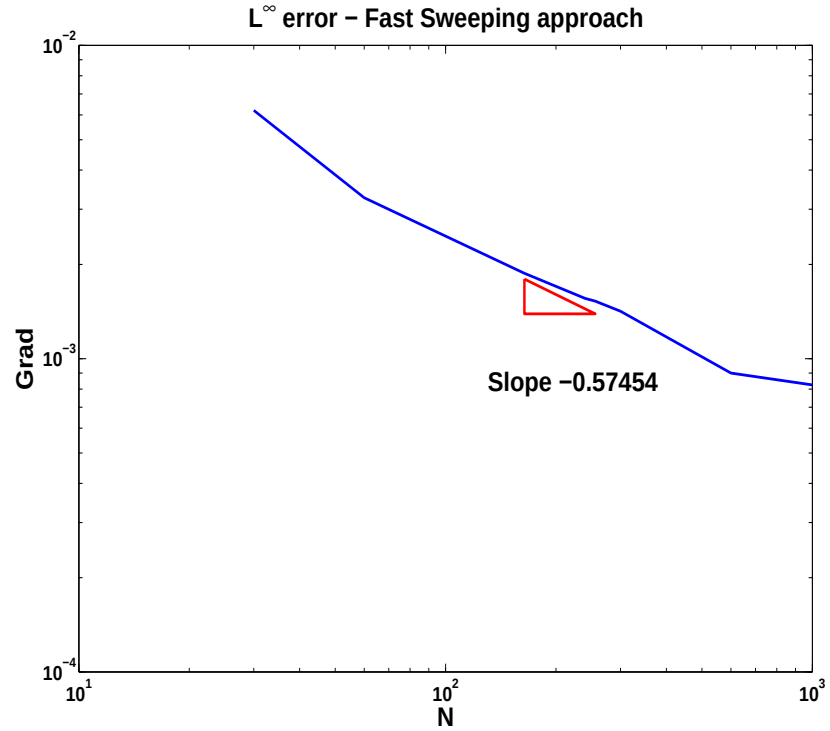

(b) Normal case

FIGURE 4.25. L^{∞} Error- Fast Sweeping Strategy

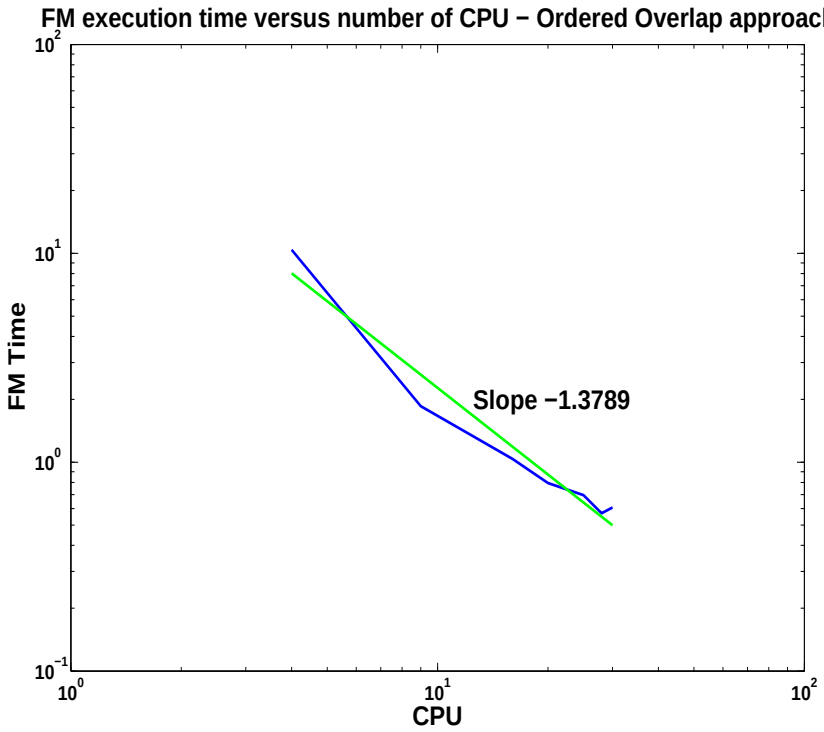

(a) Worst case

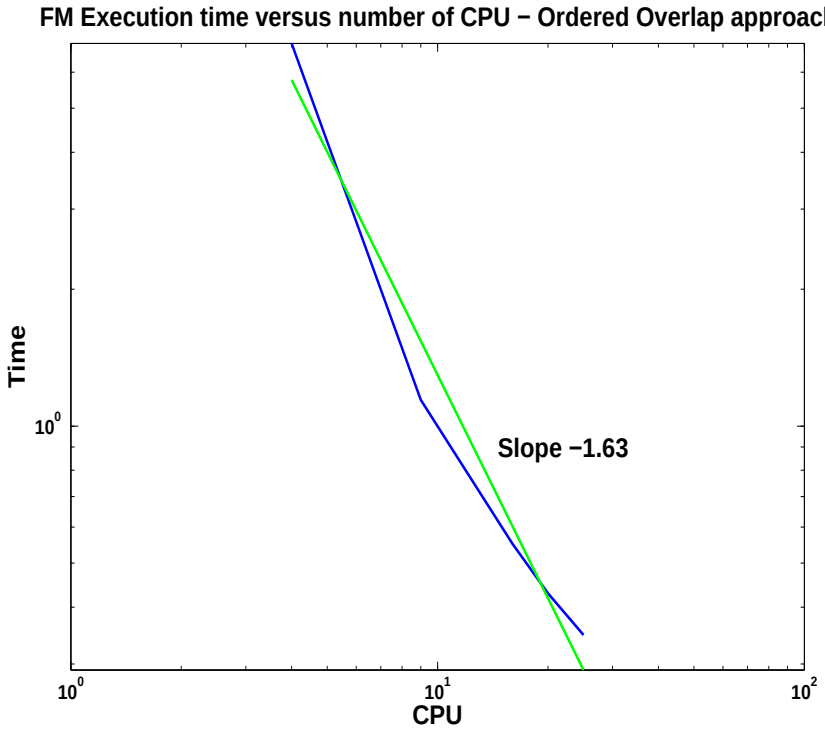

(b) Normal case

FIGURE 4.26. FM execution time with respect to the number of CPU's - Ordered Overlap Strategy

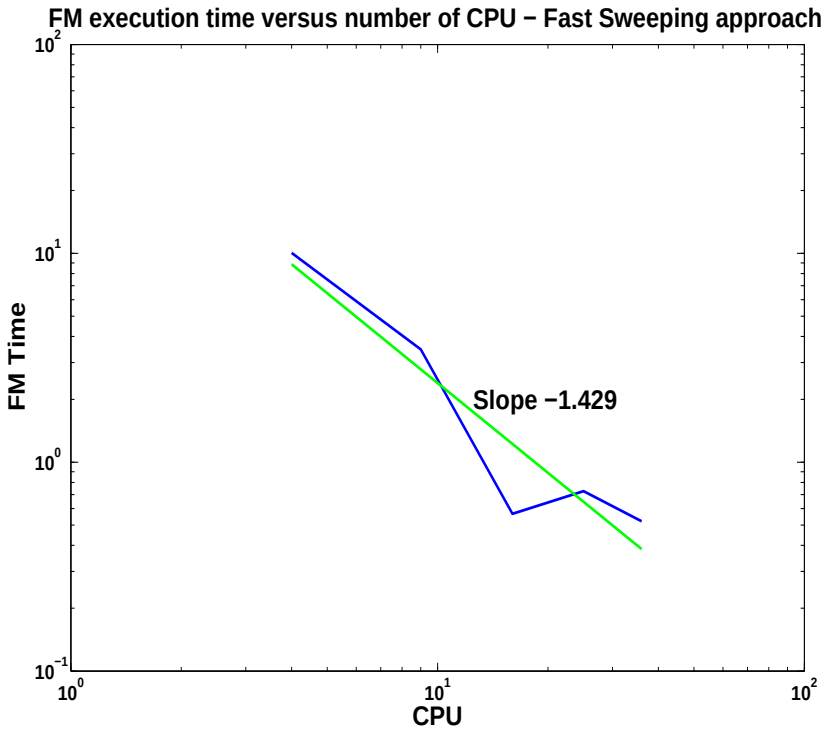

(a) Worst case

(b) Normal case

FIGURE 4.27. FM execution time with respect to the number of CPU's - Fast Sweeping Strategy

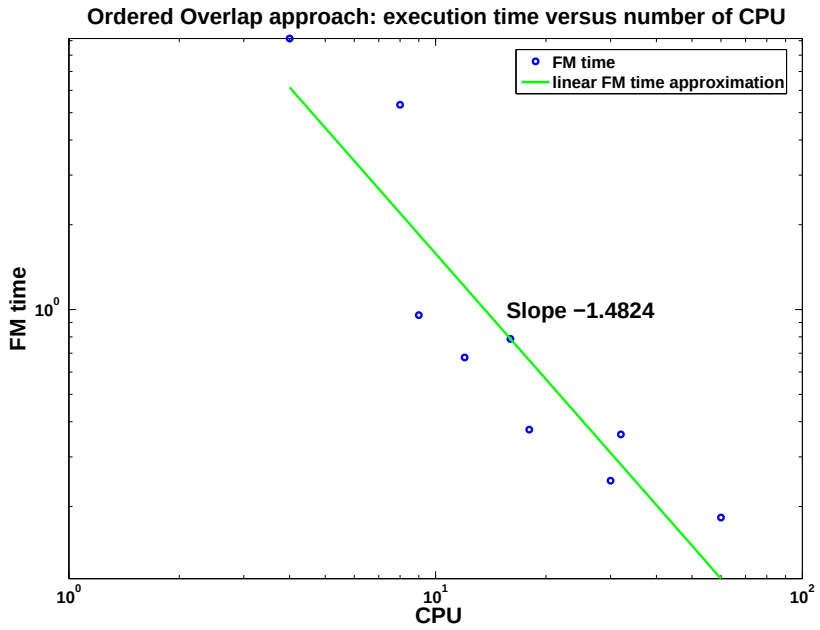

(a) Ordered Overlap Approach

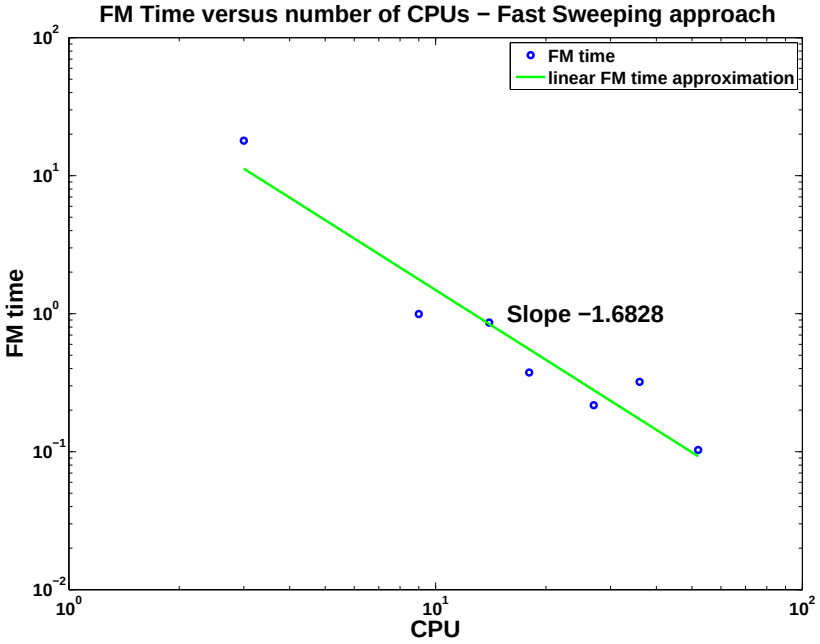

(b) Fast Sweeping Approach

FIGURE 4.28. Best case scenario: Fast Marching execution time with respect to the number of CPU's

References

[1] M. Bardi, I. Capuzzo Dolcetta, *Optimal Control and Viscosity Solutions of Hamilton-Jacobi-Bellman Equations*, Birkhäuser,1997.

[2] G. Barles, B. Perthame, *Discontinuous Solutions of Deterministic Optimal Stopping Time Problems*, Mathematical Modeling and Numerical Analysis, Vol. 21, Nr. 4, (1987), pp. 557-579.

[3] G. Barles, P.E. Souganidis, *Convergence of approximation schemes for fully nonlinear second order equations*, Asymptotic Anal. 4 (1991), pp. 271-283.

[4] M.G. Crandall, L.C. Evans and P.L. Lions, *Some Properties of Viscosity Solutions of Hamilton-Jacobi Equations*, Trans. Amer. Math. Soc. 282 (1984), pp. 487-502.

[5] M.G. Crandall and P.L. Lions, *Viscosity Solutions of Hamilton-Jacobi Equations*, Trans. Amer. Math. Soc. 277 (1983), pp. 1-42.

[6] E. Cristiani, M. Falcone, *Fast Semi-Lagrangian Schemes for the Eikonal Equation and Applications*, SIAM J. Numer. Analysis, Vol. 45, Nr. 5, (2007), pp. 1979-2011.

[7] E.W. Dijkstra, *A Note on Two Problems in Connection with Graphs*, Numerische Mathematic, 1, (1959), pp. 269-271.

[8] L.C. Evans, *Partial Differential Equations*, Graduate Studies in Mathematics, Volume 19, Amer. Math. Soc., 1998.

[9] M. Falcone, T. Giorgi, P.Loreti, *Level Sets of Viscosity Solution: Some Applications to Front and Rendez-Vous Problems*, SIAM J. Appl. Math., Vol. 54 (1994), Nr. 5, pp. 1335-1354.

[10] M. Falcone, *The Minimum Time Problem and Its Applications to Front Propagation*, in A. Visintin and G. Buttazzo, *Motion by mean curvature and related topics*, De Gruyter Verlag, Berlin, 1994, pp. 70-88.

[11] M. Falcone, R. Ferretti, *Discrete time high-order scheme for viscosity solutions of Hamilton-Jacobi-Bellman equations*, Numer. Math, 67, (1994), pp. 315-344.

[12] J.L. Hennessy, D.A. Patterson, *Computer Architecture: A Quantitative Approach*, 3rd edition, Morgan Kaufmann, 2002, pp. 713.

[13] H. Ishii, *Hamilton-Jacobi Equations with Discontinuous Hamiltonians on Arbitrary Open Subset*, Bulletin of Faculty of Science and Engineering, Chuo. Univ., 28 (1985),pp. 33-77.

[14] W. Gropp, E. Lusk, A. Skjellum, *Using MPI*, MIT Press, Cambridge, Massachusetts, 1999.

[15] D. Knuth, *The Art of Computer Programming*, Volume 3, Second Edition, Addison-Wesley, 1998, pp.80105.

[16] R.J. Leveque, *Finite Volume Methods for Hyperbolic Problems*, Cambridge University Press, 2002.

[17] P.L. Lions, *Generalized Solutions of Hamilton-Jacobi Equations*, Pitman, London, 1982.

[18] S. Osher, J.A. Sethian, *Fronts Propagating with Curvature Dependent Speed: Algorithms Based on Hamilton-Jacobi Formulations*, Journal of Computational Physics, 79 (1988), pp. 12-49.

[19] S. Balay, W.D. Gropp, L.C. McInnes, B.F. Smith , *Modern Software Tools in Scientic Computing*, Birkhauser Press, 1997, pp. 163-202.

[20] P.V. Roy, S. Haridi, *Concepts, Techniques, and Models of Computer Programming*, MIT Press, 2004, pg. 1-111, 345-405, 707-749.

[21] E. Rouy, A. Tourin, *A Viscosity Solutions Approach to Shape-from-Shading*, SIAM J. Numer. Analysis, 29 (1992), pp. 867-884.

[22] J.A. Sethian, *A Fast Marching Level Set Method for Monotonically Advancing Fronts*, Proc. Natl. Acad. Sci, Vol. 93 (1996),pp. 1591-1595.

[23] J.A. Sethian, *Level Set Methods and Fast Marching Methods: Evolving Interfaces in Computational Geometry, Fluid Mechanics, Computer Vision and Material Science*, Cambridge University Press, Cambridge, UK, 1998.

[24] J.A. Sethian, *Fast Marching Methods*, SIAM Review, Vol. 41, No. 2, (1999), pp. 199-235.

[25] M. Snir, S. Otto, S.H. Lederman, D. Walker, J. Dongarra, *MPI - The Complete Reference*, Second Edition, MIT Press, Cambridge, UK, 1998.

[26] J. Van Trier and W.W. Symes, *Upwind Finite-Difference Calculation of Travel Times*, Geophysics, 56 (1991), pp. 812-821.

[27] J. Tsitsiklis, *Efficient Algorithms for Globally Optimal Trajectories*, IEEE Trans. on Automatic Control, Vol. 40, No. 9, (1995), pp. 1528-1538

[28] H.K.Zhao, *Fast Sweeping Method for Eikonal Equations*, Math. Comp., 74,(2005), pp. 603-627.

[29] H.K.Zhao, *Parallel implementations of the Fast Sweeping Method* , Journal of Computatonal Mathematics, Vol. 25,No. 4, (2007), pp. 421-429.

Appendix A: Modules Hierarchy

The hierarchy and dependences between modules are presented in Figure 4.29. We start defining the structure and the double chained list, and after that we continue with the flags assignment rules. Next in hierarchical pyramid is the algorithm module part responsible for all the Fast Marching related procedures. The last module is the display module which manages the reading/writing of the image, from/in pgm format, the writing of the result files for graphical analysis and displaying information in between iterations. There is the string conversion module, responsible for creating the names of the simulation files. The main function assembles all the modules together and establish their order of execution.

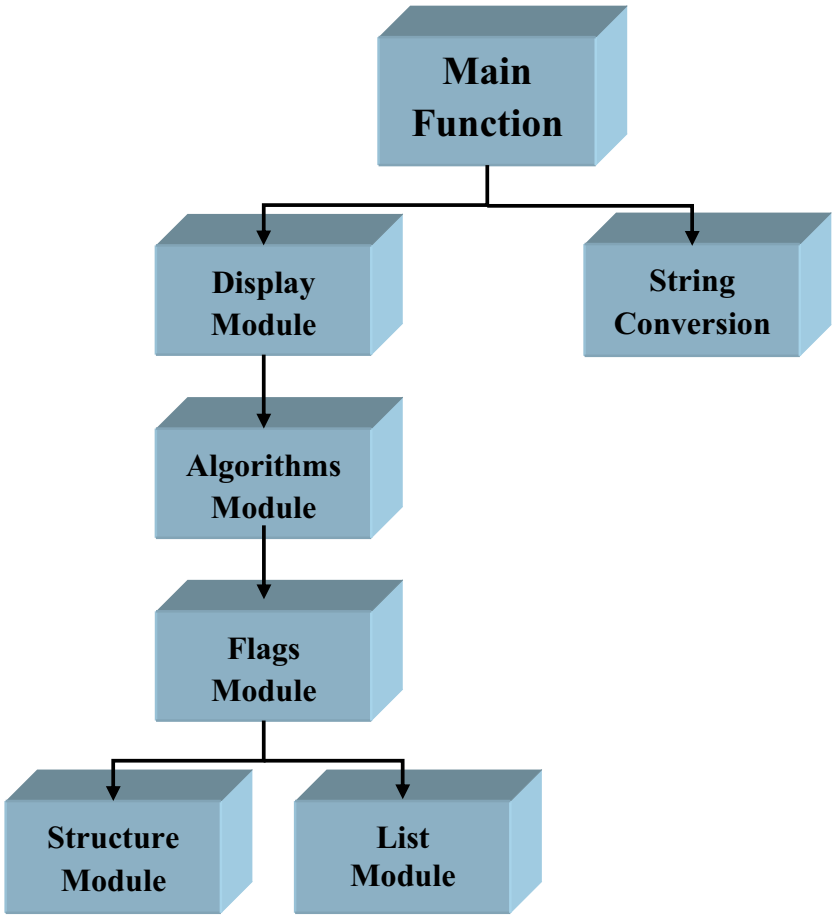

FIGURE 4.29. Modules Hierachy

In the following algorithms we present the headers of all the modules considered in the numerical implementation:

Algorithm 22 Main Function

```
#include “mpi.h”
extern “C”{
#include <pgm.h>}
#include “Stringconversion.h”
#include “DisplayMat1.h”

static char help[] = ”Read the pmg file and do the Fm algorithm ”;
int stages[19];

int main(int argc, char **argv)
{
...
}
```

Algorithm 23 Structure Module Header

```
#include <stdio.h>
#include <stdlib.h>
#include <math.h>
#include “petsc.h”
#include “petscvec.h”
#include “petscmat.h”
#include “petscda.h”
#include “petscsys.h”

typedef struct GeomStruct{
int Nx, Ny, rank;
int xs, ys, xm, ym, ghostx, ghosty, ghostxw, ghostyw;
struct neigh{
int left, right, top, bottom;
} Neighbor;
DA Val_DA;
DA Flg_DA;
} GeomStruct;

void Init_Geom(GeomStruct *geom);
void Do_Structure(GeomStruct *geom);
```

Algorithm 24 List module header

```
#include <stdio.h>
#include <stdlib.h>
#include <math.h>
#include "petsc.h"

#define S 1000.00

typedef struct ListNode{
struct position{
int row;
int col;
}entry;
struct ListNode *next;
struct ListNode *previous;
} ListNode;

struct ListNode *MakeListNode(int j, int i);
void RemoveNode(ListNode *current);
void InsertAfter(ListNode *newnode,ListNode *current);
void InsertBefore(ListNode *newnode, ListNode *current);
struct ListNode *FindPointer(int i, int j, ListNode *head, ListNode *tail);
void UpdateList(ListNode *p, PetscReal **val, ListNode *head, ListNode *tail);
void Print_List( ListNode *first, ListNode *last);
void Print_List_val(PetscReal **val, ListNode *first, ListNode *last,PetscReal
**F);
struct ListNode * FirstNarrowBand(ListNode *first, ListNode *last,PetscReal **F,
PetscReal **val);
void Do_List(int x, int y,int xw, int yw,PetscReal **val, ListNode *head, ListNode
*tail);
```

Algorithm 25 Flag Module Header

```
#include <stdio.h>
#include "petsc.h"
#include "TestStruct_Functions.h"
#include "TestList_Functions1.h"

void countNB(GeomStruct *geom,Vec L_F,Vec L, ListNode *head, ListNode *tail,
ListNode *crt);
void UpdateFlag( GeomStruct *geom,Vec L, Vec L_F, int xs, int ys, int xm, int
ym);
void UpdateNarrowBand(GeomStruct *geom,Vec L,Vec L_F, ListNode *head,
ListNode *tail);
```

Algorithm 26 Algorithms Module Header

```
#include <stdio.h>
#include <stdlib.h>
#include <math.h>
#include "petsc.h"
#include "petscvec.h"
#include "petscmat.h"
#include "petscda.h"
#include "petscsys.h"
#include "TestFlag_Functions.h"

PetscReal mini( PetscReal a, PetscReal b);
PetscReal maxi( PetscReal a, PetscReal b);
PetscReal pitagora( PetscReal a, PetscReal b);
PetscReal distance(int i, int j, PetscReal **val, GeomStruct *geom);
PetscReal distanceNB(int i, int j, PetscReal **val, GeomStruct *geom);
void UpdateNBDist(GeomStruct *geom, Vec L, Vec L_F,ListNode*head, ListNode
*tail);
void UpdateDistNbr(GeomStruct *geom, Vec L, Vec L_F, ListNode *head, ListN-
ode *tail, ListNode *crt);
void FastMarching(GeomStruct *geom,Vec L,Vec L_F, ListNode *head, ListNode
*tail, int numprocs);
PetscReal *GhostPtsH( GeomStruct *geom, PetscReal *gh, Vec L, Vec L_F, int a,
int b, int d);
PetscReal *GhostPtsV( GeomStruct *geom, PetscReal *gv, Vec L, Vec L_F, int a,
int b, int d);
PetscReal UpdateGhostPtsH1( GeomStruct *geom, Vec L, Vec L_F, ListNode
*head, ListNode *tail, PetscReal *gh, int a, int b, int c, int d );
PetscReal UpdateGhostPtsH2( GeomStruct *geom, Vec L, Vec L_F, ListNode
*head, ListNode *tail, PetscReal *gh, int a, int b, int c, int d );
PetscReal UpdateGhostPtsV1( GeomStruct *geom, Vec L, Vec L_F, ListNode
*head, ListNode *tail,PetscReal *gv, int a, int b, int c, int d );
PetscReal UpdateGhostPtsV2( GeomStruct *geom, Vec L, Vec L_F, ListNode
*head, ListNode *tail,PetscReal *gv, int a, int b, int c, int d );
void UpdateGhostPtsFlg( GeomStruct *geom, Vec L,Vec G_F,Vec L_F, ListNode
*head, ListNode *tail);
PetscReal UpdatedPtsMaxV( GeomStruct *geom, Vec L, Vec L_F, PetscReal max,
int a, int b,int c);
PetscReal UpdatedPtsMaxH( GeomStruct *geom, Vec L, Vec L_F, PetscReal max,
int a, int b,int c);
PetscReal UpdatedPtsMinV( GeomStruct *geom, Vec L, Vec L_F, PetscReal min,
int a, int b,int c);
PetscReal UpdatedPtsMinH( GeomStruct *geom, Vec L, Vec L_F, PetscReal min,
int a, int b,int c);
void UpdatedPtsFlg( GeomStruct *geom, Vec L, Vec L_F,ListNode *head, ListN-
ode *tail, PetscReal min, PetscReal max,int a, int b,int c, int d);
```

Algorithm 27 Display Module Header

```
#include <stdio.h>
#include "petsc.h"
#include "TestAlg_Functions1.h"

Vec CreateNaturalOrdering(Vec G, GeomStruct *geom);
void OutputPGM(FILE *file,Vec G, GeomStruct *geom);
void OutputPGM_f(FILE *file,Vec G,Vec G_F, GeomStruct *geom);
PetscReal Gradient_error(FILE *file, Vec G, GeomStruct *geom);
void DisplayMat(PetscReal **val, int xs, int xm, int ys, int ym, PetscReal **F);
void SaveMat(FILE *fname, PetscReal **val,int xs, int xm, int ys, int ym,
PetscReal **F);
void SavePGM(FILE *file, PetscReal **val, int xs, int xm, int ys, int ym);
void Scale_for_PGM(PetscReal **val, int xs, int xm, int ys, int ym, PetscReal
vmaxi);
void SaveFlag(FILE *file, PetscReal **F, PetscReal **val, int xs, int xm, int ys,
int ym);
void SaveList(FILE *file, PetscReal **val,PetscReal **F, ListNode *head, ListN-
ode *tail);
int Write_Geom_Struct_ASCII(int Bounds[], char F_Name[]);
int Write_2D_Scal_Struct_ASCII(PetscReal *v_in, char F_Name[], int NbRec);
int Write_2D_Vect_Struct_ASCII(PetscReal *v_in, char F_Name[], int NbRec);
int WriteCase(char *fname, char *geoname, char *resname, char *vector, int j);
```

Algorithm 28 String Conversion Module Header

```
#include <stdio.h>
#include <stdlib.h>
#include <stdarg.h>
#include <string.h>
#include "petsc.h"
#include "petscsys.h"

char *itoa(int value);
void conversion( int NumProcs, int MyRank, char filename[128], char fileprefix[4],
int i);
void conversion_pgm(int NumProcs, int MyRank, char filename[128], char filepre-
fix[4]);
```

Appendix B: PETSc Features

At certain stages of the applications, there is a need to work on a local portion of the vector, including the ghost points. This may be done by scattering a global vector into its local parts by using the two-stage commands:

```
DAGlobalToLocalBegin (DA da,Vec g,InsertMode iora,Vec l);
DAGlobalToLocalEnd (DA da,Vec g,InsertMode iora,Vec l);
```

which allow the overlap of communication and computation [19].
One can scatter the local patches into the distributed vector with the command:

```
DALocalToGlobal (DA da,Vec l,InsertMode mode,Vec g);
```

Note that this function is not subdivided into beginning and ending phases, since it is purely local.
A third type of distributed array scatter is from a local vector (including ghost points that contain irrelevant values) to a local vector with correct ghost point values. This scatter may be done by commands:

```
DALocalToLocalBegin (DA da,Vec L1,InsertMode iora, Vec L2);
DALocalToLocalEnd (DA da,Vec L1,InsertMode iora, Vec L2);
```

In our applications, there are cases where we need to use the local ghosted vectors. PETSc provides way to obtain these work vectors and return them when they are no longer needed. This is done with the routines:

```
DAGetLocalVector(DA da,Vec *l);
.... use the local vector l
DARestoreLocalVector(DA da,Vec *l);
```

Also, we can set values into the DA Vectors and access them using the natural grid indexing, by calling the routines:

```
DAVecGetArray(DA da,Vec l,void *array);
... use the array indexing it with 1 or 2 or 3 dimensions
... depending on the dimension of the DA
DAVecRestoreArray(DA da,Vec l,void *array);
```

where *array* is a multidimensional C array with the same dimension as the distributed array. The vector l can be either a global vector or a local vector. The array is accessed using the usual global indexing on the entire grid, but the user may only refer to the local and ghost entries of this array as all other entries are undefined.

Another important feature of PETSc is the way that it allows us to perform operations with vector and distributed array. For instance, for stopping criteria implementation, we check if there are any changes in the boundary of each subdomain by calling the PETSc function:

```
VecAXPY( Vec source, PetscScalar *a, Vec destination ),
```

which performs the mathematical operation:

$$destination = destination + a \times source.$$

Then, we compute the norm of the error at each edge by calling:

```
VecNorm(Vec source, NORM_INFINITY, &error_t).
```

We can also use the MPI functions to go from the local to global representation of a vector and vice versa. For instance, for each processor i we compute a total error, which represents the maximum of the left, right, top and bottom errors and using the *MPI_Allreduce* function we can find the total error:

```
errori=maxi(maxi(error_b, error_t), maxi(error_l, error_r));
MPI_Allreduce(&errori, &error, 1, MPI_DOUBLE, MPI_MAX,  MPI_COMM_WORLD).
```

In this way we use the MPI function to gather the global error on the master node.

Vita

Maria Cristina Tugurlan was born on August, 1974, in Iasi, Romania. She finished her undergraduate studies in computer science at "Gh. Asachi" Technical University of Iasi, Romania, June 1998. She earned a Master of Science degree in automatic control in July 2000 from "Gh. Asachi" Technical University of Iasi, Romania. From 1998 to 2002, she worked as instructor at "Gh. Asachi" Technical University of Iasi, Department of Automatic Control, Romania. In August 2002 she came to Louisiana State University to pursue graduate studies in mathematics. She earned a Master of Science degree in mathematics from Louisiana State University in May 2004. She is currently a candidate for the degree of Doctor of Philosophy in mathematics, which will be awarded in December 2008.